Studies of Kinetochore Mechanobiology in Drosophila

STUDIES OF KINETOCHORE MECHANOBIOLOGY IN *DROSOPHILA*

A Dissertation Presented

by

STUART CANE

Submitted to the Graduate School of the

University of Massachusetts Amherst in partial fulfillment

of the requirements for the degree of

DOCTOR OF PHILOSOPHY

February 2016

Molecular and Cellular Biology Graduate Program

STUDIES OF KINETOCHORE MECHANOBIOLOGY IN *DROSOPHILA*

A Dissertation Presented

by

STUART CANE

Approved as to style and content by:

_____
Thomas J. Maresca, Chair

_____
Wei-Lih Lee, Member

_____
Jennifer L. Ross, Member

_____
Patricia Wadsworth, Member

_____
Dominique Alfandari, Director
Molecular and Cellular Biology Graduate Program

DEDICATION

In Memory of my Parents

ACKNOWLEDGMENTS

I am indebted to Tom Maresca for several years of patient instruction, and to all the members of my Dissertation Committee – Drs. Maresca, Lee, Ross and Wadsworth – for sharing their insights and offering much-valued support and encouragement. I am also grateful for the assistance and support of my laboratory colleagues.

Portions of this Dissertation have previously appeared in *The Journal of Cell Biology* 200(2):203-18. doi: 10.1083/jcb.201211119 and *BioArchitecture* 3(3):69-76. doi: 10.4161/bioa.25734.

ABSTRACT

STUDIES OF KINETOCHORE MECHANOBIOLOGY IN *DROSOPHILA*

FEBRUARY 2016

STUART CANE, A.B., COLUMBIA UNIVERSITY

J.D., THE GEORGE WASHINGTON UNIVERSITY LAW SCHOOL

Ph.D., UNIVERSITY OF MASSACHUSETTS AMHERST

Directed by: Professor Thomas J. Maresca

Among the earliest events of mitotic cell division are formation of the bipolar, microtubule-based mitotic spindle and construction of large multiprotein structures, called kinetochores, through which the chromosomes will engage with the spindle. Spindle microtubules and kinetochores must ultimately attach in such a way as to produce *bioriented* chromosomes, in which the two sister chromatids are attached to microtubules from opposite spindle poles and are poised to segregate equally between the two daughter cells. Should a cell segregate its chromosomes without every chromosome having first become bioriented on the spindle, the daughter cells will inherit abnormal numbers of chromosomes, and the resulting condition of aneuploidy can have devastating consequences should it become sufficiently widespread in an embryo or other affected organism. Initial kinetochore-microtubule attachments, however, form stochastically, and errors are common. Error correction requires elimination of

the attachment and an attempt to reattach in the correct configuration, without the erroneous, non-bioriented attachment having become too stable to repair.

Kinetochore behavior during mitosis is responsive to forces produced by microtubule dynamics, by microtubule-associated motor proteins, or by some combination of the two. In this dissertation two different approaches are described for experimentally altering the kinetochore's usual responses to spindle forces, and to the mechanical tension that such forces generate, in order to derive insight into the cell's regulatory system for recognizing, destabilizing and correcting erroneous kinetochore-microtubule attachment states. In the first set of experiments (Chapter Two), we focused on the *Drosophila melanogaster* kinetochore protein CENP-C as a protein whose length and physical properties suggested that it could elongate in response to mechanical tension. We found that CENP-C does elongate in kinetochores that are associated with bioriented chromosomes, and we then experimentally disabled it from doing so. In this manner we tested the hypothesis that tension stabilizes bioriented attachments in large part by extending CENP-C, and with it the kinetochore as a whole, in order to pull outer kinetochore microtubule-binding proteins beyond the effective working radius of a centromere-based, attachment-destabilizing kinase activity.

The affinity with which outer kinetochore proteins, prominently including the microtubule-binding Ndc80, bind to microtubules is reduced when those proteins are phosphorylated. Hence phosphorylation of the outer region of the kinetochore tends to destabilize kinetochore-microtubule attachments. The Aurora B kinase localizes to the inner centromere throughout the period of

attachment formation and error correction, and it has therefore been postulated that the physical distance between this kinase and its outer kinetochore substrates either regulates, or contributes substantially to the regulation of, the stability of kinetochore-microtubule attachments. This “spatial positioning” model predicts that when a kinetochore attached in the bioriented configuration elongates under tension, in a process called intrakinetochore stretch, phosphorylation of outer kinetochore Aurora B substrates is progressively reduced and the attachment becomes increasingly stable. The cell would accordingly tend to stabilize attachments that are bioriented and under tension, as it should, while erroneous attachments would remain unstable. We sought to test the model by experimentally reducing or eliminating intrakinetochore stretch, hypothesizing that the cell’s inability to distance the outer kinetochore from the inner centromere would preclude dephosphorylation of the outer kinetochore and prevent the formation of stable attachments.

Having determined that CENP-C is a mediator of intrakinetochore stretch in *Drosophila*, we found that when we shortened CENP-C, by removing a stretchable portion of the protein, we impaired the cell’s ability to form stable attachments. We also found that, consistent with a key premise of the spatial positioning model, inhibition of Aurora B activity partially restored the cell’s capacity to stabilize kinetochore-microtubule attachments. Further, we showed that by inserting an unrelated peptide linker into CENP-C in lieu of the section we had originally removed, we could likewise partially rescue the attachment instability phenotype.

In a second set of experiments (Chapter Three) we again altered the usual distribution of forces within the spindle and at the kinetochore. In this instance our strategy was not to destabilize attachments but rather, by applying artificially elevated levels of tension to an erroneously attached kinetochore pair – a syntelically attached pair, in which both sister kinetochores attach to microtubules from the same spindle pole – to overcome the Aurora B-based error correction system and stabilize the erroneous attachment. To implement this strategy we employed the *Drosophila* chromokinesin NOD, a plus end-directed kinesin-10 motor that localizes to chromosome arms, where it contributes to the polar ejection force that pushes chromosomes away from the poles and toward the spindle midzone.

A syntelically attached kinetochore pair, being pulled by depolymerizing microtubules toward only one spindle pole, would ordinarily experience little or no opposing force that might cause those kinetochores to come under tension. It would therefore be expected that the syntelic attachment, being incapable of placing the kinetochores under a meaningful degree of tension, would for that reason be recognized as erroneous, leading to detachment under the influence of Aurora B and correction of the error. Our experimental goal was to introduce a significant opposing force, increase the tension experienced by the syntelically attached kinetochore pair, and thereby stabilize the erroneous attachment. This we accomplished by overexpressing NOD and artificially increasing the magnitude of the polar ejection force – a force that opposes the unidirectional microtubule-based pulling force acting on syntelically attached kinetochores but

is ordinarily not strong enough to place those kinetochores under tension. NOD overexpression, consequently, introduced stability to an erroneous, typically highly unstable, state of attachment.

The dissertation examines the implications of those results further in the succeeding chapter. Among the questions addressed in Chapter Four is whether there are spindle assembly checkpoint signaling differences between stable syntelic attachments and bioriented attachments. In general, the checkpoint delays anaphase onset until the error correction system has completed its work and all chromosomes are in the correct, bioriented configuration. But at our stable syntelic attachments we have overridden the usual error correction process and the kinetochores, though not bioriented, are nonetheless attached to microtubules and under tension. Under these conditions the checkpoint should be satisfied and anaphase inhibition should cease, and indeed our NOD-overexpressing cells do progress from metaphase to anaphase, albeit more slowly than non-perturbed *Drosophila* S2 cells. Consistent with that observed anaphase delay, our data show that the checkpoint protein Mad1 is depleted more slowly from stable syntelic attachments than from bioriented attachments, and that detectable levels of Mad1 sometimes remain associated with the syntelic attachments even at anaphase onset. We also found that BubR1, a second checkpoint protein, is never fully depleted from the syntelic attachments, even after a drug-induced two-hour metaphase arrest that should facilitate such depletion. Taken together, the data suggest that the checkpoint inactivation

process is more muted at the stable syntelic attachments, leading to a cell-wide delay in mitotic progression.

From a very broad perspective, it can be argued that the CENP-C results and the NOD results converge in that both tend to undermine any notion that kinetochore-centered regulatory processes behave in an on-off, all-or-nothing fashion (a concept that also arises in Chapter Four, in connection with checkpoint signaling and the potency of anaphase inhibition). There is a developing consensus in the literature holding that attachment stability is carefully modulated, likely by some combination of differential phosphorylation of kinetochore proteins (via spatial positioning and perhaps other, allied mechanisms) and the mechanics of bond formation at or near the plus ends of dynamic microtubules. We have endeavored to encapsulate those emerging principles in the inclusive, though distinctly preliminary, model presented at the close of Chapter Four.

TABLE OF CONTENTS

Page

LIST OF FIGURES

Figure Page

CHAPTER 1

INTRODUCTION

1.1 The Kinetochore in Eukaryotic Cell Division

During each round of eukaryotic cell division, shortly after DNA replication each somatic cell dramatically reorganizes its microtubule cytoskeleton to generate an elegant and astonishing microtubule-based bipolar structure called the mitotic spindle. Microtubules are highly dynamic polymers, continually undergoing polymerization and depolymerization. In the context of the mitotic spindle, it is microtubule depolymerization that ultimately provides the force that moves separated chromatids, after their loss of cohesion, toward the two opposite spindle poles around which the daughter cells will form (Cheerambathur and Desai, 2014; Cheeseman, 2014; Duro and Marston, 2015; McIntosh, 2012). The spindle microtubules do not, however, apply force directly to the DNA or histone constituents of the chromosome. Rather, in order to move chromosomes the spindle microtubules exert their force upon an intervening structure: the kinetochore. That is to say, the microtubules attach to the kinetochore and, as they depolymerize during chromosome segregation the force generated by their depolymerization is transmitted to the chromosome through the kinetochore. The kinetochore, when stably attached to spindle microtubules in the correct configuration, is therefore said to function as a load-bearing structure (Rago and Cheeseman, 2013; Umbreit and Davis, 2012).

A kinetochore forms at a region of heterochromatin called a centromere. After DNA replication, sister chromatids are joined through their centromeres,

and when this junction becomes situated between a pair of sister kinetochores it is referred to as the “inner centromere.” Once the kinetochore has formed adjacent to the inner centromere, a series of movements within the spindle results in its becoming so located and configured as to allow it to be acted on by the forces that are generated by spindle microtubules. Those forces can then effect changes within the structure of the kinetochore itself, with profound consequences for the creation of productive interactions between chromosomes and the spindle and, ultimately, for the dividing cell’s ability to apportion its genetic material equally between the two forming daughter cells. Preliminarily, therefore, an examination of kinetochore structure is necessary to lay the groundwork for what follows.

1.2 Overview of Kinetochore Structure

The kinetochore is a complex assemblage containing multiple copies of a very large number of proteins; in human kinetochores, more than 100 different constituent proteins have been identified (Cheeseman, 2014). By electron microscopy the fully assembled kinetochore appears as a trilaminar structure, with two distinct electron-dense “plates” separated by an intervening, electron-translucent central zone (Maiato et al., 2004; Maiato et al., 2006). When the kinetochore is not attached to spindle microtubules, a “fibrous corona” also emanates from the outer face of the outer kinetochore plate (Chan et al., 2005; Cheeseman and Desai, 2008; McEwen et al., 1998), serving as a binding locus for certain motor proteins and proteins associated with the Spindle Assembly Checkpoint (Chan et al., 2005; Maiato et al., 2004; Musacchio and Salmon,

2007) – of which more will be said below. This overall ultrastructure is characteristic of human and other vertebrate kinetochores as well as those of *Drosophila melanogaster* (Maiato et al., 2006), the model organism used in all of the experiments to be described in this dissertation.

Investigators in this field often remark upon the extent to which various features and components of the kinetochore are conserved across nearly all eukaryotes (Cheeseman and Desai, 2008; Lampert and Westermann, 2011; Meraldi, 2012; Santaguida and Musacchio, 2009). But the molecular composition of the *Drosophila* kinetochore does differ in certain respects from the kinetochore composition seen in other model organisms. As described in Section 1.2.1 below, the inner region of the *Drosophila* kinetochore contains far fewer proteins than are found in the vertebrate inner kinetochore. Of greatest significance for present purposes is the fact that in vertebrate kinetochores there are two different proteins that link the inner region of the kinetochore to the outer, microtubule-binding region, whereas only one such protein linkage is found in *Drosophila*.

In the experiments described in Chapter Two we consider whether, to what extent, and with what consequences the kinetochore stretches and elongates when attached to a chromosome in the proper configuration. Such questions are by no means uniquely relevant for *Drosophila*, and indeed similar questions have been explored both in other metazoans and in yeast. Our study is informed throughout by insights derived from the study of those other organisms. A representation of the vertebrate kinetochore, at three different

levels of resolution, is shown in Figure 1.1. The right-hand panel of the figure depicts, as alluded to immediately above, two different proteins linking the inner and outer regions of the kinetochore: (i) CENP-C, which is also found in the *Drosophila* kinetochore and will be a central focus of Chapter Two, and (ii) CENP-T, which is absent from the *Drosophila* kinetochore. Putting that (very significant) difference aside, the figure's right-hand panel is nonetheless useful for its depiction of the relative locations of the CENP-A chromatin (see Section 1.2.1), the inner and outer regions of the kinetochore, and the kinetochore-microtubule contact site.

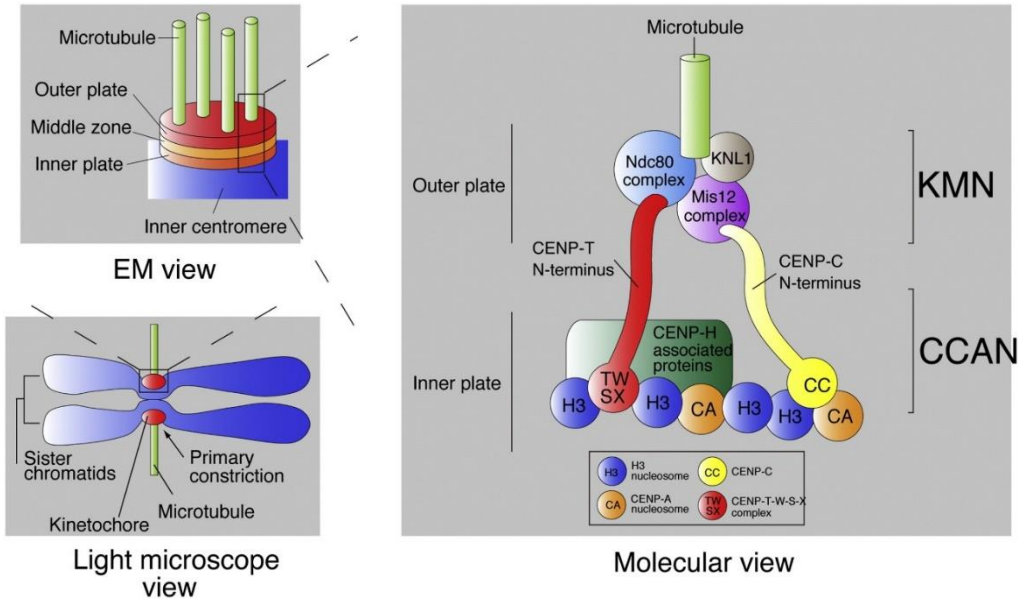

Figure 1.1: The vertebrate kinetochore. In the two left-hand panels, a Light Microscope View situates a pair of sister kinetochores in relation to their associated sister chromatids, and an EM View depicts the kinetochore's trilaminar architecture and the underlying inner centromere. The Molecular View, at right, schematically represents the protein composition of the inner and outer regions of the vertebrate kinetochore. As described in Sections 1.2.1 and 1.2.2 below, "CCAN" refers to the Constitutive Centromere-Associated Network and "KMN" refers to the network of outer kinetochore proteins consisting of KNL1, the Mis12 complex and the Ndc80 complex. Reprinted from Takeuchi and Fukagawa (2012), *Experimental Cell Research* 318(12):1367-1374, with permission from Elsevier.

1.2.1 The Inner Kinetochore

The inner and outer “plates” of the kinetochore are now universally referred to simply as the Inner Kinetochore and the Outer Kinetochore. The inner kinetochore includes, as its foundation, a region of centromeric heterochromatin in which are interspersed, among the conventional nucleosomes, other nucleosomes containing a unique, centromere-specific variant of Histone H3 (Blower and Karpen, 2001; Sullivan et al., 2001). The presence of this histone variant, referred to as CENP-A in most organisms and as Cid (for *C*entromere *Id*entifier) in *Drosophila*, is the defining epigenetic feature that specifies the site at which a kinetochore will form. Aside from the presence of CENP-A/Cid, which is universal (Phansalkar et al., 2012), the *Drosophila* inner kinetochore is somewhat differently constituted than the vertebrate inner kinetochore.

In *Drosophila*, only two additional proteins are considered to be part of the inner kinetochore: Cal1 and CENP-C. Localization of Cid, Cal1 and CENP-C to the centromere is interdependent, that is, none of the three localizes properly in the absence of either one of the others. Cal1 is proposed to act as a chaperone for delivery of Cid to the centromeric chromatin (Chen et al., 2014) and/or as a “bridging factor” (Schittenhelm et al., 2010) linking the other two inner kinetochore components, binding Cid through its N terminus and CENP-C through its C terminus.

CENP-C, of which a great deal more will be said at later points in the dissertation, directly binds DNA *in vitro* (Guse et al., 2011; Yang et al., 1996) and localizes to the centromere constitutively in cells, through a C-terminal domain

that (in *Drosophila*) is found in the region of amino acids 1009-1205. Within this region lies the distinctive “CENP-C motif,” which is generally well conserved across eukaryotes but is “highly diverged” in *Drosophila* species (Heeger et al., 2005). A single point mutation within this motif abolishes the centromere localization of *Drosophila* CENP-C (Heeger et al., 2005). Proper CENP-C localization may occur through DNA binding alone, given that no direct interaction between CENP-C and CENP-A/Cid has been shown in *Drosophila* (Schittenhelm et al., 2010) – but such a conclusion seems premature as of now, and a potential for direct binding is seen *in vitro* using the human CENP-C motif and a chimeric histone that resembles CENP-A in relevant respects (Kato et al., 2013). The CENP-C N terminus binds directly to Nnf1, a constituent of the outer kinetochore Mis12 complex (Przewloka et al., 2011). The particular domain within CENP-C’s N terminus that is required for Nnf1 binding has not been identified with certainty, though some or all of the amino acid 1-71 region mediates that interaction in humans (Screpanti et al., 2011). CENP-C thus forms a linkage – in *Drosophila*, likely the only linkage – between the inner and outer regions of the kinetochore (Przewloka et al., 2011; Screpanti et al., 2011). The *Drosophila* CENP-C N terminus, through its direct association with the Mis12 complex, provides a foundation for assembly of the entire outer kinetochore. CENP-C plays a similar foundational role in human cells, but in that context there are conflicting reports as to whether there also exists a parallel and CENP-C-independent pathway for outer kinetochore assembly based on CENP-T (Rago et al., 2015) or whether, instead, CENP-T localization to the kinetochore is itself

CENP-C-dependent – placing CENP-C at the foundation of a single outer kinetochore assembly pathway (Klare et al., 2015).

In sharp contrast to the minimalist version of the inner kinetochore found in *Drosophila*, the inner kinetochore in human and other vertebrate cells includes, in addition to CENP-C, fifteen other proteins that localize to the centromere throughout the cell cycle. Collectively the sixteen constitutively localized proteins have been termed the Constitutive Centromere-Associated Network (CCAN) (Cheeseman and Desai, 2008). The CCAN includes CENP-C and several different protein subgroups: CENP-H/I/K, CENP-L/M/N, CENP-O/P/Q/R/U, and the CENP-T/W/S/X complex (Perpelescu and Fukagawa, 2011), though modestly different groupings have also been proposed (Suzuki et al., 2014). The CENP-T/W/S/X complex is of particular significance functionally for two distinct, but closely related, reasons.

First, like CENP-C, CENP-T possesses both DNA-binding activity in the region of its C terminus (Hori et al., 2008) and an N-terminal outer kinetochore-interacting domain – though in this case the interaction is with the Ndc80 complex (specifically, the Spc24/Spc25 heterodimer) rather than the Mis12 complex (Nishino et al., 2013). CENP-T thus has the capacity to link centromere DNA to the outer kinetochore, though recent data suggests a greater likelihood that CENP-T, instead, links centromere-bound *CENP-C* to the outer kinetochore in vertebrate cells (Klare et al., 2015). In either case CENP-T is centrally involved in linking the inner and outer regions of the vertebrate kinetochore. The CENP-T homolog Cnn1 also interacts with the Spc24/Spc25 heterodimer in

budding yeast (Malvezzi et al., 2013; Schleiffer et al., 2012), but the roles of Cnn1 and the CENP-C homolog Mif2 in the process of outer kinetochore assembly in yeast do not appear to have been specifically compared.

Second, CENP-T is an extendible protein (Suzuki et al., 2011) that elongates when subjected to tension at bioriented kinetochore-microtubule attachments during metaphase (Suzuki et al., 2014). This mechanical deformation, called *intrakinetochore stretch* (see Section 1.3.5 below), has the effect of distancing the outer kinetochore from the inner kinetochore and, correspondingly, from the proteins that localize to the inner centromere. We hypothesize that CENP-C is also an extendible protein, at least in *Drosophila*. The investigation reported below as Chapter Two is premised on the contention that in *Drosophila*, from which CENP-T is absent, it is CENP-C that undergoes intrakinetochore stretch and, further, that the stretching of CENP-C plays a pivotal role in enabling the dividing *Drosophila* cell to segregate its chromosomes properly.

1.2.2 The Outer Kinetochore

The outer kinetochore includes three constituent parts: the protein KNL1, the Mis12 Complex and the Ndc80 Complex. Collectively these outer kinetochore constituents are generally referred to throughout the literature by the initials KMN, hence, the KMN Network. (KNL1 actually forms a heterodimer with Zwint-1 – an upstream participant in the recruitment of Spindle Assembly Checkpoint proteins to the kinetochore (Varma et al., 2013) – but references to a

"KNL1 Complex" are seldom encountered.) For convenience the following discussion begins with the innermost network component (Mis12 complex) and concludes with the principal mediator of kinetochore-microtubule attachment (Ndc80 complex), but it should be borne in mind that KNL1 does not lie physically between the two other network components in a linear sequence along the spindle's long axis (Schittenhelm et al., 2009), and that it forms its own interaction with spindle microtubules (DeLuca and Musacchio, 2012).

1.2.2.1 The Mis12 Complex

The Mis12 complex both recruits the two other KMN network components and serves as a bridge between the two and, by binding to CENP-C, also links the inner and outer regions of the kinetochore (Foley and Kapoor, 2013; Petrovic et al., 2014). In *Drosophila* the complex includes three constituent proteins (Nnf1, Mis12 and Nsl1), while a fourth protein (Dsn1) that is present in the vertebrate (and *C. elegans*) Mis12 complex is not found in *Drosophila* (Przewloka et al., 2009). *Drosophila* is also somewhat unusual in that the subunits of the complex do not localize to the centromere simultaneously; rather, the Mis12 protein itself is found at the centromere during interphase whereas Nsl1 does not localize to the centromere until mitotic entry (Venkei et al., 2011). As for Nnf1, two distinct (paralogous) versions are found in *Drosophila*, and there is a conflict in the literature concerning whether only one version (Venkei et al., 2011) or both (Schittenhelm et al., 2007) are found at the centromere during interphase.

In humans, the full complex takes the form of a ~22 nm rod (Petrovic et al., 2010). (The complex is of a comparable length in budding yeast, where it has been described both as “comma”-shaped (Maskell et al., 2010) and as a “bi-lobed rod-like structure” (Hornung et al., 2011).) The individual subunits were believed for some time to be organized in a linear sequence (Nnf1, Mis12, Dsn1, Nsl1) (Petrovic et al., 2010), but more recently it has instead been proposed that, at least in human cells, Nsl1 more likely extends along the entire length of the ~22 nm rod (Petrovic et al., 2014). It has been shown that in *Drosophila*, it is the Nnf1 subunit that interacts with the N terminal portion of CENP-C as part of the inner-to-outer kinetochore linkage (Przewloka et al., 2011). Meanwhile at the other, outermost end of the rod, Nsl1, through its C terminal region, interacts both with KNL1 and with the Spc24/Spc25 portion of the Ndc80 complex (Petrovic et al., 2010).

1.2.2.2 KNL1

The largest single protein constituent of the KMN network, KNL1, binds directly to microtubules through its N terminus, but this interaction is not essential for the formation of load-bearing kinetochore-microtubule attachments, for which the Ndc80 complex is primarily responsible (Cheeseman et al., 2006; Espeut et al., 2012; Ghongane et al., 2014). Primarily, KNL1 is regarded as a scaffold or hub for the recruitment of other kinetochore proteins. Localization of most of the components of the Spindle Assembly Checkpoint to unattached kinetochores depends on KNL1, with the proteins Bub1, Bub3 and BubR1 interacting directly with KNL1, and Bub1, in turn, responsible (along with a distinct kinetochore

complex called RZZ) for recruitment of Mad1 and Mad2. KNL1 is also the site for localization of two phosphatases that play important roles in stabilizing kinetochore-microtubule attachments: PP1, which interacts directly with KNL1, and PP2A, whose interaction with KNL1 is mediated by BubR1 (Caldas and DeLuca, 2014).

1.2.2.3 The Ndc80 Complex

The four-protein Ndc80 complex is well characterized organizationally and is assembled from a pair of two-protein subcomplexes. Nearer to the inner kinetochore is a heterodimeric subcomplex formed by the proteins Spc24 and Spc25, which form a coiled coil along most of their length and two C-terminal globular domains through which they associate with the Nsl1 component of the adjacent Mis12 complex. (No Spc24 homolog has been confidently identified in *Drosophila*, though it has been suggested that a smaller, otherwise uncharacterized *Drosophila* protein could correspond to the Spc24 C-terminal globular domain (Schittenhelm et al., 2007).) More distant from the inner kinetochore are the proteins Nuf2 and Ndc80, which likewise form a heterodimer structured as a coiled coil along most of the proteins' length, with globular domains near their N termini through which both proteins associate with the microtubule lattice upon formation of kinetochore-microtubule attachments. Although their relative contributions have not yet been fully described (Cheerambathur and Desai, 2014), microtubule binding is generally understood to be mediated both by Calponin Homology domains found within the N-terminal

globular regions of Nuf2 and Ndc80 and by a short unstructured “tail” in the N-terminal region of Ndc80 (Cheeseman et al., 2006; Sundin et al., 2011).

The two coiled coils within the Ndc80 complex are organized in an end-to-end fashion and impart to the complex an overall “dumbbell” shape, wider at the ends and comparatively slender along the length of the complex (Foley and Kapoor, 2013). The overall complex measures approximately 50 nm in length – somewhat more when measured in isolation using electron microscopy (Wei et al., 2005), and somewhat less when measured by “K-SHREC” (see below) in an intact kinetochore and in its native orientation relative to the CENP-A-to-microtubule axis (Suzuki et al., 2014). The Ndc80 protein features a hinge or loop region that briefly interrupts the Ndc80/Nuf2 coiled coil structure, adds flexibility to the overall complex (DeLuca and Musacchio, 2012; Tooley and Stukenberg, 2011; Varma et al., 2012), and is involved in the conversion of lateral kinetochore-microtubule interactions to an “end-on” configuration (Shrestha and Draviam, 2013).

1.3 Kinetochore-Microtubule Attachments

1.3.1 Attachment Formation

The initial interaction between kinetochores and spindle microtubules is a lateral one, in which one member of a pair of sister kinetochores, or possibly both (Tanaka, 2010), associate(s) laterally or “side-on” with the lattice of a single microtubule emanating from one of the spindle poles. The laterally attached kinetochore is then rapidly transported poleward by kinetochore-associated

dynein (Yang et al., 2007), and shortly thereafter the lateral attachment is converted to the end-on configuration. In human cells, it appears that this conversion requires both the plus end-directed motor CENP-E (kinesin-7 family) and the microtubule-depolymerizing motor MCAK (kinesin-13 family) (Shrestha and Draviam, 2013). In any event, kinetochore attachment to the plus ends of spindle microtubules may or may not initially produce the attachment configuration necessary to support an equal partitioning of chromosomes at anaphase.

Because the sister chromatids (and their associated sister kinetochores) ordinarily face in opposite directions, spindle geometry and chromosome structure generally favor the attachment of sister kinetochores to microtubules that originate from opposite poles (Indjeian and Murray, 2007). That is the correct configuration to support proper chromosome segregation, and is referred to as the amphitelic or "bioriented" attachment state. Nonetheless, as attachments first become established in prometaphase, mono-oriented (monotelic) attachments – in which one kinetochore attaches to microtubules from one spindle pole while its sister kinetochore remains unattached – are also seen, as are two different kinds of aberrant attachments: (i) syntelic attachments, in which both members of a sister kinetochore pair attach to microtubules from the same spindle pole; and (ii) merotelic attachments, in which a single kinetochore attaches simultaneously to microtubules from both poles (Figure 1.2). Left uncorrected, any of the three non-bioriented attachment states can lead to chromosome missegregation and incorrect transmission of the cell's

genetic material, producing aneuploid daughter cells with unequal numbers of chromosomes. To avoid this fate, the cell requires a system for detecting, and then correcting, erroneous attachments between kinetochores and spindle microtubules.

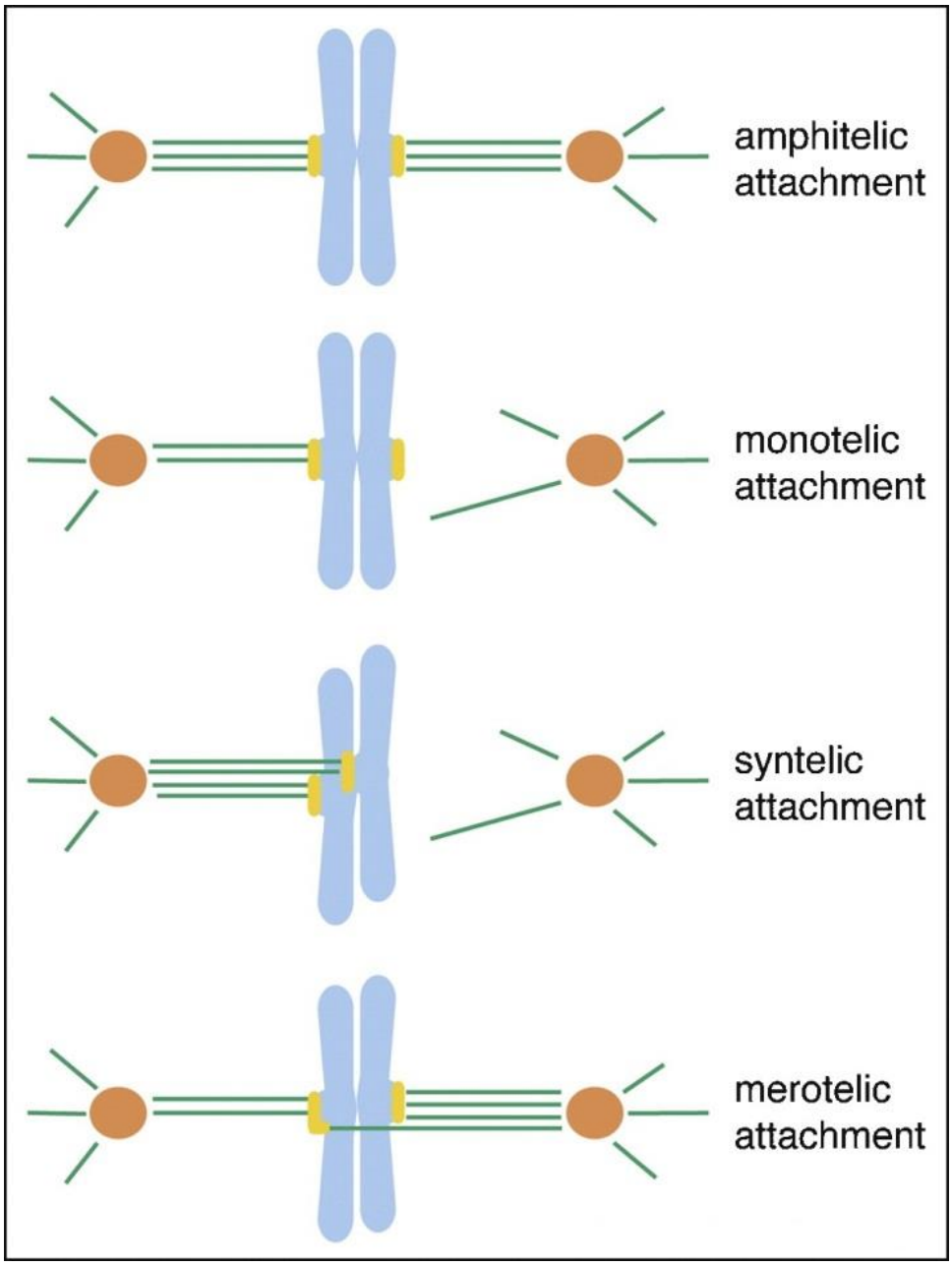

Figure 1.2: Kinetochore-microtubule attachment states. Amphitelic (bioriented) attachments are selectively stabilized, whereas the cell's Aurora B-based error correction system selectively destabilizes erroneous attachments to allow further attempts to achieve a bioriented attachment state. Reprinted from Kelly and Funabiki (2009), *Current Opinion in Cell Biology* 21(1):51-58, with permission from Elsevier.

1.3.2 The Aurora B Kinase and Error Correction

As previously noted (Section 1.2.2.3), kinetochore-microtubule binding is mediated, on the kinetochore side of the interaction, principally by the Ndc80 complex. Key components of the interaction include the basic N-terminal tail of Ndc80 and certain Lysine residues in the Calponin Homology domains of Ndc80 and Nuf2 (Santaguida and Musacchio, 2009) and, on the microtubule side of the interaction, an unstructured, acidic C-terminal tail (or “E-hook”) associated with each tubulin subunit – all of which suggests a significant electrostatic contribution to the binding affinity of the Ndc80 complex for spindle microtubules (Ciferri et al., 2008). (Structural data also shows that the Ndc80 CH domain forms a “toe” that occupies the hinge region between tubulin monomers, interacting simultaneously with the globular regions of adjacent α- and β-tubulin subunits and therefore sensitive to protofilament bending (Alushin et al., 2012; Alushin et al., 2010).) Consistent with this, the phosphorylation of Ndc80 complex components, by introducing additional negative charge and disrupting electrostatic interactions at the kinetochore-microtubule binding interface, has the effect of reducing kinetochore-microtubule binding affinity and destabilizing nascent attachments (DeLuca et al., 2011; Foley and Kapoor, 2013). Impairment of attachment stability in this fashion is linked to the presence of nine phosphorylation sites in the Ndc80 N-terminal tail (Zaytsev et al., 2014), all of which are substrates of the Aurora B kinase. Sites in KNL1 (and, in humans, the Mis12 complex component Dsn1) have also been identified as Aurora B targets (Welburn et al., 2010). Aurora B, accordingly, is a crucial participant in a regulatory process that

selectively destabilizes kinetochore-microtubule attachments involving phosphorylated outer kinetochore proteins (Hauf et al., 2003). The outer kinetochore phosphorylation signifies that the kinetochore is not experiencing physical tension, and the absence of tension signifies that the kinetochore is associated with a chromosome that is not bioriented on the spindle. This erroneous attachment must be released and corrected before mitosis can safely proceed.

Aurora B is a serine/threonine kinase, a population of which associates with three other proteins – INCENP, Borealin and Survivin – to form the Chromosomal Passenger Complex (CPC). CPC localization changes predictably over the course of mitotic progression, but in prometaphase and metaphase a CPC subcomplex, in which Borealin and Survivin interact stably with the N terminus of INCENP, targets the CPC to the inner centromere. There Aurora B, the enzymatic component of the complex, interacts with and is activated by the C terminus of INCENP. INCENP thus forms a scaffold that unites the targeting proteins Borealin and Survivin (both of which interact with phosphorylated histones within the centromeric chromatin) with Aurora B. An unstructured central region of INCENP bridges the chromatin-bound and kinase-bound regions (van der Horst and Lens, 2014) and, owing to that structural organization, it has been proposed that INCENP could serve as a flexible “dog leash” tethering the active kinase to an inner centromere anchor (Maresca and Salmon, 2010; Samejima et al., 2015; Santaguida and Musacchio, 2009). As a consequence of this combination of CPC localization and CPC organization, Aurora B is well

positioned to phosphorylate kinetochore substrates just when kinetochore-microtubule attachments are being formed and erroneous attachments must be recognized and corrected (Carmena et al., 2012; van der Waal et al., 2012).

1.3.3 The Spindle Assembly Checkpoint

The commencement of anaphase represents the moment when attachment errors become irrevocable and uncorrectable. Therefore, while the Aurora B-based error correction pathway is causing non-bioriented attachments to be destabilized and eliminated, the cell must also engage a system for delaying anaphase onset until no unattached kinetochores remain and all attachments have adopted the correct, bioriented configuration. This system, the Spindle Assembly Checkpoint (SAC), assembles at the kinetochore and functions by generating a diffusible Mitotic Checkpoint Complex (MCC) consisting of Mad2, BubR1, Bub3, and Cdc20.

Recruitment of the checkpoint machinery requires phosphorylation of KNL1, which generates a binding site for localization of Bub1 and Bub3. Bub 1 at the kinetochore is required for localization of BubR1 and Mad1, which then interact with the MCC component Mad2. In the cytoplasm the MCC incorporates its fourth subunit, Cdc20, and by preventing Cdc20 activity the MCC further prevents the activation of a ubiquitin ligase called the Anaphase Promoting Complex or Cyclosome, of which Cdc20 is a necessary cofactor. All of this has the ultimate effect of delaying the proteolytic degradation of two inhibitors of further mitotic progression, Cyclin B and Securin (Foley and Kapoor, 2013;

London and Biggins, 2014; Musacchio and Salmon, 2007). Clearly the Aurora B error correction pathway and the SAC are intimately related, with engagement of the SAC persisting throughout error correction and SAC inactivation occurring only after the last non-bioriented attachment has been corrected.

1.3.4 Attachment Stabilization: The Dual Role of Tension

A key attribute of the bioriented attachment configuration is that, as poleward forces are applied to a bioriented kinetochore pair from opposite spindle poles, tension is generated across the kinetochores and the centromeric chromatin. It is for that reason that the absence of tension acts as a signal to the kinetochore of chromosome mal-orientation and as a trigger for attachment destabilization and error correction. Conversely, application of tension has the effect of stabilizing attachments that are correctly configured (Akiyoshi et al., 2010; Tanaka, 2010). The insight that tension plays a role in stabilizing kinetochore-microtubule attachments is often associated with Bruce Nicklas (Nicklas and Koch, 1969), who observed that erroneously configured meiotic bivalents with both chromosomes attached to a single spindle pole could be prevented from “reorienting” to the correct attachment state by an artificial application of tension – *i.e.*, that tension served to stabilize the erroneous attachment configuration – whereas in unperturbed cells such incorrect orientations were readily corrected. Subsequently, a series of papers published in the 1990s, including (Gorbsky and Ricketts, 1993; McIntosh, 1991; Nicklas et al., 1995), established that spindle-based tension exerts its attachment-stabilizing (and anaphase-promoting) effect through a mechanism that involves

dephosphorylation of kinetochore proteins: a “mechanochemical linkage” (Li and Nicklas, 1995) uniting tension, kinetochore dephosphorylation, error correction and satisfaction of the Spindle Assembly Checkpoint. This mechanochemical framework is now understood to revolve around the phosphoregulation of kinetochore-microtubule attachment stability by Aurora B acting on KMN network substrates (Foley and Kapoor, 2013).

Recently it has come to be understood that tension can also regulate kinetochore-microtubule attachment stability directly, rather than indirectly through its effect on phosphorylation levels at the outer kinetochore. In an *in vitro* experimental system lacking Aurora B, Akiyoshi *et al.* applied increasing, physiologically relevant, levels of tension to a bead-bound kinetochore particle with an attached microtubule in a laser trap. They found that over a 1-5 piconewton force range, application of increasing force caused the kinetochore-microtubule attachment to become increasingly stable, as reflected in a greater mean lifetime for the attached state, before stability of the attachment began to decline in response to tension levels beyond that range (Akiyoshi et al., 2010). The application of tension in this system also decreased the microtubule catastrophe frequency and increased the rescue frequency, stabilizing the kinetochore-microtubule attachment by disfavoring microtubule disassembly at the binding interface. These results may stem from catch bond-like behavior (Akiyoshi et al., 2010; Sarangapani and Asbury, 2014; Umbreit and Davis, 2012), and at all events demonstrate the existence of a purely mechanical (as distinct from mechanochemical) role for tension in attachment stabilization. It is now

considered likely that tension promotes attachment stability both directly and indirectly, in proportions that are yet to be determined (Foley and Kapoor, 2013). These issues are explored in greater depth in Chapter Four, and a proposed combinatorial model in which the two manifestations of tension could generate several different levels of overall attachment stability is presented in Figure 4.5.

1.3.5 Intrakinetochore Stretch and the Spatial Positioning of Kinetochore Elements

If tension were to elongate the kinetochore, and increase the distance between the outer kinetochore and the centromeric chromatin housing the CPC, this would point toward a potential explanation for the connection between tension and the phosphorylation state of the outer kinetochore. And kinetochore elongation under tension at metaphase has in fact been shown to occur (Maresca and Salmon, 2009; Uchida et al., 2009). When a bioriented chromosome is pulled in opposite directions by spindle-based tension, two distinct kinds of stretching are produced: (i) centromere stretch, which increases the distance between sister kinetochores, and (ii) intrakinetochore stretch, which increases the distance between the inner kinetochore and the outer kinetochore. Both phenomena have been indirectly visualized by application of a super-resolution microscopy approach known as Kinetochore Speckle High-Resolution Colocalization microscopy (K-SHREC) or Delta analysis (Varma et al., 2013; Wan et al., 2009).

In this technique, each member of a pair of sister kinetochores is labeled with two different fluorescent markers, one fluorophore labeling each end of a

spatial interval, or a single structure, whose length is to be measured. At this point each labeled site (for example, a GFP-labeled inner kinetochore and an RFP-labeled outer kinetochore) is represented by two distinct fluorescent spots when the cell is imaged in the appropriate channel of the fluorescence microscope; in this example, there would be two spots of GFP fluorescence marking the inner kinetochores of the sister pair and two spots of RFP fluorescence marking the outer kinetochores of the same sister pair. Interkinetochore distance (or "K-K distance") for a given kinetochore pair is calculated as the distance between the centroids of the two inner kinetochore fluorescent spots associated with that pair; and *centromere stretch* is then calculated as the difference between the mean K-K distance for a group of pairs measured in the absence of tension (*e.g.*, following microtubule depolymerization) and the mean K-K distance for a group of pairs measured in an intact spindle at metaphase. Intrakinetochore distance, or "Delta," is calculated by subtracting the K-K distance for a sister pair from the outer-kinetochore-to-outer-kinetochore distance for that pair and then dividing the result by two. The difference between the mean Delta for a group of bioriented metaphase pairs and the mean Delta for a group of tensionless pairs represents intrakinetochore stretch.

Using K-SHREC, intrakinetochore stretch was definitively shown to occur in *Drosophila* cells in response to spindle-based tension. Further, treatment of the cells with 20 nM Taxol produced an experimental condition in which bioriented chromosomes exhibited normal levels of intrakinetochore stretch but

only sharply reduced levels of centromere stretch. Experimentation under this condition showed that centromere stretch and intrakinetochore stretch are distinct and separable phenomena and that intrakinetochore stretch, rather than centromere stretch, correlates with the outer kinetochore dephosphorylation and SAC inactivation that are associated with chromosome biorientation.

These results mesh seamlessly with a previously proposed mechanistic explanation for the mechanochemical linkage among tension, outer kinetochore phosphorylation and the stabilization of kinetochore-microtubule attachments. This explanatory framework, known as the “spatial positioning” or “spatial separation” model, posits that with biorientation the outer kinetochore, and the Ndc80 complex in particular, is pulled away from centromeric Aurora B, and that the increased spatial separation between the two makes a significant contribution to the establishment of stable attachments. The 40 nm increase in the distance between CENP-A/Cid and the Ndc80 complex under metaphase tension in *Drosophila* due to intrakinetochore stretch (Maresca and Salmon, 2009) is consistent with a role for spatial positioning in promoting stabilization of bioriented attachments (Maresca and Salmon, 2010).

This spatial positioning model first arose (Tanaka et al., 2002) from an observation that, in budding yeast, activity of the Ipl1 kinase (the budding yeast homolog of *Drosophila* and vertebrate Aurora B) is necessary for the “reorientation” (correction) of erroneous, monopolar linkages between kinetochores and Spindle Pole Bodies; once tension is introduced, however, erroneous linkages no longer turn over and reorientation/error correction no

longer occurs. Thus Ipl1 activity leads to phosphorylation of kinetochore substrates and their phosphorylation leads to unstable attachments, but under tension the result is quite different: Ipl1 activity may or may not persist, but kinetochores become dephosphorylated and the erroneous attachments become stable. This could happen either because tension "turns off" the kinase, perhaps by "unraveling" the centromeric chromatin, or because tension simply pulls the kinetochores away from active, unimpaired Ipl1. In the latter case, attachment stability will depend on the relative spatial positions of Ipl1 and its kinetochore substrates. Tanaka *et al*. deemed the two alternative mechanisms "equally possible," but shortly thereafter two other groups, working with human (Andrews et al., 2004) and PtK1 cells (Cimini et al., 2006), specifically embraced the physical separation/spatial positioning alternative.

The alternative mechanisms were directly tested several years later (Liu et al., 2009) with a FRET-based phosphorylation sensor capable of being targeted to different chromosomal locations in HeLa cells. When targeted to the inner centromere, where Aurora B is found, the sensor was seen to be phosphorylated irrespective of the presence or absence of tension (constitutive phosphorylation), demonstrating that tension does not exert its effect by inactivating or inhibiting the kinase. In contrast, when targeted to a kinetochore the sensor was seen to be phosphorylated in the absence of tension but dephosphorylated when tension was present. The authors concluded, therefore, that tension affects attachment stability by increasing the distance between centromeric Aurora B and its outer kinetochore substrates. Consistent with this, attachment instability is at its most

severe when the most spatially distant Aurora B phosphorylation sites among the KMN proteins are phosphorylated, and is more modest when Aurora B phosphorylation extends only to sites physically closer to the kinase (Welburn et al., 2010).

Lastly, just as a spatial positioning model predicts that, even in the presence of tension, kinetochore extension is required if stable attachments are to form, it also implies that an inordinately long extension (kinetochore "hyper-stretch") would prevent re-phosphorylation of Aurora B substrates and generate "hyper-stable" erroneous attachments that would likely go uncorrected. A comparable phenomenon was demonstrated by DeLuca *et al.*, who induced persistent dephosphorylation of Ndc80 in mammalian cells by mutating all of the Aurora B target sites within the N-terminal tail, after which they observed chromosome congression and alignment defects (DeLuca et al., 2011). They attributed those defects to hyper-stable attachments, and that explanation was borne out by the cells' inefficiency in releasing and correcting syntelic attachments in a monastrol washout experiment. Accordingly, if the spatial positioning model is valid, constraints on extendibility should exist to prevent kinetochore hyper-stretch and the formation of hyper-stable, uncorrectable erroneous attachments.

In fact, such a system of constraints has recently been described in HeLa cells by Suzuki *et al*., who showed that several CCAN components (CENP-C, CENP-T and the CENP-H/I complex) combine to keep overall intrakinetochore stretch at a bioriented attachment (measured as the change in CENP-A-to-

Spc24/Spc25 distance; elongation of the Ndc80 complex was not observed) well short of the hyperextension that, they also showed, leads to substantially reduced levels of Ndc80 phosphorylation in late prometaphase (Suzuki et al., 2014).

The constraint mechanism revealed in their work turns out to be somewhat complex. So long as the system was maximally constrained, with CENP-C, CENP-T and CENP-H all present, the linkage between CENP-A and the Ndc80 complex exhibited only limited compliance, or stretchability. Even for a bioriented kinetochore pair, beyond a certain level of tension Delta (intrakinetochore distance) became invariant, and thereafter tension only made K-K separation greater, increasing interkinetochore stretch without producing a corresponding increase of intrakinetochore stretch.

Turning next to a less-than-fully constrained system, in a series of protein depletion experiments Suzuki *et al*. observed instances of hyper-intrakinetochore stretch, which consisted of two distinct components. First, depletion of CENP-C (or, somewhat more dramatically, co-depletion of CENP-C and CENP-H/I) substantially increased CCAN compliance, such that intrakinetochore stretch now increased along with interkinetochore stretch: With CENP-C and CENP-H both gone, total CENP-A to Spc24/Spc25 distance in late prometaphase was ~90 nm, as compared with ~30 nm in controls – and ~25 nm of that length increase was attributable to CENP-T stretch. CENP-T depletion likewise increased CCAN compliance and allowed greater freedom for CENP-C to stretch, but in that case the effect was somewhat less pronounced.

A second component of hyper-stretch was also identified: In the absence of any one of CENP-C, CENP-H or CENP-T, the underlying centromeric chromatin itself became “de-compacted,” with the fluorescent signal representing GFP-labeled CENP-A visibly elongated along the kinetochore-kinetochore axis in 10%-20% of all cells, and the CENP-A to CENP-T (C terminus) length increasing from 15 nm to 52 nm for bioriented attachments in late prometaphase. It thus appears that these cells have evolved a way to suppress two different sources of hyper-stretch, further underscoring the importance of controlling the spatial positioning, and thus the phosphorylation state, of microtubule-binding proteins at the outer kinetochore.

CHAPTER 2

ELONGATION OF THE *DROSOPHILA* KINETOCHORE PROTEIN CENP-C IS REQUIRED FOR THE FORMATION OF STABLE KINETOCHORE-MICROTUBULE ATTACHMENTS

2.1 Introduction

During mitosis, all pairs of sister chromatids must become bioriented on the spindle, with the two sisters attached through their kinetochores to microtubules originating at opposite spindle poles, in order for the genetic material to be partitioned equally in anaphase. Failure of one or more chromosomes to become bioriented before anaphase onset can lead to chromosome missegregation and the production of aneuploid daughter cells, with potentially ominous results for the progeny of those cells and ultimately for the organism as a whole (Gordon et al., 2012; Orr et al., 2015; Ricke et al., 2011). The formation, stabilization and maintenance of a bioriented kinetochore-microtubule attachment is typically preceded by an error correction process, in which the same molecular binding partners form a non-bioriented attachment but then dissociate from one another, the attachment having been identified as incorrect, destabilized and eliminated (Lampson and Cheeseman, 2011). No such incorrect attachments can be allowed to persist. As the cell proceeds toward anaphase, bioriented kinetochore-microtubule attachments must become stable whereas all incorrect attachments must be released in order to facilitate correction of the error.

The different fates of bioriented and non-bioriented attachments are attributable to the presence or absence of tension across the

kinetochore/centromere region. The bioriented attachment state generates tension, and it has long been understood that tension stabilizes kinetochore-microtubule attachments (Nicklas and Ward, 1994). At least in part, the stabilizing role of tension occurs through a regulatory pathway that involves the phosphorylation state of outer kinetochore substrates of the Aurora B kinase (Foley and Kapoor, 2013). Aurora B is a component of the four-protein Chromosomal Passenger Complex, which localizes to the inner centromere throughout the period of attachment formation, error correction and attachment stabilization before migrating to the spindle midzone in anaphase.

Phosphorylation of Aurora B target sites within the N-terminal region of Ndc80 reduces the affinity with which Ndc80 binds to microtubules (Cheeseman et al., 2006; DeLuca et al., 2006). Phosphorylation of those target sites is high at non-bioriented attachments that experience little or no tension, and then decreases once biorientation is achieved and the attachment comes under tension (Ciferri et al., 2008; DeLuca et al., 2011). Meanwhile, the spindle forces that give rise to tension also stretch the kinetochore, increasing the distance between the inner centromere and the kinetochore-microtubule binding interface (Maresca and Salmon, 2009; Uchida et al., 2009). Taken together, these factors have given rise to a model holding that tension affects the proximity of centromeric Aurora B to the microtubule binding site and that this proximity, through its effect on outer kinetochore phosphorylation, determines the stability of kinetochore-microtubule attachments (Lampson and Cheeseman, 2011; Welburn et al., 2010). This regulatory framework is referred to as the spatial

positioning or spatial separation model. And while the role that CPC/Aurora B proximity to the attachment site plays in this system remains in dispute, it is, at all events, well accepted that the formation of stable attachments coincides with a tension-dependent movement of the kinetochore-microtubule binding interface away from the inner region of the kinetochore.

In *Drosophila* specifically, the outer kinetochore is ~40 nm more distant from the inner kinetochore at bioriented attachments during metaphase than it is at unattached kinetochores that are not under tension, and this displacement is attributable to the intrakinetochore stretch produced by transmission of force from dynamic microtubules to the outer region of the kinetochore (Maresca and Salmon, 2009). Intrakinetochore stretch increases the distance between outer kinetochore substrates of Aurora B and the kinase activity centered at the inner centromere. According to the spatial positioning model it is intrakinetochore stretch, and the repositioning of the outer kinetochore relative to the Aurora B activity at the inner centromere, that are responsible (and required) for enhancing the stability of correct, bioriented kinetochore-microtubule attachments (Cheeseman, 2014; Lampson and Cheeseman, 2011; Maresca and Salmon, 2010).

In order to investigate the role of spatial positioning in attachment stabilization we have focused on the *Drosophila* kinetochore protein CENP-C, a long and largely disordered protein that links the inner and the outer kinetochore. We hypothesized that the disordered region of CENP-C stretches under tension at metaphase, and that CENP-C stretch contributes to the repositioning of outer

kinetochore attachment factors and the stabilization of bioriented attachments. We employed super-resolution microscopy to verify and quantify CENP-C stretch and then made truncated mutant versions of CENP-C with varying lengths and capacities for stretch. We now show that *Drosophila* CENP-C does elongate when it experiences tension on the spindle, and that shortening CENP-C, or eliminating its ability to stretch in response to tension, leads to an impairment of the cell's ability to form stable kinetochore-microtubule attachments. To the extent that CENP-C stretch is then restored, the cell also recovers the capacity to form stable attachments. Our results demonstrate that, as predicted by the spatial positioning model, the cell's capacity to form stable attachments is progressively reduced with reduction of the distance between the centromere and the kinetochore-microtubule contact site. Conversely, the cell's capacity to form stable attachments is progressively enhanced with incremental increases in the distance from the centromere to the attachment site.

2.2 Results

2.2.1 A disordered central region of *Drosophila* CENP-C undergoes intrakinetochore stretch at metaphase

In *Drosophila*, the kinetochore protein CENP-C is 1411 amino acids in length and represents the only known link between the inner and outer regions of the kinetochore (Orr et al., 2010; Schleiffer et al., 2012), binding to chromatin at the centromere through its C terminus and to the outer kinetochore protein Nnf1, a component of the Mis12 complex, through its N terminus. The C terminal portion of CENP-C also interacts with Cal1, a protein essential for CENP-C

localization to the kinetochore and whose own localization to the kinetochore is likewise CENP-C dependent (Schittenhelm et al., 2010), and this portion of CENP-C may also have important phosphatase-recruitment (Lipinszki et al., 2015) and RNA-binding functions (Rosic et al., 2014). Between CENP-C's outer kinetochore-binding N-terminal domain (expected to lie within the first 71 amino acid residues in human cells (Screpanti et al., 2011)) and its DNA-binding C-terminal region (somewhere among residues 1000 through 1200 (Heeger et al., 2005)) lies a lengthy region of computationally predicted structural disorder. Owing to the predicted disorder characterizing a substantial segment of CENP-C, we hypothesized that this protein could act as a mediator of intrakinetochore stretch in *Drosophila*, and that, if so, experimentally reducing or eliminating CENP-C elongation could afford a means of investigating the role of spatial positioning in stabilizing kinetochore-microtubule attachments and facilitating the cell's progression from metaphase to anaphase.

To evaluate whether CENP-C elongates when the kinetochore is subjected to spindle forces at metaphase in attached, bioriented chromosomes, we employed a version of the protein bearing a TagRFP-T fluorophore at its N terminus and EGFP at the C terminus. In mitotic *Drosophila* S2 (Schneider) cells expressing this recombinant CENP-C under the control of its native promoter, the recombinant protein localized normally, as evidenced by the appearance at centromeres of roughly circular spots in both the red and green channels of the fluorescence microscope. The recombinant CENP-C also localized properly in cells from which endogenous CENP-C had been depleted by RNAi, and rescued

the kinetochore null phenotype that is associated with CENP-C depletion in *Drosophila* (Orr and Sunkel, 2011).

We then employed Delta analysis (K-SHREC) as described in (Wan et al., 2009) and (Varma et al., 2013) to obtain measurements, on a chromosome by chromosome basis, of the average distance between the CENP-C N and C termini for the CENP-C molecules of the kinetochore pairs associated with each chromosome. This measurement technique relies on software that maps, for the two members of a pair of sister kinetochores, both the centroid of the fluorescent spot representing the N-terminal TagRFP fluorophore and the centroid of the (simultaneously imaged) fluorescent spot representing the C-terminal EGFP fluorophore. The TagRFP centroid-to-centroid distance and the EGFP centroid-to-centroid distance for that pair having been determined, the shorter distance (green-to-green) is subtracted from the longer (red-to-red) and the result is then halved. In this manner an average intrakinetochore green-to-red distance is obtained for each kinetochore pair, representing the average length of the combined population of fluorescently labeled CENP-C molecules localized to the two sister kinetochores of that pair.

Using this technique, we measured a mean end-to-end length of 24.4 ± 1.4 nm (Mean ± SEM; N = 111 kinetochore pairs) for the fluorescently labeled full length CENP-C at metaphase. A statistically equivalent length was also measured in cells from which the endogenous CENP-C had been depleted by RNAi, indicating that length measurements for the recombinant CENP-C were not affected by the presence of the endogenous protein. In contrast, a mean

end-to-end CENP-C length of 3.4 ± 2.0 nm (Mean ± SEM; N = 103 pairs) was measured in colchicine-treated cells, in which spindle microtubules had depolymerized and all kinetochores were therefore unattached. These results demonstrate that, when attached to microtubules, *Drosophila* CENP-C undergoes a ~20-25-nm elongation under the spindle forces present at metaphase (Figure 2.1).

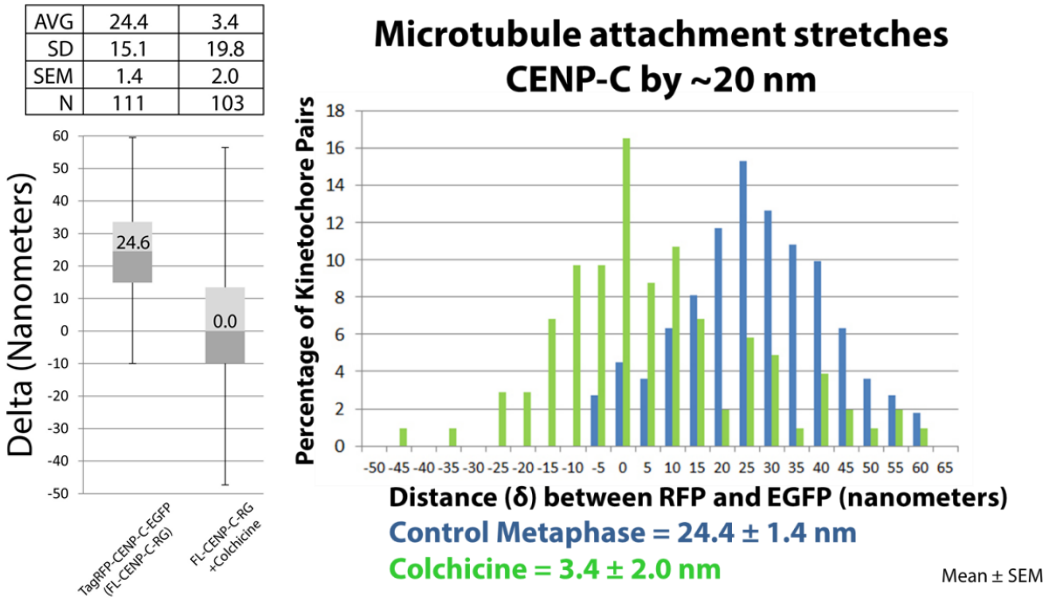

Figure 2.1: CENP-C stretches by ~20-25 nm at metaphase. We found by K-SHREC that full length CENP-C (here designated "FL-CENP-C-RG" to reflect RFP and GFP labeling) is ~24 nm longer when attached to microtubules at metaphase than it is in colchicine-treated cells, in which all kinetochores are unattached. N = 111 kinetochore pairs (untreated metaphase cells), 103 kinetochore pairs (colchicine treated cells).

2.2.2 Absence of CENP-C stretch is associated with kinetochore-microtubule attachment instability

To examine the effect of eliminating CENP-C elongation we sought to truncate the protein by removing a structurally disordered segment that, we suspected, would likely be extendible when subjected to a pulling force within the spindle. CENP-C has been broadly characterized as an extreme example of disorder among kinetochore proteins (Westermann and Schleiffer, 2013), hinting at the feasibility of our proposed strategy. We consulted a protein disorder prediction program, DISOPRED3 (Jones and Cozzetto, 2015; Ward et al., 2004), and found that, consistent with the foregoing characterization, upon analysis of the amino acid sequence of *Drosophila* CENP-C the program generated an intrinsic disorder profile/plot starkly portraying an extensive region of (predicted) disorder encompassing nearly the entire length of the protein – 1272 amino acid residues out of a total of 1411 (Figure 2.2). Such disordered protein regions not only have the capacity to behave in a spring-like fashion (van der Lee et al., 2014) but are also known to function as flexible linkers for the specific purpose of regulating the length between globular domains (Tompa, 2002). Indeed we noted that there are short regions at either end of CENP-C that were computationally predicted to adopt a stably folded structure. These would presumably represent CENP-C's C-terminal DNA-binding domain and the N-terminal domain that interacts with the outer kinetochore Mis12 complex.

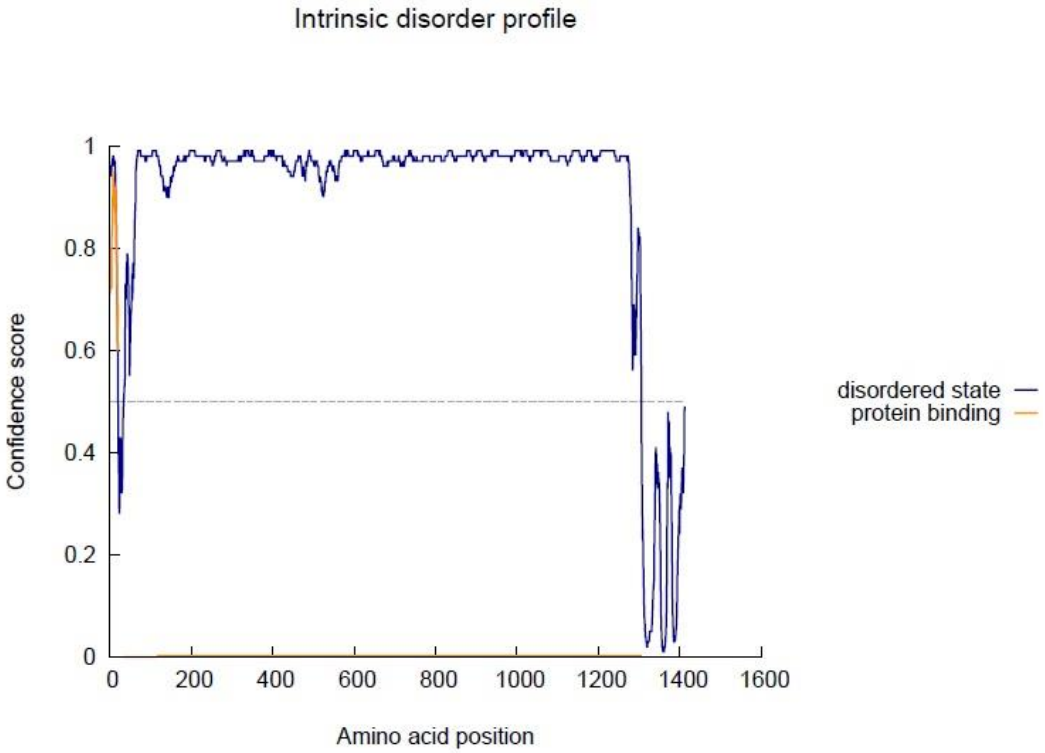

Figure 2.2: Much of the CENP-C molecule is predicted to exhibit structural disorder. By computational prediction, CENP-C is characterized by structural disorder throughout most of its length. The intrinsic disorder profile shown here was generated by the DISOPRED3 disorder prediction program (Jones and Cozzetto, 2015; Ward et al., 2004), which was accessed through the PSIPRED "workbench" server at University College London (Buchan et al., 2013). The region of predicted disorder lies between CENP-C's N-terminal (outer kinetochore-binding) and C-terminal (DNA-binding) regions.

We generated our truncated mutant CENP-C (here denoted “Minimal CENP-C”) by removing length from within the region that we thought likely to exhibit the extendibility, and ideally to fulfill the sort of length-regulating role, associated with an intrinsically disordered protein. We expected that by removing a considerable part of that region we would substantially reduce, or even wholly eliminate, CENP-C’s ability to stretch under tension. The Minimal CENP-C mutant consists of amino acids 1-82 at the N terminus and 990-1411 at the C terminus, and we have verified both its constitutive localization to the kinetochore and its functionality in recruiting the KMN network (Figure 2.3). Consistent with expectations, we found that Minimal CENP-C does not elongate at metaphase to any measurable extent. The metaphase length of Minimal CENP-C, as measured using Delta analysis, is effectively zero (-3.5 ± 1.3 nm (Mean ± SEM); N = 111 kinetochore pairs) (Figure 2.4). We therefore conclude that Minimal CENP-C represents a non-stretchable derivative of the native, stretchable protein, and that the kinetochore-microtubule binding interface is ~25 nm closer to the CENP-C C terminus in Minimal CENP-C cells than in wild type cells (Figure 2.5).

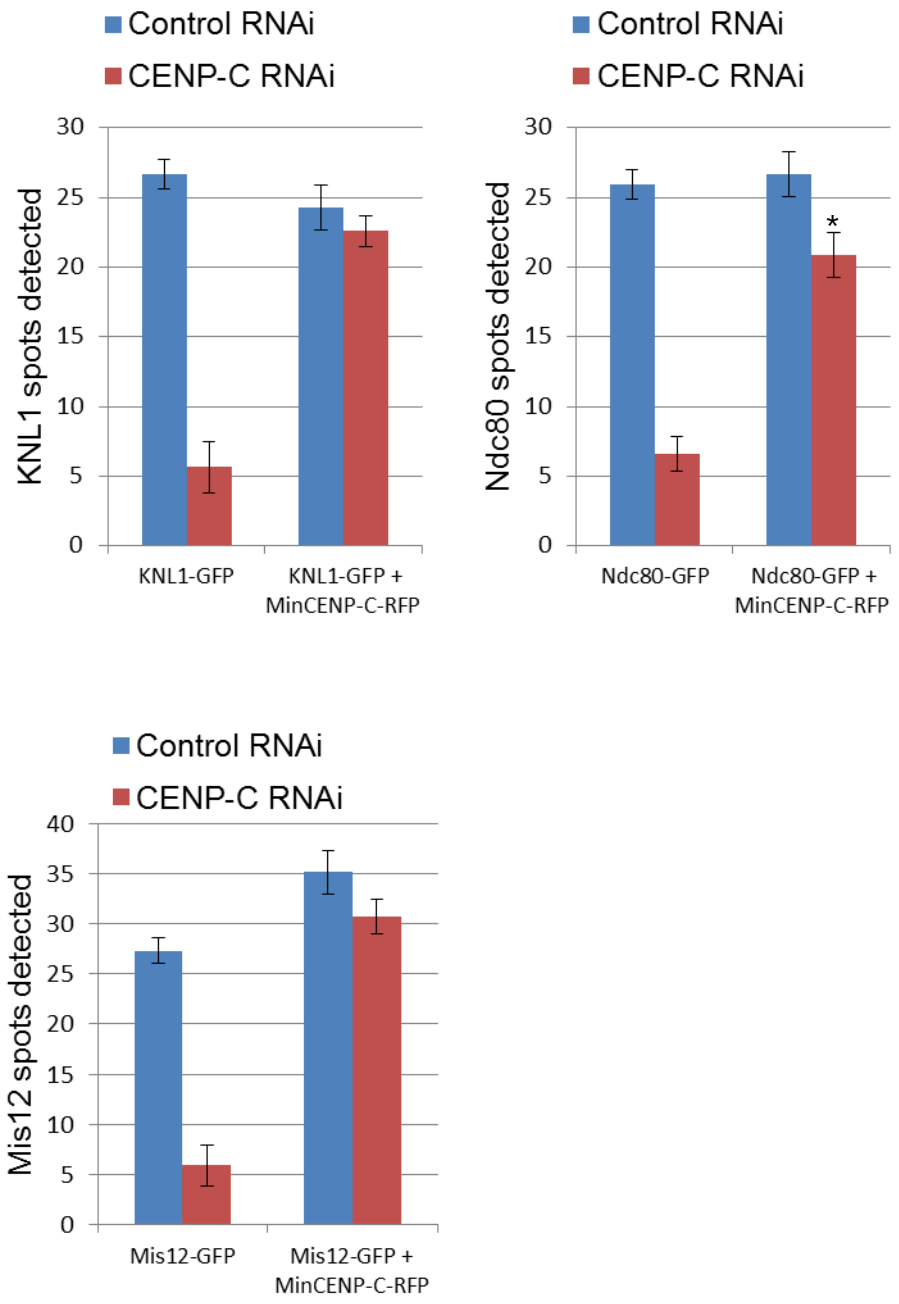

Figure 2.3: KMN proteins localize to the kinetochore in Minimal CENP-C cells. We employed an automated counting feature of the MetaMorph image analysis software to count GFP "spots" representing kinetochore-localized KNL1, Mis12 or Ndc80. Minimal CENP-C was somewhat less efficient at recruiting Ndc80 than at recruiting KNL1 or Mis12. There were 26.7 ± 1.6 localized Ndc80 spots in the Minimal CENP-C controls, compared with 20.9 ± 1.6 localized Ndc80 spots in the Minimal CENP-C cells depleted of endogenous CENP-C. Error bars show SEM. N ≥ 23 cells per condition, for cell lines without Minimal CENP-C; N ≥ 27 cells per condition for the Minimal CENP-C cell lines. * indicates $P < .05$.

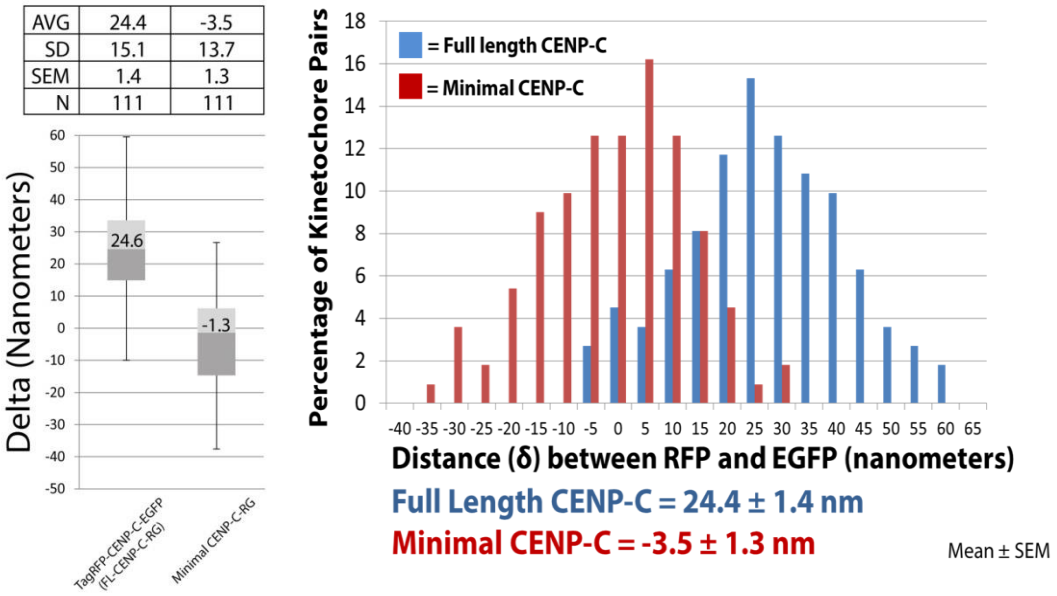

Figure 2.4: Minimal CENP-C does not stretch. We found by K-SHREC that the kinetochores in Minimal CENP-C cells, after RNAi depletion of the full length protein, do not undergo stretch at metaphase. Minimal CENP-C length at metaphase is comparable, instead, to the length of the full length protein measured in the absence of microtubule attachments. N = 111 kinetochore pairs for each set of measurements.

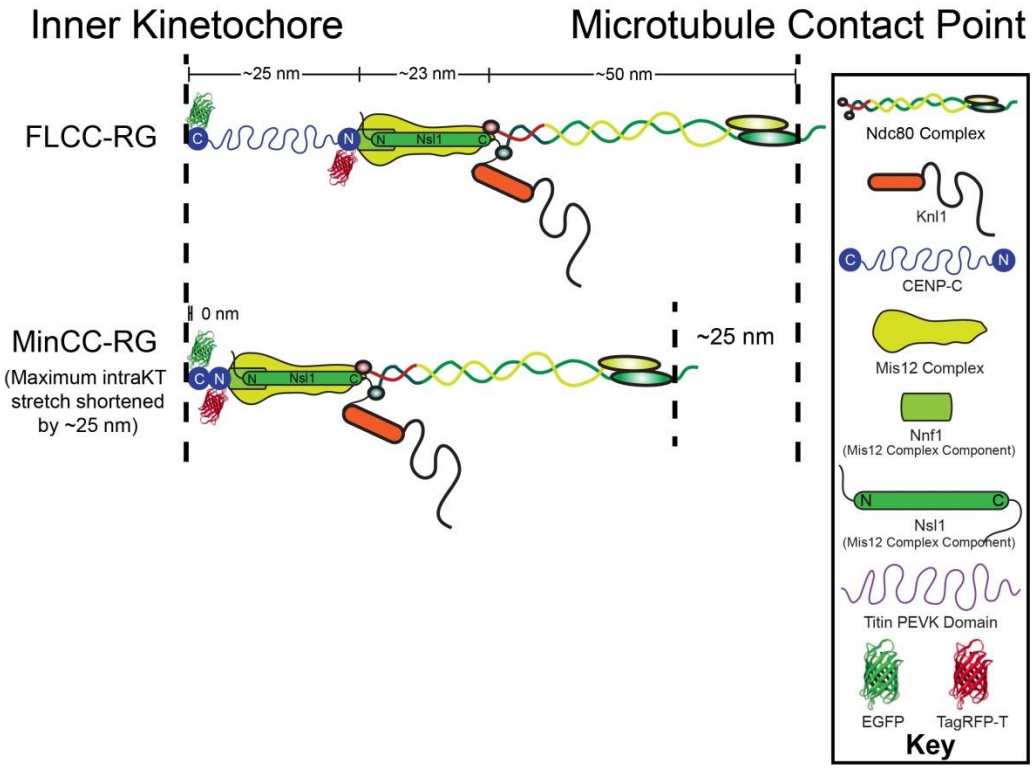

Figure 2.5: The kinetochore-microtubule binding site is closer to the inner kinetochore in Minimal CENP-C cells. The metaphase distance from the inner kinetochore (CENP-C C terminus) to the microtubule binding site is ~25 nm shorter in cells expressing only Minimal CENP-C than in cells expressing the full length protein.

Live cells expressing only the Minimal version of CENP-C were seen to exhibit, with varying degrees of severity, a distinct chromosome alignment deficiency and an associated failure to form stable kinetochore-microtubule attachments. In cells exhibiting this phenotype, chromosomes (marked by their labeled kinetochores) either formed a partial or fragmentary metaphase plate from which individual chromosomes repeatedly fell away, or else failed entirely to form a coherent metaphase plate but, rather, fell away from the midzone in large numbers and moved poleward and then anti-poleward along the spindle periphery. In the most severely affected cells, numerous individual chromosomes appeared to move cyclically between polar and equatorial regions of the spindle, seemingly without their kinetochores ever having formed stable end-on attachments to spindle microtubules. Examples are shown by kymograph in Figure 2.6.

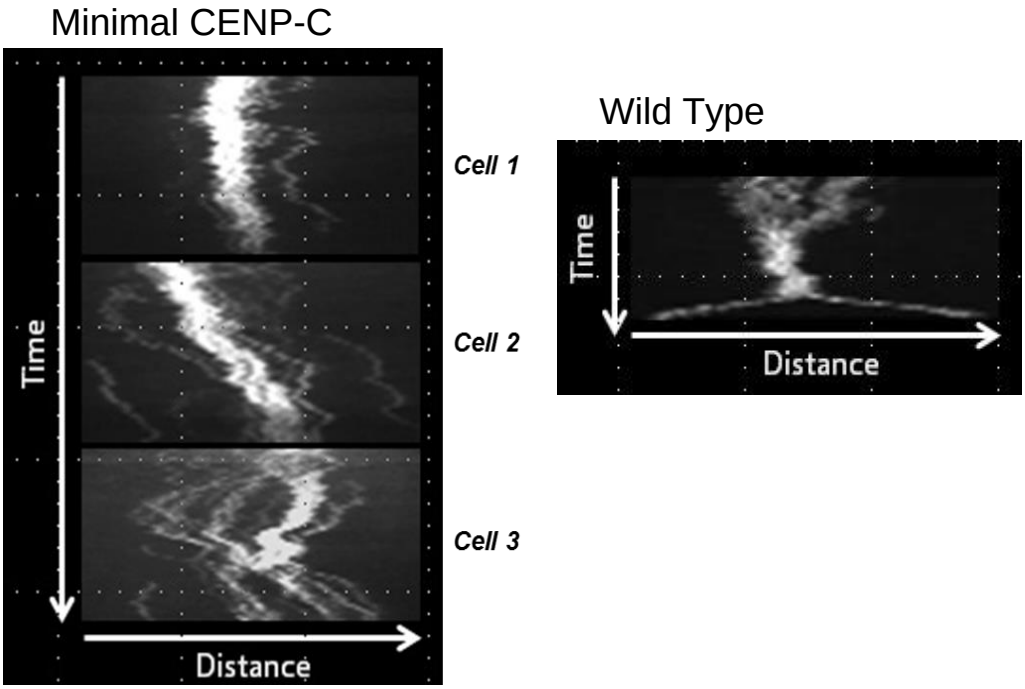

Figure 2.6: Minimal CENP-C cells exhibit a distinctive "hurricane"-like behavior in mitosis. Disorganized movements of fluorescently labeled Minimal CENP-C kinetochores are shown at left, in three different cells exhibiting, with different degrees of severity, what we have referred to as the "Hurricane" phenotype. Normal kinetochore behavior during the transition from metaphase to anaphase is shown at right.

In fixed Minimal CENP-C cells examined by immunofluorescence, we counted substantial numbers of misaligned kinetochore pairs after depletion of the endogenous protein. In this assay, we classified each cell as presenting either a Metaphase chromosome alignment (no misaligned kinetochore pairs), a relatively moderate degree of chromosome misalignment (1-4 misaligned pairs) or a more severe degree of misalignment (≥ 5 misaligned pairs). In Minimal CENP-C cells in which the endogenous CENP-C was also present, 84 ± 4 percent of all cells examined had all of their chromosomes aligned in the Metaphase configuration (Mean ± SD; three experiments, N = 150 cells), whereas 69.3 ± 1.2 percent of Minimal CENP-C cells from which the endogenous protein was depleted by RNAi exhibited either the moderate (32.7 ± 6.4%) or the more severe (36.6 ± 6.1%) levels of chromosome misalignment (Mean ± SD; three experiments, N = 153) (Figure 2.7A).

A relative lack of stable end-on kinetochore-microtubule attachments in the Minimal CENP-C cells was further reflected in reduced levels of tubulin adjacent to kinetochores following a ten-minute exposure of the cells to cold (4ºC) (Rieder, 1981): In cold-treated CENP-C-depleted Minimal CENP-C cells, tubulin fluorescence intensity adjacent to the kinetochores was 69.5 ± 4 percent of the corresponding value measured in non-depleted Minimal CENP-C control cells (Mean ± SEM; three experiments, N = 396 control cells and N = 345 CENP-C RNAi cells) (Figure 2.7B).

A. Chromosome Alignment **B.** Cold Stability

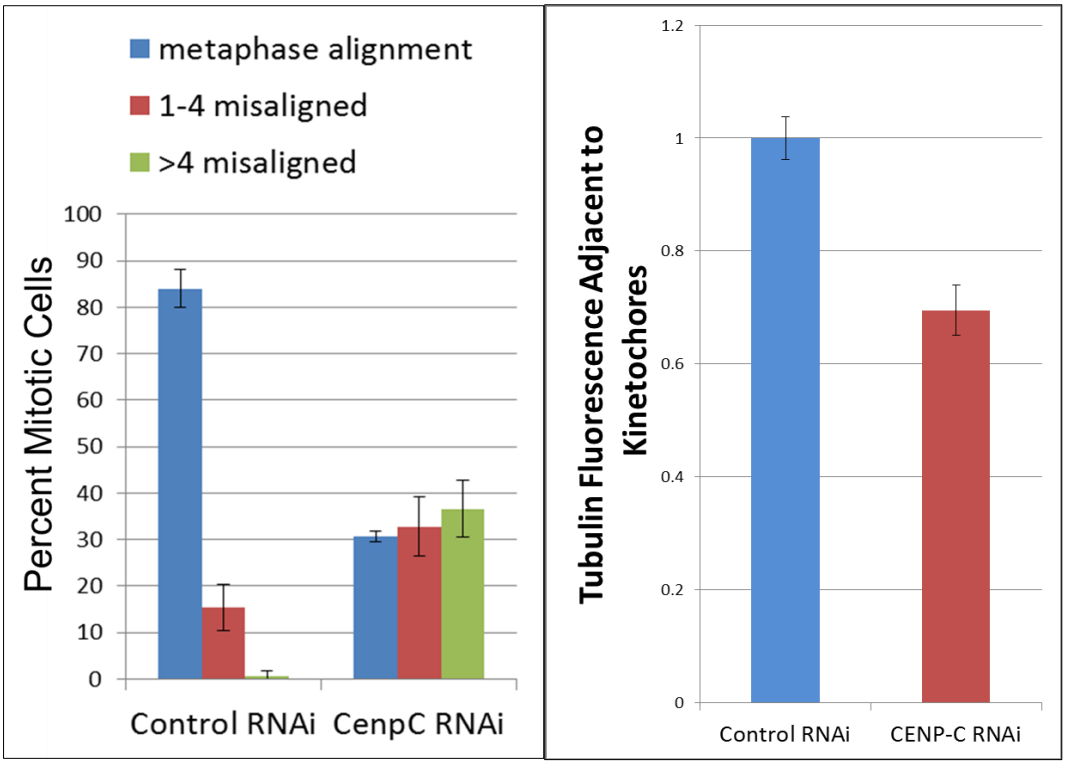

Figure 2.7: Chromosome alignment and k-fiber cold stability are impaired in Minimal CENP-C cells. *(A)* After depletion of endogenous CENP-C, at least one misaligned chromosome pair is seen in 69.3 percent of mitotic Minimal CENP-C cells. The corresponding value is only 16 percent in the control condition. Data reflect three independent experiments with N = 50 cells per condition in each experiment. Error bars = Standard Deviation. *(B)* Cold stability of kinetochore microtubules, an indicator of attachment stability, is severely compromised in Minimal CENP-C cells. Data reflect three independent experiments, with N = 395 kinetochore pairs (control), N = 342 kinetochore pairs (CENP-C RNAi). Control values are normalized to 1.0. Error bars = SEM.

In addition, kinetochores in the cold-treated Minimal CENP-C cells often appeared to associate laterally with robust microtubule bundles that did not resemble kinetochore microtubules assembled into kinetochore fibers. These cells had also formed unusually dense microtubule foci, near each spindle pole, within which kinetochores appeared to have become embedded far from their expected location in a metaphase-arrested cell. We conclude, accordingly, that S2 cells expressing only the non-stretchable Minimal version of CENP-C form less-stable kinetochore-microtubule attachments than wild type cells.

2.2.3 Chromosome misalignment in cells with shortened CENP-C is Aurora B dependent

The spatial positioning model of kinetochore-microtubule attachment stabilization posits that attachment instability is caused by proximity of the attachment site to active Aurora B kinase at the centromere. The model therefore predicts that the chromosome misalignment seen in our Minimal CENP-C cells, to the extent that it reflects kinetochore-microtubule attachment instability, should be ameliorated by Aurora B inhibition. To test this prediction we treated CENP-C-depleted Minimal CENP-C cells with the Aurora B inhibitor Binucleine 2 (Smurnyy et al., 2010; Ye et al., 2015) for one hour at a concentration of 1 μM, or with an equal volume of DMSO as a control, before fixing the cells and examining chromosome alignment. Proper chromosome alignment was restored in part by treatment with this inhibitor, after which only 42 ± 6 percent of the Aurora B-inhibited cells exhibited either a moderate (26% ± 4%) or severe (16% ± 8.7%) chromosome misalignment phenotype (Mean ± SD;

three experiments, N = 150 cells) (Figure 2.8). This result is consistent with a key prediction of the spatial positioning model and supports the conclusion that kinetochore-microtubule attachment instability in the Minimal CENP-C cells is associated with Aurora B kinase activity.

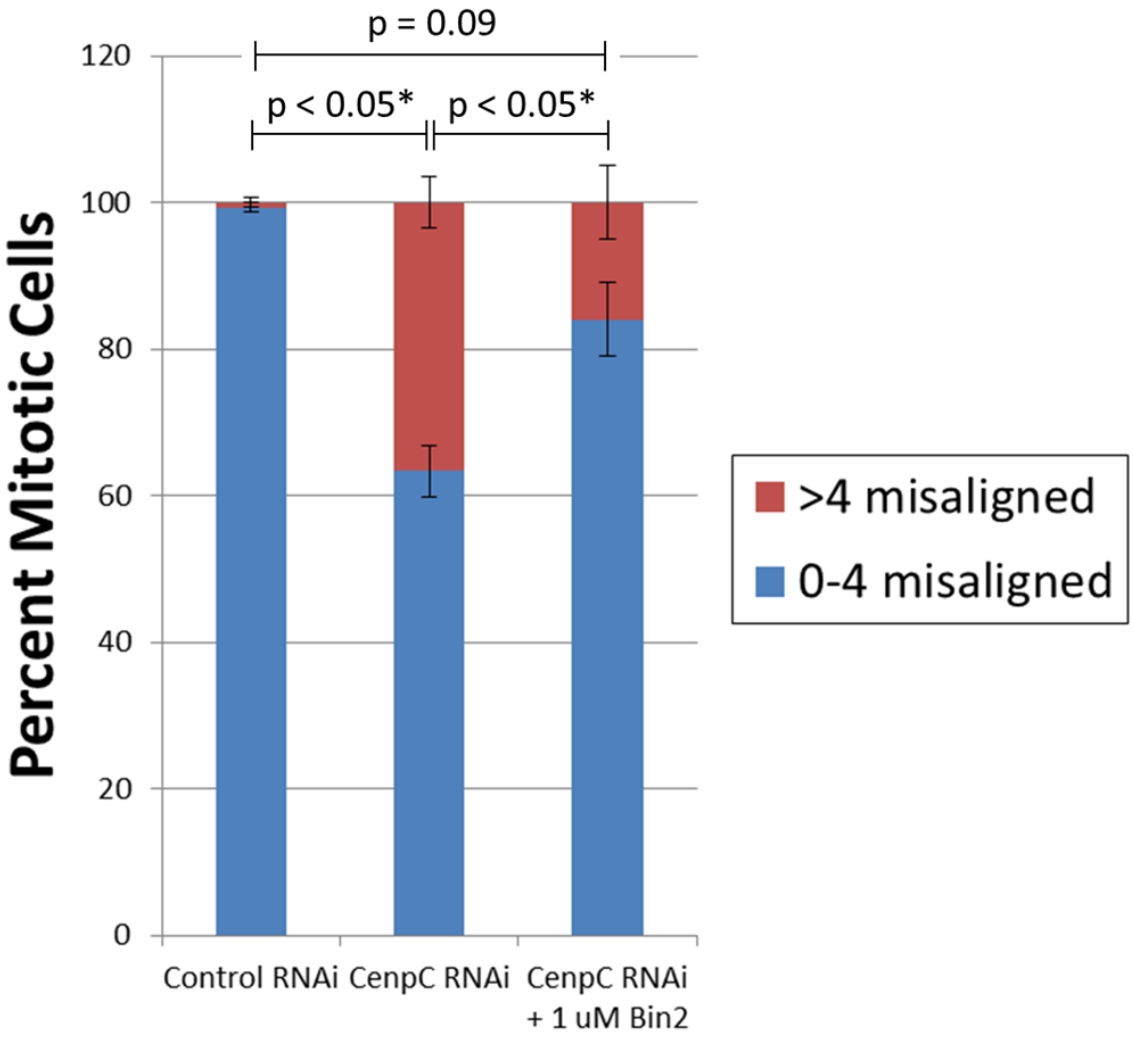

Figure 2.8: The Minimal CENP-C chromosome alignment defect is partially rescued by the Aurora B-specific inhibitor Binucleine 2. Treatment with 1 μM Binucleine 2 for one hour reduced the percentage of Minimal CENP-C cells with five or more misaligned kinetochore pairs, in the CENP-C RNAi condition, from 36.6 ± 6.1 percent to 16 ± 8.7 percent. Data reflect three independent experiments, N = 50 cells per condition in each experiment. Error bars = Standard Deviation.

2.2.4 Further shortening of the kinetochore leads to higher levels of chromosome misalignment and attachment instability

We reasoned that if outer kinetochore distance from centromeric Aurora B regulates the stability of kinetochore-microtubule attachments, further shortening of the kinetochore should exacerbate the attachment instability phenotype seen in the Minimal CENP-C cells. To test this, we produced a cell line in which the DNA-binding C-terminal region of CENP-C was fused to the Mis12 complex protein Nsl1. We refer to the fused protein as "Nsl1-CENP-C." Nsl1 is the Mis12 complex component that associates directly with the Ndc80 complex (in addition to KNL1) (Petrovic et al., 2010), and thus, irrespective of any other feature of Mis12 complex organization, maximal shortening of the distance from the CENP-C C terminus to the kinetochore-microtubule binding interface should be achieved by fusing the CENP-C C terminus directly to Nsl1, bypassing Nnf1 and Mis12 and nullifying whatever length those proteins would otherwise contribute to the kinetochore.

We found by the Delta method that in Nsl1-CENP-C cells, the distance between the GFP fluorophore at the CENP-C C terminus and the RFP fluorophore at the Nsl1 N terminus is 22.9 ± 2.1 nm (Mean ± SEM; N = 105 kinetochore pairs) (Figure 2.9A). In assessing the significance of this result it is necessary to bear in mind (Chapter One, Section 1.2.2.1) that Nsl1 recruits the other components of the outer kinetochore to its C terminus, which, in our Nsl1-CENP-C fusion protein, lies immediately adjacent to the DNA binding region of CENP-C. Thus the Nsl1 portion of the Nsl1-CENP-C protein lies wholly outside

of the inner-to-outer kinetochore linkage pathway, leaving only the CENP-C C terminus to contribute length to the kinetochore – a contribution that, per the Minimal CENP-C length measurement reported above (Section 2.2.2), is effectively nil. In short, Nsl1-CENP-C is 23 nm long but adds no length at all to the kinetochore.

The 23 nm length of the Nsl1-CENP-C protein is nonetheless a very important finding. It means that at metaphase the kinetochore-microtubule binding interface is ~50 nm closer to the centromeric Aurora B activity in Nsl1-CENP-C cells than in wild type cells: ~25 nm of CENP-C stretch has been eliminated and ~25 nm of Nsl1 length has been removed from the linkage pathway (Figure 2.9B). Likewise, at metaphase the kinetochore-microtubule binding interface is ~25 nm closer to centromeric Aurora B activity in Nsl1-CENP-C cells than in Minimal CENP-C cells, again reflecting the removal of Nsl1 from the linkage pathway. Knowledge of those distances greatly enhances our understanding of the attachment stability data as it relates to the validity of the spatial positioning hypothesis. In addition, knowing that the Nsl1-CENP-C protein is 23 nm long gives us a baseline for determining how much length will have been added when, in a rescue experiment described below, we insert a stretchable peptide linker between the Nsl1 and CENP-C components of the protein. Finally, it is interesting to note that our measurement very closely approximates the length of the entire Mis12 complex (~22 nm) as measured in human cells (Petrovic et al., 2010), lending support to the view (Petrovic et al.,

2014; Petrovic et al., 2010) that Nsl1 is so oriented as to span the entire length of the human Mis12 complex.

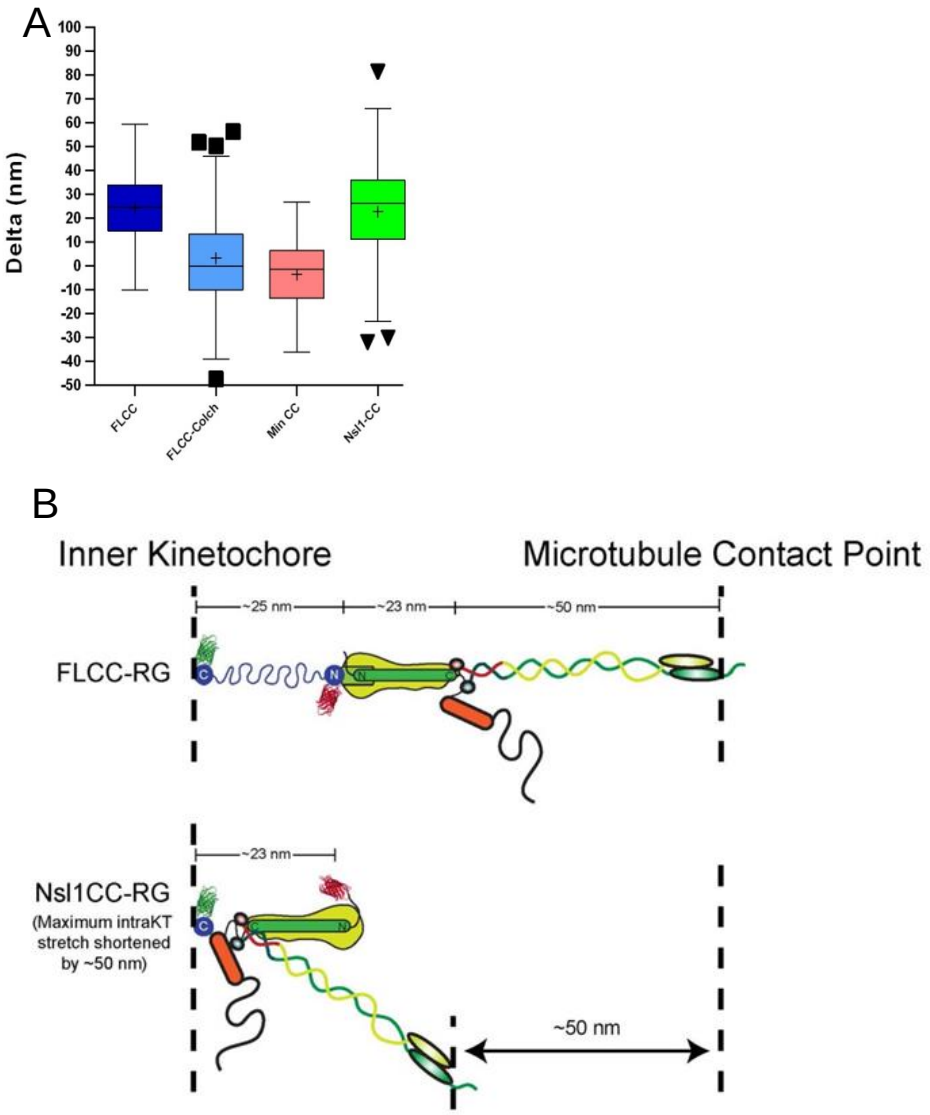

Figure 2.9: Nsl1-CENP-C kinetochores are ~50 nm shorter than wild type kinetochores. *(A)* Length of the Nsl1-CENP-C protein, compared with Minimal CENP-C, full length CENP-C, and full length CENP-C in the absence of kinetochore-microtubule attachments. For Nsl1-CENP-C, Delta = 22.9 ± 2.1 nm (Mean ± SEM; N = 105 kinetochore pairs; mean is marked by the cross). *(B)* At metaphase, the microtubule binding interface is ~50 nm closer to the centromeric chromatin in Nsl1-CENP-C cells than in cells with full length CENP-C. The CENP-C stretch (~25 nm) has been lost, and the Mis12 complex (~23 nm) falls outside of the inner-to-outer kinetochore linkage pathway.

In any event, the removal of 23 nm of kinetochore length from Minimal CENP-C to make Nsl1-CENP-C is indeed reflected phenotypically. Nsl1-CENP-C localized correctly, and the Nsl1 portion of the protein recruited the microtubule-binding kinetochore protein Nuf2 (an Ndc80 complex component) to the kinetochore constitutively (Figure 2.10). But moving the microtubule binding site ~25 nm closer to the centromere in this cell line further compromised both chromosome alignment and k-fiber cold stability (Figures 2.11A and 2.11B). In the Nsl1-CENP-C cell line, 70 ± 5.3 percent of the cells had more than four misaligned chromosomes after depletion of the endogenous CENP-C (Mean ± SD; three experiments, N = 150 cells), compared with only 3.3 ± 1.15 percent exhibiting misalignment of that degree among control Nsl1-CENP-C cells (Mean ± SD; three experiments, N = 150 cells). With respect to the cold stability of kinetochore fibers, after ten minutes of exposure to cold, the amount of tubulin remaining adjacent to metaphase kinetochores in CENP-C-depleted Nsl1-CENP-C cells was only 46.7 ± 2.6 percent of the corresponding amount measured in control Nsl1-CENP-C cells with the endogenous CENP-C present (Mean ± SEM; three experiments, N = 279 control cells and N = 300 CENP-C RNAi cells); as previously noted, k-fiber persistence was considerably greater (69.5% of control level) in cold-treated Minimal CENP-C cells.

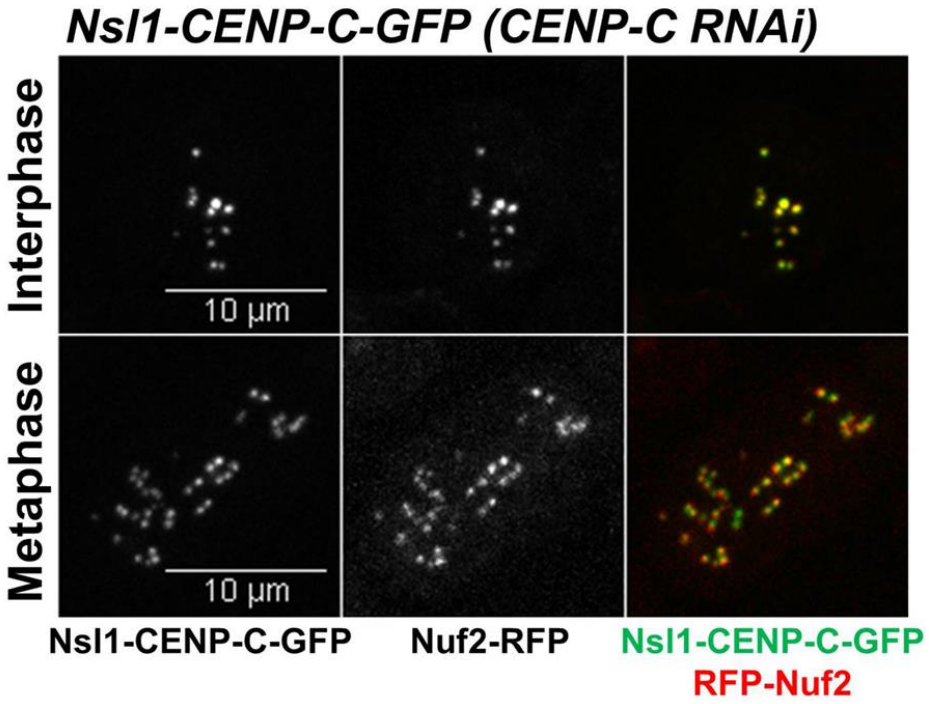

Figure 2.10: Nsl1-CENP-C recruits Nuf2 to the kinetochore. These images show RFP-labeled Nuf2 (an Ndc80 complex component) at the kinetochore in live Nsl1-CENP-C-GFP cells, both during interphase and in mitosis. The Ndc80 complex interacts directly with Nsl1, and Nsl1 is now fused to the CENP-C C terminus. The CENP-C C terminus localizes constitutively to centromeric chromatin.

A. Chromosome Alignment

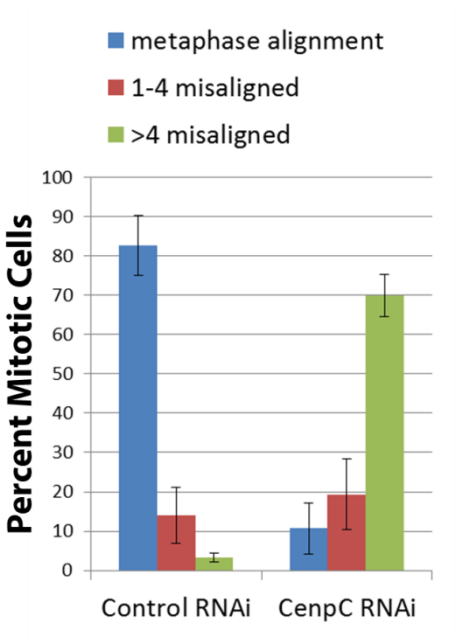

B. Cold Stability

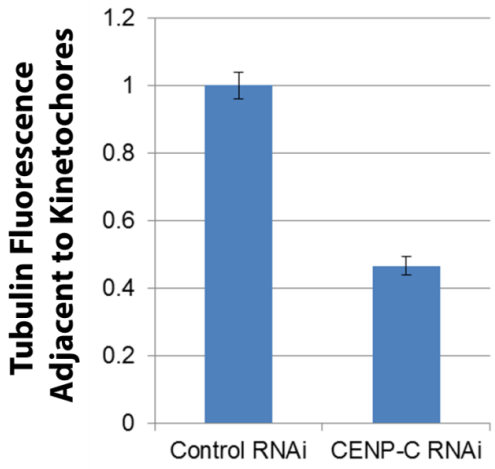

Figure 2.11: Nsl1-CENP-C cells exhibit severe defects in chromosome alignment and attachment stability. (*A)* After depletion of endogenous CENP-C, at least one misaligned chromosome pair is seen in 89.3 percent ± 6.4 percent of mitotic Nsl1-CENP-C cells. The corresponding value is only 17.3 percent ± 7.6 percent in the control condition. Data reflect three independent experiments with N = 50 cells per condition in each experiment. Error bars = Standard Deviation. *(B)* Cold stability of kinetochore microtubules is significantly compromised in Nsl1-CENP-C cells, to a greater extent than in Minimal CENP-C cells. Tubulin fluorescence intensity adjacent to the kinetochores for the CENP-C-depleted Nsl1-CENP-C cells, after a ten-minute cold treatment, was only 46.7 percent ± 2.6 percent of the intensity seen in cold-treated controls. Data reflect three independent experiments, with N = 279 kinetochore pairs (Control RNAi), N = 300 kinetochore pairs (CENP-C RNAi). Control values are normalized to 1.0. Error bars = SEM.

As with the Minimal CENP-C cells, the chromosome misalignment phenotype seen in the Nsl1-CENP-C cells was found to be Aurora B dependent. Chemical inhibition of Aurora B activity by a one-hour treatment with Binucleine 2 yielded a partial rescue of the phenotype, eliminating much of the disparity between the Nsl1-CENP-C and Minimal CENP-C cells with regard to chromosome misalignment (Figure 2.12). Treatment with a 1 μM concentration of the inhibitor left only 55.3 ± 6.1 percent of Nsl1-CENP-C cells with more than four misaligned chromosomes (Mean ± SD; three experiments, N = 150 cells) and treatment with 5 μM inhibitor further reduced that figure to 44 ± 10.5 percent (Mean ± SD; three experiments, N = 150 cells). By way of comparison (Section 2.2.2), among (non-Binucleine-treated) Minimal CENP-C cells only 36.6% had more than four misaligned kinetochore pairs in the CENP-C-depleted condition.

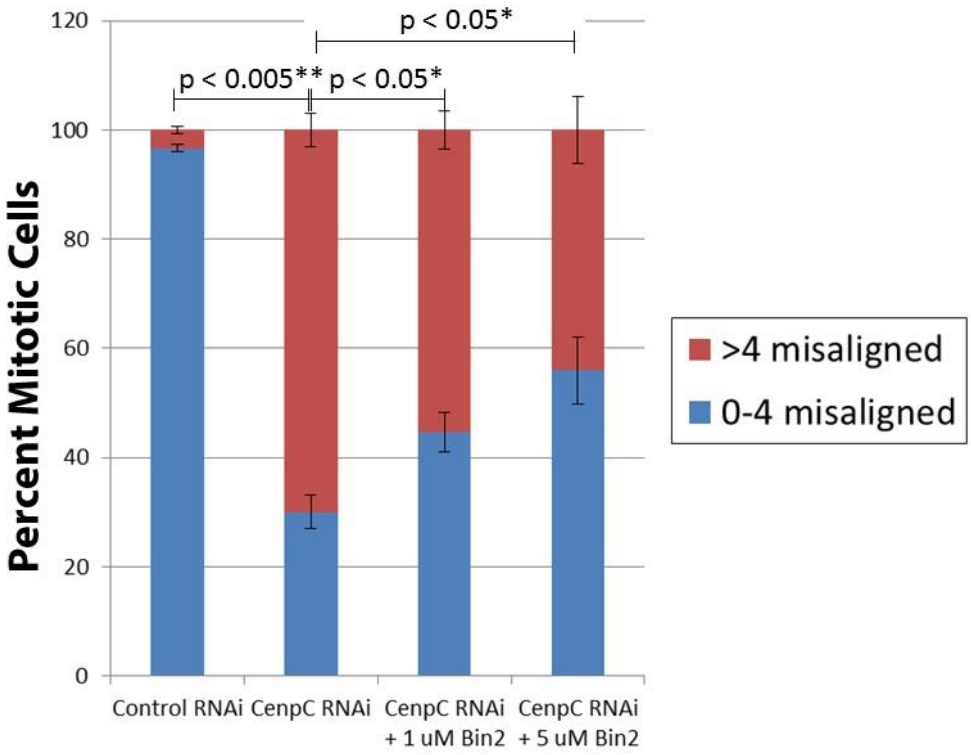

Figure 2.12: The Nsl1-CENP-C alignment defect is partially rescued by Aurora B inhibition. Treatment with 1 μM Binucleine 2 for one hour reduced the percentage of Nsl1-CENP-C cells with five or more misaligned kinetochore pairs, in the CENP-C RNAi condition, from 70 ± 5.3 percent to 55.3 ± 6.1 percent. Raising the concentration of inhibitor to 5 μM further lowered the percentage of Nsl1-CENP-C cells with five or more misaligned pairs to 44 ± 10.5 percent (Mean ± SD), a level comparable to that seen in (untreated) Minimal CENP-C cells. Data for each condition reflect three independent experiments, with N = 50 cells per condition in each experiment.

The foregoing results demonstrate a worsening of both chromosome alignment and k-fiber cold stability as the microtubule binding interface was brought another 23 nm closer to the inner centromere. And among live Nsl1-CENP-C cells that exhibited chaotic kinetochore movements suggestive of attachment instability, the phenotype was generally comparable to the most severe forms of that behavior seen in the Minimal CENP-C cells. Collectively these results support the hypothesis that kinetochore-microtubule attachment stability is increasingly compromised, in an Aurora B-dependent manner, as the inner-to-outer kinetochore distance is progressively reduced in S2 cells.

A definitive understanding of the role of Aurora B inhibition in this context is somewhat elusive, however, because there is evidence in the literature indicating that centromere Aurora B level is not wholly independent of kinetochore attachment state. At least in certain human cell lines, centromere Aurora B levels are higher at misaligned chromosomes and lower at bioriented chromosomes, possibly to supplement spatial position-based regulation by ensuring that bioriented attachments are not counterproductively destabilized (Salimian et al., 2011). Aurora B enrichment at erroneous attachments depends, moreover, on the activity of Aurora B itself (and on the activity of a second kinase, Plk1). Aurora B inhibition could therefore be operating on two different levels in our experiment, by reducing the phosphorylation of outer kinetochore substrates in our CENP-C truncation mutants and possibly also reducing the centromere Aurora B levels ordinarily found in association with erroneous kinetochore-microtubule attachments.

We examined the level of active, phosphorylated Aurora B at the inner centromere in control and CENP-C-depleted Nsl1-CENP-C cells. In cells expressing GFP-labeled Nsl1-CENP-C we determined the centromere phospho-Aurora B levels by immunofluorescence, calculating the ratio of phospho-Aurora B fluorescence to DAPI signal for a single region within each centromere. The results of these experiments were not conclusive. In two of the experiments we found a significantly higher level of centromere phospho-Aurora B in the CENP-C-depleted cells than in controls, but in a third experiment we found the levels to be essentially indistinguishable. Overall, normalized background-corrected phospho-Aurora B fluorescence in the CENP-C-depleted cells was 21% ± 3.5% higher than in controls (Mean ± SEM; three experiments, N > 300 centromeres per condition) (Figure 2.13). The results are consistent with the feedback mechanism proposed by Salimian *et al.* whereby centromere Aurora B both regulates (via spatial positioning), and is also regulated by, kinetochore attachment state (Salimian et al., 2011). Experimental inhibition of Aurora B would presumably impact both prongs of this regulatory scheme. In any case, however, we have amply demonstrated that the attachment instability seen in our CENP-C truncation mutants depends on Aurora B activity.

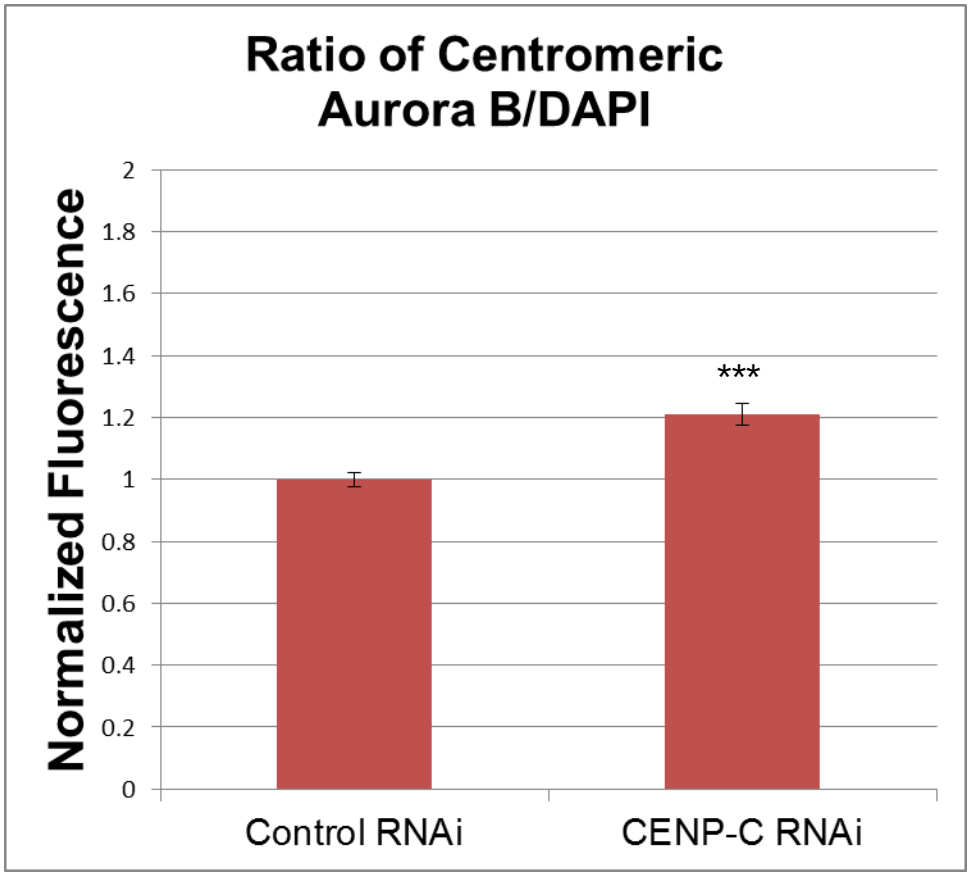

Figure 2.13: Nsl1-CENP-C cells have elevated Aurora B levels at the inner centromere. Although results varied considerably among the three experiments, we found centromere phospho-Aurora B levels to be 21 percent ± 3.5 percent higher in CENP-C-depleted Nsl1-CENP-C cells than in controls. Mean ± SEM; three experiments, N = 327 centromeres (Control RNAi), 307 centromeres (CENP-C RNAi). *** indicates $P < .005$.

2.2.5 Preliminary data suggests a likelihood of increased outer kinetochore phosphorylation in Nsl1-CENP-C cells

Assuredly the very strongest prediction of the spatial positioning model, as it pertains to our strategy of curtailing intrakinetochore stretch, is that our truncated CENP-C mutants should exhibit higher levels of outer kinetochore phosphorylation than cells expressing full length CENP-C. This prediction, for technical reasons, we have largely been unable to test. We have attempted an immunofluorescence experiment with our Nsl1-CENP-C cells, using an antibody against human KNL1 phosphorylated at Serine 60, but the antibody does not appear to react strongly with *Drosophila* KNL1, and only dim and indistinct signal has been produced. In order to obtain quantifiable fluorescence intensity data we have tried modifying our standard immunofluorescence protocol to incorporate a brief (30-60 second) detergent treatment before fixation, but this has typically either had no discernible effect or else has been too destructive. We were able to obtain (encouraging) data from a single experiment, the results of which are shown in Figure 2.14.

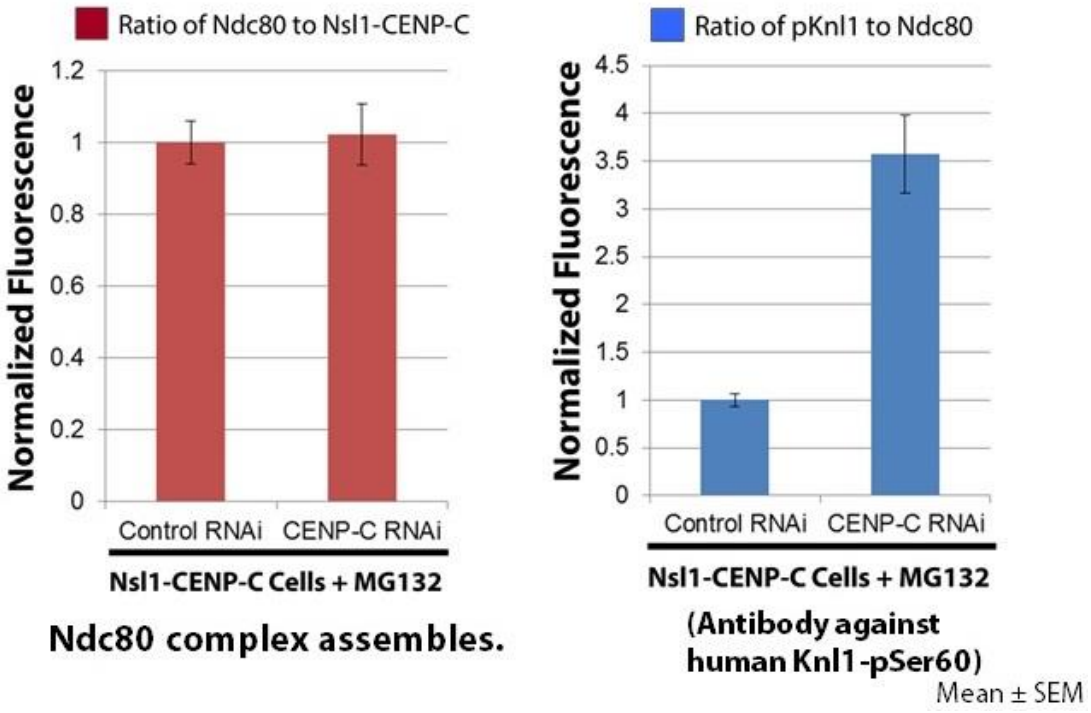

Figure 2.14: KNL1 is more phosphorylated at Nsl1-CENP-C kinetochores. We have obtained results from one experiment examining outer kinetochore phosphorylation. We found that the outer kinetochore was being successfully recruited to the Nsl1-CENP-C (ratio of Ndc80/Nsl1-CENP-C fluorescence was at wild type levels), and that KNL1 phosphorylation (as measured by the ratio of pKNL1 to Ndc80 fluorescence) was substantially increased in CENP-C-depleted Nsl1-CENP-C cells.

2.2.6 The chromosome alignment defect seen in shortened-kinetochore cells is partially rescued by addition of a stretchable segment of a non-kinetochore protein

In light of the attachment instability observed among our CENP-C truncation mutants, we asked whether normal attachments would form if we were to add physical length back to CENP-C, by inserting a non-functional peptide linker wholly unrelated to CENP-C. In a series of length restoration experiments we inserted a widely used flexible linker, $(GGGGS)_8$ or "2xFL2," and then a widely used α-helical linker, $A(EAAAK)_{32}A$ or "4xHL3" (Arai et al., 2001; Lu and Feng, 2008), into Minimal CENP-C. We also generated a series of cell lines containing versions of Minimal CENP-C augmented with $(GGGGS)_{16}$, $A(EAAAK)_{64}A$, $A(EAAAK)_{96}A$ and $A(EAAAK)_{128}A$ (respectively "4xFL2," "8xHL3," "12xHL3" and "16xHL3"). We took this approach further by inserting into Minimal CENP-C a 740-amino acid segment of Nup153, a natively unfolded "FG Nucleoporin" with an abundance of highly unstructured "FG-repeat" domains (Fahrenkrog and Aebi, 2003; Lim et al., 2006). In the more promising of these experiments, we measured a length of 7.5 ± 0.8 nm for Minimal CENP-C augmented by $A(EAAAK)_{64}A$/8xHL3 (Mean ± SEM; N = 110 kinetochore pairs) and a length of 10.1 ± 1.1 nm for the construct containing an intrinsically disordered region of Nup153 (Mean ± SEM; N = 143 kinetochore pairs). The additional length generated by inserting these various peptides is shown in Figure 2.15. We were unfortunately not able to replicate the initially promising result that we had obtained with the 8xHL3 insertion, and despite considerable effort we were never able to generate a stable cell line expressing a recombinant

form of CENP-C that incorporated the Nup153 insert. In no case could we restore the ~20-25 nm of metaphase elongation that we had measured for native, full length CENP-C at the outset of our study. In principle, however, under a large enough pulling force several of the linkers that we tested might have been expected to elongate by even more than 20 nm.

AVG	24.4	-3.5	7.5	1.8	1.6	10.1
SD	15.1	13.7	8.8	10.3	9.6	13.6
SEM	1.4	1.3	0.8	0.9	0.9	1.1
N	111	111	110	139	125	143

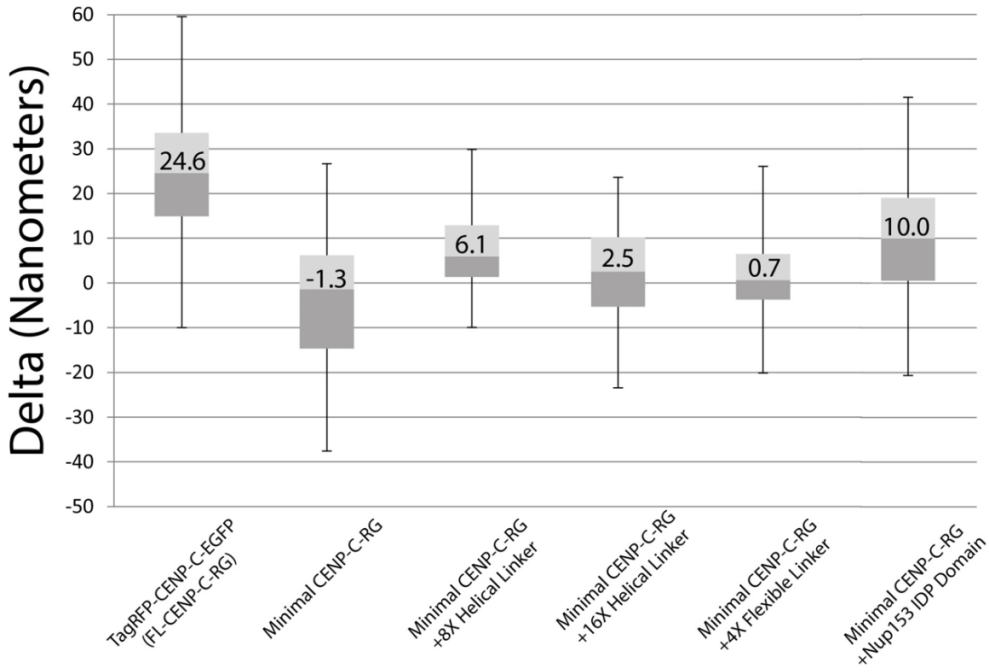

Figure 2.15: Modest Minimal CENP-C length increases are seen with the insertion of either of two different peptide linkers. The plot shows lengths measured by K-SHREC for the full length and Minimal versions of CENP-C (two left columns) and for Minimal CENP-C variants containing (i) the 8xHL3 helical linker, (ii) the 16xHL3 helical linker, (iii) the 4xFL2 flexible linker, and (iv) an intrinsically disordered domain from the Nucleoporin Nup153.

Upon reflection, our linker insertion efforts were instructive and prompted us to reevaluate the force-extension behavior of an intrinsically disordered, flexible peptide linker like the stretchable middle region of CENP-C. Such linkers are often characterized as entropic springs, in which the force required to extend the disordered peptide region by a particular increment of length varies with the loss of conformational entropy that the stretch will produce. Subjected to an outward pulling force of a given magnitude, a shorter linker will lose more entropy by stretching than a longer one, will generate a stronger restoring force, and will therefore not stretch as far. We reasoned that in order to approximate the ~20 nm metaphase stretching of native CENP-C, a sensible approach would be to insert an intrinsically disordered peptide with a roughly equivalent number of amino acid residues. Therefore, in an effort to approximate the behavior of the 907 amino acid region that we had deleted in making the Minimal CENP-C mutant, we proposed to insert an intrinsically disordered peptide approximately 1000 amino acids in length into each recombinant CENP-C variant. Our objective was to compare the extent to which extendibility would be restored by inserting this peptide into each recombinant protein and, more importantly, the extent (if any) to which restoration of adequate length and extendibility to the mutants might restore wild type function and rescue the non-stretchable CENP-C phenotype.

In seeking to identify a suitable intrinsically disordered peptide we were assisted by the searchable Database of Protein Disorder (DisProt) (Sickmeier et al., 2007). This database guided us, based on sequence similarity to CENP-C

amino acids 83-989, to the disordered “PEVK domain” of human Titin. The largest known protein in nature, Titin is found in the sarcomere in both skeletal and cardiac muscle. Owing to its tremendous importance from a medical perspective, Titin’s elongation in response to mechanical force has been, and continues to be, extensively studied. Titin’s stretching behavior arises in significant part from its PEVK domain – so called for the abundance of Proline, Glutamic Acid, Valine and Lysine residues in the domain’s highly repetitive amino acid sequence – which has been characterized as an intrinsically disordered, permanently unstructured peptide region that behaves as an entropic spring (Anderson and Granzier, 2012; Tompa, 2005; van der Lee et al., 2014). Given its structural disorder and extendibility, we expected that a PEVK insert of appropriate length might effectively replace the deleted portions of CENP-C with regard to both general physical characteristics and susceptibility to elongation by spindle forces during mitosis.

For these reasons we inserted a 982 amino acid segment of a PEVK region from human Titin into both the Minimal CENP-C and Nsl1-CENP-C proteins, producing new variants that we refer to as “Minimal CENP-C-Titin” and “Nsl1-CENP-C-Titin.” By the Delta method we determined that the mean length of Minimal CENP-C-Titin at metaphase was 19.6 ± 1.4 nm (Mean ± SEM; N = 100 kinetochore pairs), meaning that Minimal CENP-C-Titin is only ~5 nm shorter than full length CENP-C (Figure 2.16). Maximum intrakinetochore stretch was restored nearly to wild type levels, and phenotypically this produced a partial rescue. In Minimal CENP-C-Titin cells from which the endogenous CENP-C was

depleted, the percentage of cells with fewer than five misaligned kinetochore pairs was 85.3 ± 3.3 percent (Mean ± SD; three experiments, N = 150 cells). (All control cells examined had four or fewer misaligned pairs.) The corresponding percentage seen in Minimal CENP-C cells, without the Titin insert, had been 63.4 ± 6.1 percent. In fact the alignment result for the Minimal CENP-C-Titin cells was remarkably similar to the partial rescue obtained by treating Minimal CENP-C cells with 1 μM Binucleine 2, the Aurora B inhibitor (84 ± 8.7 percent of cells having fewer than five misaligned pairs) (Figures 2.17A and 2.17B; and compare Figure 2.8 above).

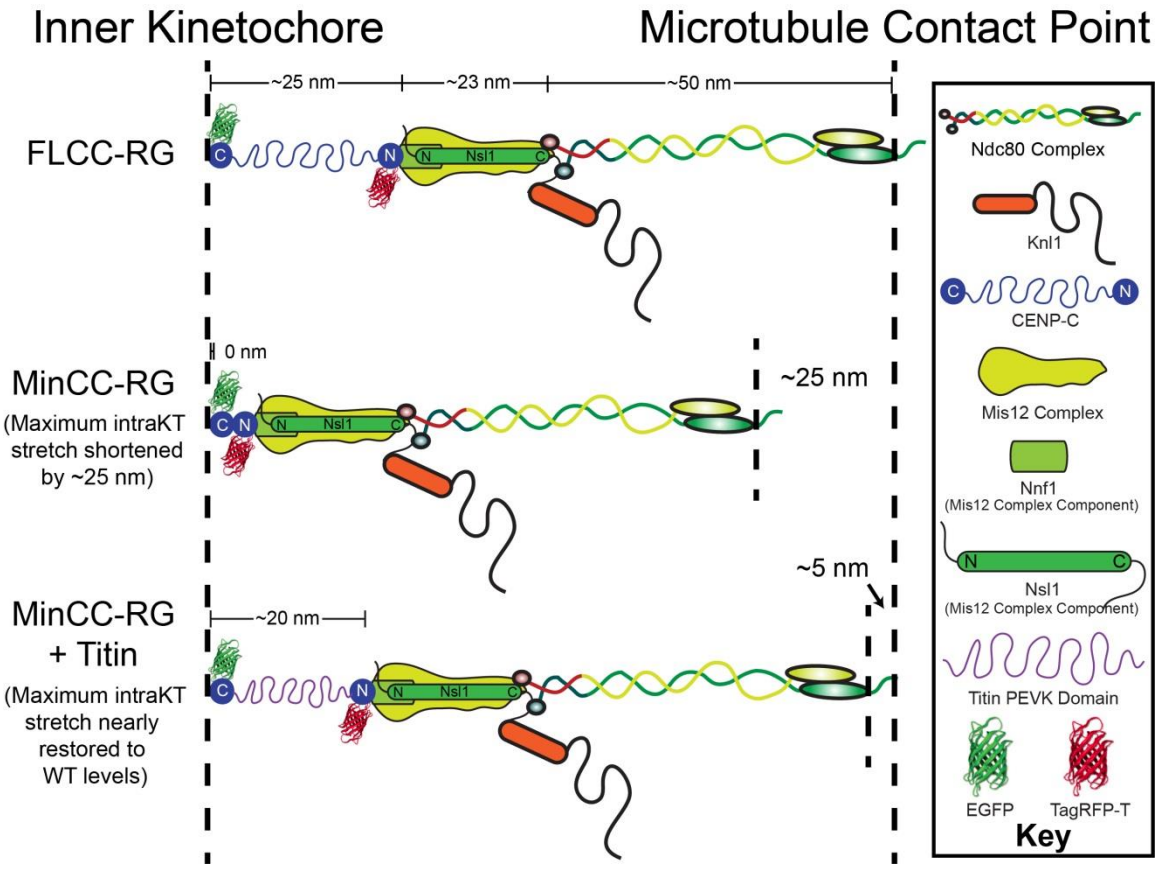

Figure 2.16: The Titin PEVK insert restores ~20 nm of length to Minimal CENP-C. This rendering of the Minimal CENP-C protein before and after insertion of the Titin PEVK segment shows that, with the Titin insert, the distance from the CENP-C C terminus to the microtubule attachment site is restored almost fully to the distance measured for full length CENP-C (here labeled FLCC).

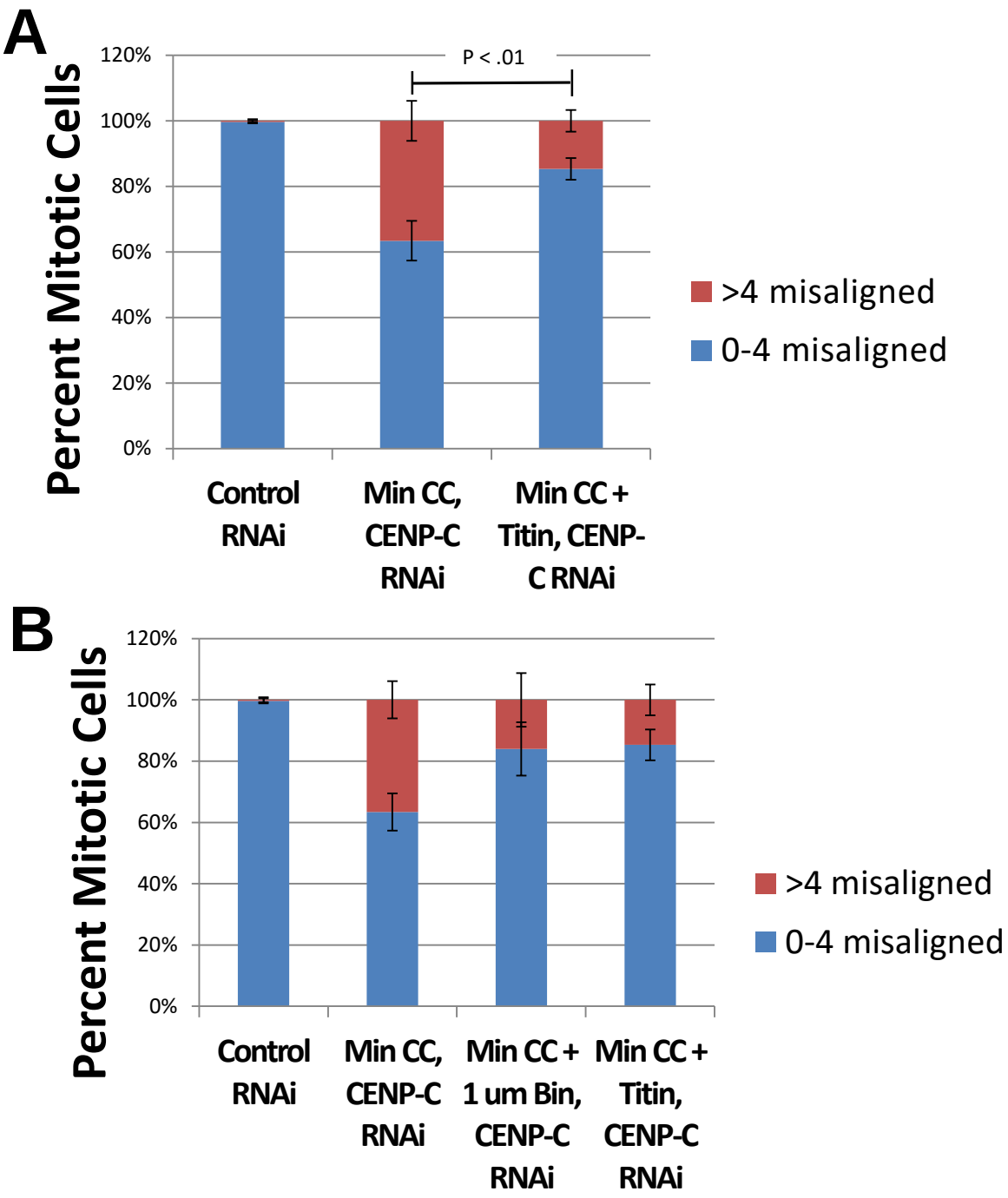

Figure 2.17: Addition of the Titin insert partially rescues the Minimal CENP-C chromosome misalignment phenotype. *(A)* The percentage of Minimal CENP-C cells with fewer than five misaligned kinetochore pairs increases from 63.4 ± 6.1 to 85.4 ± 3.3 percent following insertion of the Titin PEVK segment (Mean ± SD; three experiments, N = 150 cells). *(B)* The comparable percentage for Minimal CENP-C cells treated with 1 μM Binucleine 2 is 84% ± 8.7% (Figure 2.9) and is shown here for comparison.

In the Nsl1-CENP-C-Titin cells, the mean distance measured from the CENP-C C terminus to the Nsl1 N terminus, after addition of the Titin PEVK insert, was 43.5 ± 2.2 nm (Mean ± SEM; N = 95 kinetochore pairs) (Figures 2.18A and 2.18B). This agrees exceptionally well with *a priori* expectations, given the ~20 nm of Titin PEVK stretch seen in Minimal CENP-C-Titin and the ~23 nm length that we had measured for the Nsl1-CENP-C protein. Phenotypically, restoration of a 20 nm stretchable element to Nsl1-CENP-C caused the percentage of cells with more than four misaligned kinetochore pairs to drop, in the CENP-C RNAi condition, from 70% (Nsl1-CENP-C) to 36.5% ± 6.8% (Nsl1-CENP-C-Titin; Mean ± SD, three experiments, N = 126 cells). This partial rescue was comparable to, and not statistically different from, the partial rescue obtained by treating the Nsl1-CENP-C cells with 5 μM Binucleine 2 (Figure 2.19); and the chromosome alignment data for the Nsl1-CENP-C-Titin cells was also statistically equivalent to the corresponding data for the original Minimal CENP-C cells, without Aurora B inhibition and without a Titin insert (36.6% ± 6.1% of those cells had more than four misaligned kinetochore pairs; Figures 2.7, 2.8).

A

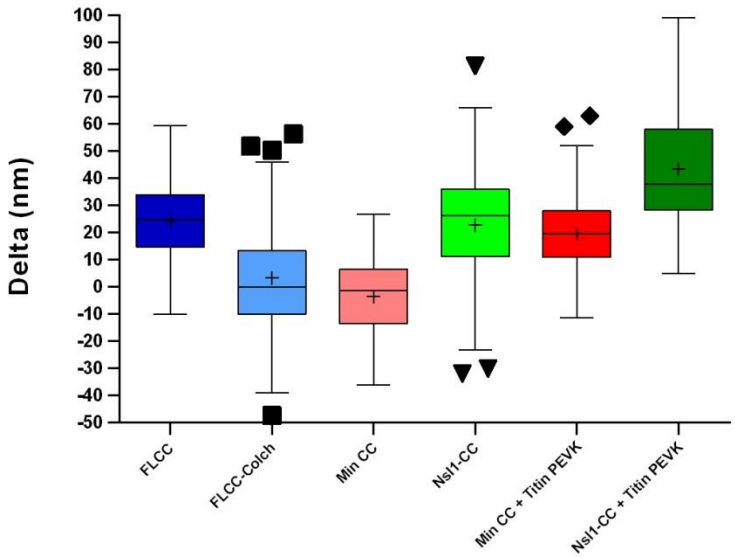

B

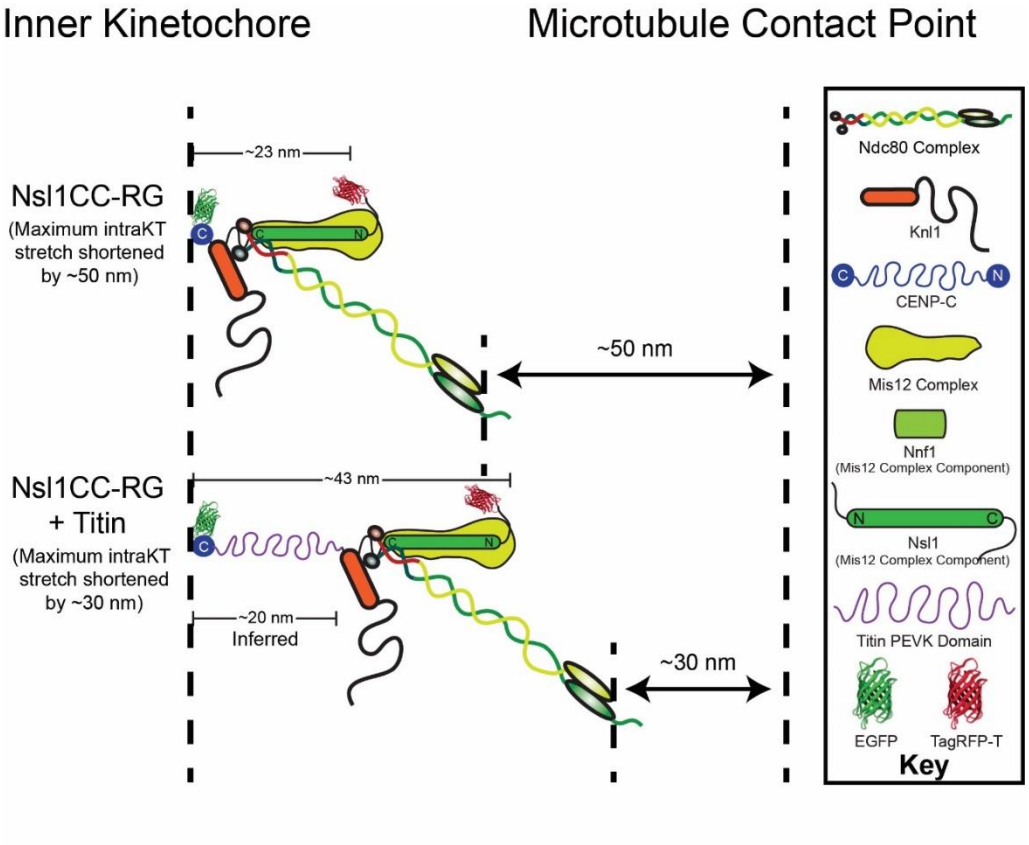

Figure 2.18: The Titin PEVK insert restores ~20 nm of length to Nsl1-CENP-C. *(A)* With the addition of the Titin insert, the length of Nsl1-CENP-C (far right column), as measured by K-SHREC, is 43.5 ± 2.2 nm (Mean ± SEM; N = 95

kinetochore pairs). *(B)* The distance from the CENP-C C terminus to the microtubule binding site has, accordingly, increased by ~20 nm.

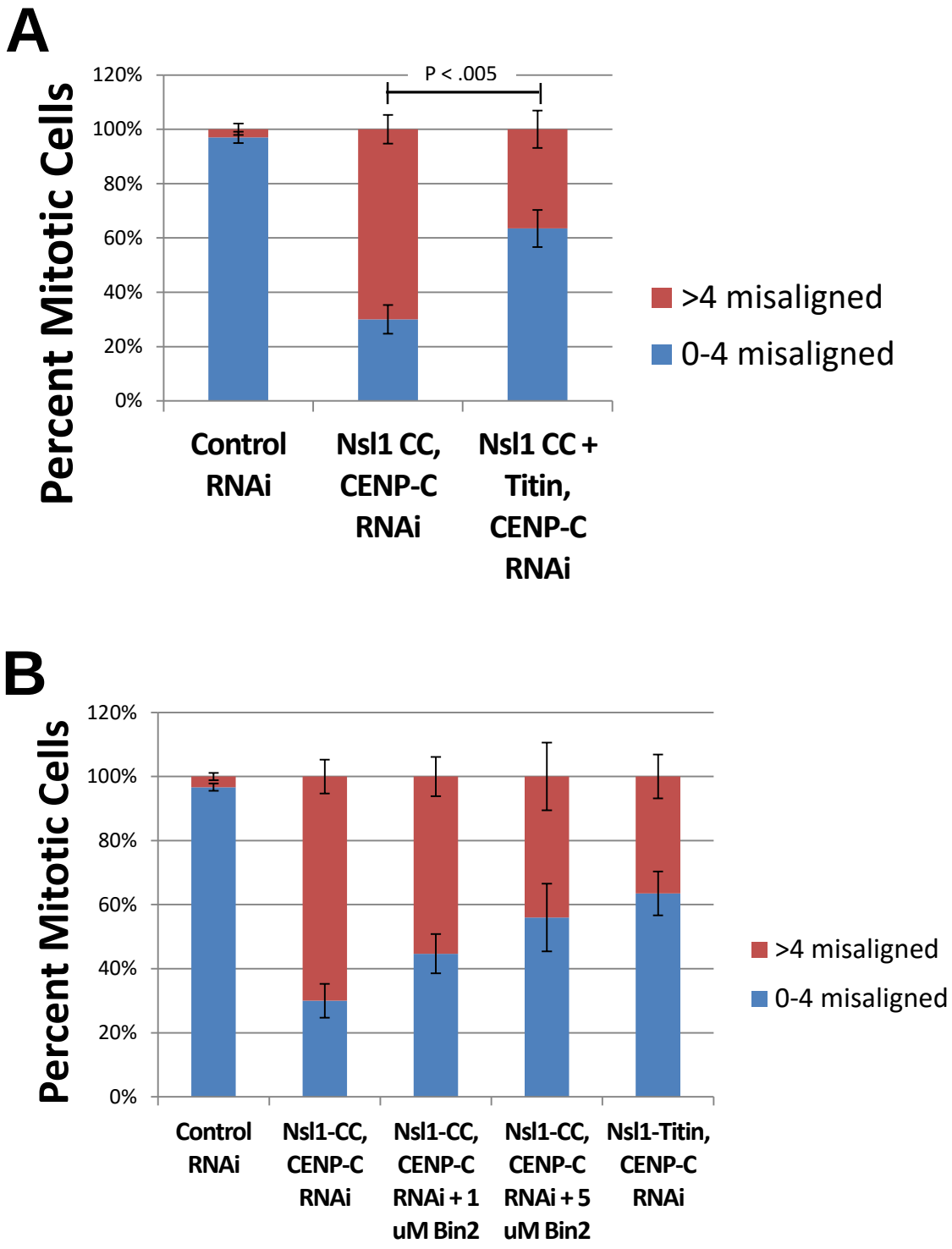

Figure 2.19: Addition of the Titin insert partially rescues the Nsl1-CENP-C chromosome misalignment phenotype. *(A)* The percentage of Nsl1-CENP-C cells with fewer than five misaligned kinetochore pairs increases from 30% ± 5.3% (Nsl1-CENP-C) to 63.5% ± 6.8% (Nsl1-CENP-C-Titin; Mean ± SD, three experiments, N = 126 cells). *(B)* The comparable percentage for Nsl1-CENP-C cells treated with 5 μM Binucleine 2 is 56% ± 10.6% (Figure 2.12) and is shown here for comparison.

2.3 Discussion

Through the use of artificially truncated, non-stretchable versions of *Drosophila* CENP-C, we found that kinetochore-microtubule attachment stability responds predictably to changes in the distance between the inner centromere and the microtubule attachment site. Shortening the distance led to greater attachment instability, whereas restoring length produced a corresponding recovery of the cell's ability to form stable attachments. In the absence of a linkage capable of adequately elongating in response to spindle forces, intrakinetochore stretch was reduced or eliminated and the outer kinetochore could not successfully be repositioned with respect to the inner centromere. It was in that circumstance that we observed chromosome alignment defects indicative of attachment instability.

Importantly, we found that the deleterious effects of shortening CENP-C and disabling intrakinetochore stretch could be reduced, and the characteristic instability phenotype partially rescued, either by inhibiting the kinase activity of Aurora B or by restoring adequate length to the shortened version of CENP-C. Our results are therefore consistent in all respects with the behavior that would be predicted by the spatial positioning model. Collectively our findings provide compelling evidence for the role of CENP-C as a mediator of intrakinetochore stretch in *Drosophila*, and for the role of intrakinetochore stretch in adjusting the stability of attachments by repositioning the kinetochore-microtubule binding site relative to the inner kinetochore as tension is applied. It is also noteworthy that as we reduced CENP-C's ability to elongate we observed a graded response

similar in concept to the system of graduated phosphorylation states described by Welburn *et al*. (Welburn et al., 2010).

It has been argued that, while the spatial positioning model may have amassed considerable support over a number of years, alternative explanations for tension-based attachment stabilization must still be considered (Sarangapani and Asbury, 2014). The most recent arguments to that effect seem rooted to some extent in a report (Campbell and Desai, 2013) finding that budding yeast can biorient and properly segregate their chromosomes with active Aurora B clustered on spindle microtubules rather than between sister kinetochores. The explanation proposed was that kinetochore structural changes at bioriented attachments make Aurora B substrates less accessible to the kinase for some reason other than mere spatial distance. We would suggest that the difference between this explanation and the spatial positioning model has been somewhat overstated. In the spatial positioning model, too, Aurora B substrates are made less accessible to the kinase due to tension-based changes in kinetochore structure. In either case the selective stabilization of bioriented attachments depends, at least to a considerable degree, on the physical accessibility of Aurora B substrates. While current formulations of the spatial positioning model are well supported, it would be unsurprising to learn that they are in some respects incomplete, or that an exclusive focus on the Aurora B at the inner centromere may be unnecessarily limiting. We anticipate further testing and refinement of spatially oriented and other tension based models of attachment stabilization.

By highlighting the extent to which kinetochore function turns on the extension and relaxation of flexible protein elements, this work also underscores the role of protein disorder in events occurring at the cell biological level, including at the kinetochore (Tantos et al., 2015; Wright and Dyson, 2015). Citing a combination of *in vitro* experiments and computational simulations, Zaytsev *et al*. recently proposed that the Ndc80 N-terminal tail exhibits conformational instability and that its structural disorder allows phosphoregulation of microtubule attachments to proceed in a measured and gradual fashion (Zaytsev et al., 2014). Also potentially relevant for kinetochore biology is the role of intrinsically disordered proteins as platforms for assembly of large complexes (Hegyi et al., 2007; Tantos et al., 2015). KNL1 could well represent an example of this. It has been noted that tension applied to the kinetochore at bioriented attachments allows PP1 to bind KNL1 by stretching KNL1, moving it beyond the reach of Aurora B activity that otherwise inhibits PP1 binding (Godek et al., 2015). Others have also recently pointed to KNL1 as an example of a kinetochore protein whose structural flexibility allows it to make available, as needed, a wide assortment of different binding motifs (Ghongane et al., 2014). KNL1, which interacts with microtubules and with the outer kinetochore component Nsl1, also has the capacity to bind Zwint-1, the checkpoint proteins Bub1, BubR1, and Bub 3, and the PP1 and PP2A phosphatases.

The work reported here identifies protein disorder as a source of intrakinetochore stretch, of variability in the spatial positioning of the outer kinetochore, and of a refined system for regulating attachment stability. The

presence of structural disorder in both CENP-C and (in vertebrate systems) CENP-T suggests that disordered proteins are particularly well suited for the role of linking the inner and outer regions of the kinetochore and adjusting the distance that separates them. We are inclined to speculate that these disordered kinetochore linkers have evolved so as to allow such a tunable regulatory system to develop.

2.4 Materials and Methods

2.4.1 Cell culture

Drosophila S2 cells were cultured at 24°C in Schneider's media (Life Technologies) supplemented with 10% heat inactivated fetal bovine serum (Life Technologies) and 0.5X antibiotic-antimycotic cocktail (Life Technologies).

2.4.2. Generation of S2 cell lines

The full length *Drosophila melanogaster* CENP-C gene (CG31258) was amplified from cDNA clone RE68959 with a 5' SpeI site and 3' BstXI site, and the resulting product was inserted into the multiple cloning site of a pMT/V5 His-B vector (Invitrogen). The TagRFP-T gene was inserted immediately upstream, between a 5' KpnI site and a 3' SpeI site, and the native CENP-C Promoter (consisting of the 890 bp immediately upstream of the CENP-C coding sequence) was inserted upstream of the RFP fluorophore between a 5' XbaI site and a 3' KpnI site. The EGFP gene was inserted downstream of the CENP-C gene, between a 5' BstXI site and a 3' SacII site. To produce the Minimal CENP-

C construct, in lieu of the full length CENP-C gene, a 246 bp sequence corresponding to amino acid residues 1-82 was inserted after the RFP fluorophore between upstream and downstream SpeI sites; 1266 bp corresponding to amino acids 990-1411 were then inserted adjacent to the aa 1-82 CENP-C segment, between an upstream SpeI site and a downstream BstXI site, with the EGFP fluorophore following immediately thereafter as in the full length construct. At this point, in order to facilitate the later insertion of linker peptides into Minimal CENP-C, a second version of the construct was also generated by inserting an XhoI site immediately 5' to the preexisting SpeI site separating the N-terminal (82 aa) and C-terminal (422 aa) portions of CENP-C.

To create Nsl1-CENP-C, the 246 bp region of the Minimal CENP-C construct corresponding to the N-terminal 82 amino acids of CENP-C was excised and the Nsl1 gene (amplified from cDNA clone RE03006) was inserted in its stead, between the (preexisting) 5' SpeI and 3' XhoI sites. Linker peptides later inserted into Nsl1-CENP-C, or into Minimal CENP-C, were inserted at the XhoI site, resulting in each linker being flanked by a 5' SalI (or SalI-derived) site and a 3' XhoI site. The Nup153 gene (Isoform A) was amplified from cDNA clone LD46479, and the Titin PEVK segment was synthesized by GenScript. The flexible linker $(GGGGS)_8$ ("2xFL2") and the helical linker $A(EAAAK)_{32}A$ ("4xHL3"), both gifts from Dr. Wei-Lih Lee of the University of Massachusetts Amherst, were inserted into Minimal CENP-C at the XhoI site between the N- and C-terminal CENP-C portions of the construct, and the inserted sequence was then amplified and reinserted one, two or three times in succession to make the series of

additional Minimal CENP-C derivatives containing 4xFL2, 8xHL3, 12xHL3 and 16xHL3 inserts.

All cell lines were generated by transfecting DNA constructs into S2 cells using the Effectene Transfection Reagent system (Qiagen) according to product directions. The transfected cells were grown in Schneider's media (Invitrogen) containing 10% heat-inactivated Fetal Bovine Serum (Invitrogen). After four days, the cells were transferred to a 25 cm^2 flask. The cells were then grown in media containing Blasticidin S or Hygromycin B, depending on the construct, and observed at least twice weekly until cell death ceased. From that point cells were maintained in media containing no Blasticidin or Hygromycin (as applicable).

2.4.3 Production of double-stranded RNAs (dsRNAs)

DNA templates for the CENP-C coding region and 3' untranslated region were produced to contain approximately 500 bp of complementary sequence flanked with the T7 promoter sequence. dsRNAs were synthesized overnight at 37°C from the DNA templates using the T7 RiboMax™ Express Large Scale RNA Production System (Promega). For RNAi experiments, media was aspirated off semi-adhered cells at 25% confluence and replaced with 1 ml of serum-free Schneider's medium containing ~20 µg of dsRNA. After one hour, 1 ml of fresh Schneider's + FBS was added to the wells and incubated for two days at 24°C.

2.4.4 Live-cell imaging

Cells were seeded onto Concanavalin A (Sigma) treated acid-washed coverslips (Corning) for one hour. The coverslips were assembled into rose chambers containing Schneider's media and imaged at room temperature. For K-SHREC/Delta analysis, two color Z-series were acquired through the depth of the spindle at 0.2 µm intervals for both the TagRFP and EGFP channels simultaneously, on a TiE inverted microscope (Nikon) equipped with a DV2 beam splitter (Photometrics) and a cooled charge-coupled device Orca ER camera (Hamamatsu), using a 100X 1.4 NA Plan Apo violet-corrected series differential interference contrast objective (Nikon). For time-lapse imaging of live cells, coverslips and rose chambers were prepared and assembled as above. Z-series were acquired at 0.5 µm intervals once every minute for a period not exceeding 60 minutes. At the first and last time points for each cell, Z-series were acquired in both the TagRFP and EGFP channels to verify that the relevant CENP-C-derived protein was expressing both fluorophores in that cell. At all other time points the Z-series were acquired only in the EGFP channel, in order to minimize phototoxicity and photobleaching. Time-lapse imaging was performed on a TiE inverted microscope (Nikon) with a CSU-X1 spinning disk confocal head (Yokogawa) and an iXON EMCCD camera (Andor Technology), using a Nikon 100X 1.4 NA Plan Apo violet-corrected series DIC objective (Nikon). MetaMorph software (Molecular Devices) was used to control both imaging systems.

2.4.5 Immunofluorescence

In a tissue culture dish, cells were seeded onto an acid-washed coverslip (Corning) treated with Concanavalin A (Sigma Aldrich) and allowed to adhere for one hour, after which the cells were immediately subjected to paraformaldehyde fixation or, if applicable, the coverslip was immersed in Schneider's media to a final volume of 2 ml and treated with 5 μM MG132 for one hour before fixation. If applicable, cells were also treated for one hour with 1 μM, 5 μM or 10 μM Binucleine 2 or an equal volume of DMSO for controls.

Cells were fixed with 10% paraformaldehyde for ten minutes after a brief rinse with BRB80 buffer. Cells were then permeabilized for eight minutes in 1xPBS+ 1% Triton X-100, washed three times for 5 minutes each in 1xPBS + 0.1% Triton, and blocked in boiled donkey serum for 30-60 minutes. All primary antibodies were diluted in boiled donkey serum. Anti-Phospho-Aurora A/B/C (Rabbit mAb #2914 – Cell Signaling Technology), Mouse anti-α-tubulin (DM1α – Sigma-Aldrich) and Rabbit anti-phospho-KNL1 (a gift of Iain Cheeseman, Massachusetts Institute of Technology) antibodies were used at a 1:1000 dilution, and a Chicken anti-Ndc80 antibody was used at 1:100. All secondary antibodies (Jackson ImmunoResearch Laboratories, Inc.) were diluted 1:200 to a final concentration of 3 μg/ml in boiled donkey serum. After secondary treatment, coverslips were washed two times with 1xPBS + 0.1% Triton, followed by incubation with DAPI (1:1000) at a final concentration of 1 μg/ml for five minutes, and two additional washes. Cover slips were sealed in mounting media containing 20 mM Tris, pH 8.0, 0.5% N-propyl gallate, and 90% glycerol.

2.4.6 Cold stability assay

In a tissue culture dish, cells were seeded onto an acid-washed coverslip (Corning) treated with Concanavalin-A (Sigma Aldrich) and allowed to adhere for one hour, after which the coverslip was immersed in Schneider's media to a final volume of 2 ml and treated with 5 μM MG132 for one hour. The cells were placed inside a 4°C cold room where they were kept for ten minutes, after which the Schneider's media was removed, the cells were briefly rinsed with ice-cold BRB80 buffer and were then immediately fixed with ice-cold 10% paraformaldehyde. Control cells were maintained at room temperature throughout an equivalent MG132 treatment, briefly rinsed with room temperature BRB80 and fixed with room temperature paraformaldehyde. For both control and cold-treated cells, after fixation the standard immunofluorescence protocol (Section 2.4.5 above) was carried out at room temperature.

After immunostaining, the cells were imaged on the Spinning Disk confocal microscope. Two color Z-series were acquired through the depth of the spindle at 0.2 μm intervals for both the kinetochores (signal emitted by EGFP fused to the applicable CENP-C derivative) and the microtubules (signal emitted by a Cy3-conjugated secondary antibody). In MetaMorph, coplanar kinetochore pairs were identified and a 5 pixel x 5 pixel region of interest was overlaid on the tubulin immediately adjacent to each member of the pair, with the regions oriented along the axis described by the kinetochore pair. Integrated fluorescence intensity representing the Cy3 signal was recorded for each of the two regions of interest, and each intensity measurement was background

corrected by subtracting the intensity of a 5 pixel x 5 pixel square placed within the cytoplasm. Each coplanar kinetochore pair thus generated two background-corrected tubulin fluorescence intensity values. In CENP-C-depleted cells, regions of interest were deliberately positioned so as to exclude tubulin bundles clearly not in an end-on attachment state with respect to their associated kinetochores (*i.e.*, non-"k-fiber" bundles), and also to exclude tubulin in the immediate vicinity of a spindle pole. To the extent feasible, tubulin intensity was measured for kinetochores at or near the spindle equator, though this was often not possible for kinetochore pairs in cells with highly disorganized spindles.

Fluorescence intensity values for the cold treatment experiments were also corrected for differences in overall staining quality and brightness as between control and cold-treated coverslips. For each coverslip, tubulin fluorescence intensity was determined for two regions of interest within each of ten well preserved midbodies, all as corrected for cytoplasmic background signal. A brightness correction factor was then derived from the mean background-corrected fluorescence intensity of the twenty midbody regions imaged for each coverslip.

2.4.7 Chromosome misalignment assay

Misaligned kinetochore pairs were identified by imaging fixed cells with fluorescently labeled kinetochores (EGFP) and microtubules (Cy3) and then manually counting the misaligned pairs as seen on the acquired image. In certain instances it was possible to count misaligned pairs by visual examination

of the EGFP signal under 100x magnification, without first imaging the cell. Kinetochore pairs falling more than 20 percent of the spindle length away from the metaphase plate (or from the best-organized partial metaphase plate) were scored as “misaligned” irrespective of their orientation relative to the spindle axis. Kinetochore pairs closer to the metaphase plate were scored as “misaligned” only if not oriented correctly with respect to the spindle axis.

2.4.8 Phospho-Aurora B Quantification (Nsl1-CENP-C cells)

Using standard immunofluorescence procedures, cells expressing GFP-labeled Nsl1-CENP-C were fixed, incubated with an anti-phospho-Aurora A/B/C antibody (previously determined to bind centromeric phospho-Aurora B) and a Cy3-conjugated secondary antibody, and stained with DAPI. Z-series were imaged in the EGFP, RFP and DAPI channels. A Z plane showing a distinct kinetochore pair with a strong GFP signal was identified and a 7 pixel x 7 pixel region of interest was placed in the area between the sister kinetochores; this region was then transferred to the Cy3 image, a second 7 pixel x 7 pixel region was placed in the cytoplasm to correct for background signal, and the integrated fluorescence intensity for both the centromere/phospho-Aurora B region and the cytoplasmic/background region were recorded. The two regions were then transferred to the DAPI image, and DAPI signal intensity was recorded for the centromere and background regions. Finally, the ratio of background-corrected phospho-Aurora B fluorescence to background-corrected DAPI signal was determined.

2.4.9 KMN Localization assay (Minimal CENP-C cells)

In fixed cells expressing the outer kinetochore protein of interest (KNL1, Mis12 or Ndc80) labeled with GFP, kinetochores incorporating the labeled protein appeared as distinct spots of GFP fluorescence. For approximately thirty cells in each condition (six coverslips), the spots of GFP fluorescence were counted by the MetaMorph software in a wholly automated fashion using its in-built cell counting function. Parameters governing the automated counting (minimum and maximum size, and minimum signal intensity above background, required for inclusion as a "countable" spot) were specified such that no single spot was recognized as more than one kinetochore. Parameters for the automated counting were held constant across the control and CENP-C RNAi conditions for each protein of interest. Four-day RNAi treatments were used for these experiments.

2.4.10 K-SHREC/Delta analysis

We employed Delta analysis substantially as described by its originators for use in living cells in (Varma et al., 2013), but without using antibodies or applying a tilt correction. In the K-SHREC experiment involving colchicine-treated CENP-C, the cells were treated with 25 μM colchicine for one hour before imaging.

2.4.11 Western blotting

A total of 10 μg of protein was loaded into a 10% SDS-PAGE gel, run out and transferred to a nitrocellulose membrane (BioRad) in transfer buffer

containing 10% methanol. All antibodies were diluted in TBS with 0.1% Tween and 5% milk. The membrane was incubated with an anti-CENP-C antibody (gift of Barbara Mellone, University of Connecticut) at 1:7500 and then a guinea pig HRP secondary antibody (Jackson ImmunoResearch), and imaged with a GBox system controlled by GeneSnap software (Syngene). The same procedure was then followed with an anti-Ndc80 antibody (1:1000 dilution) and a chicken HRP secondary.

CHAPTER 3

ELEVATED POLAR EJECTION FORCES STABILIZE KINETOCHORE-MICROTUBULE ATTACHMENTS

3.1 Introduction

Establishing bioriented chromosomes with sister kinetochores attached to microtubules from opposing spindle poles is essential for maintaining genomic integrity though cell division. Mitotic forces select for bioriented attachments through tension-dependent stabilization of kt-MT attachments (Akiyoshi et al., 2010; Li and Nicklas, 1995; Nicklas et al., 2001). Polar ejection forces (PEFs) have been implicated in chromosome alignment since their discovery (Rieder et al., 1986; Rieder and Salmon, 1994). PEFs are predominantly generated by kinesin-10 family members – chromokinesins that are proposed to walk chromosome arms away from poles and towards the plus ends of spindle microtubules. Perturbation of chromokinesin function in multiple model systems disrupts the proper and timely congression of chromosome arms (Afshar et al., 1995a; Antonio et al., 2000; Funabiki and Murray, 2000; Goshima and Vale, 2003; Levesque and Compton, 2001; Magidson et al., 2011; Powers et al., 2004; Stumpff et al., 2012; Theurkauf and Hawley, 1992; Tokai-Nishizumi et al., 2005; Wandke et al., 2012; Wignall and Villeneuve, 2009; Zhang et al., 1990) but the extent to which PEFs contribute to chromosome alignment remains unclear as inhibition of chromokinesins in several cell types results in subtle or even undetectable effects on congression (Dumont et al., 2010; Kitajima et al., 2011).

An under-appreciated feature of chromosomal positioning by PEFs is the potential regulation of kinetochore function by kinesin-10 motors. PEFs are well-positioned to impact kt-MT interactions by producing forces along chromosome arms that are transmitted through the kinetochore and it has been hypothesized that PEFs could regulate motility of bioriented chromosomes by creating tension at kinetochores (Rieder and Salmon, 1994; Skibbens et al., 1993). Furthermore, misaligned chromosomes where one (monotelic) or both (syntelic) kinetochores are attached to a single pole could come under tension when kinetochore-dependent poleward pulling forces are opposed by PEFs (Cassimeris et al., 1994; Rieder et al., 1995). In fact, applying tension with microneedles to unipolar bivalents attached to the same spindle pole in spermatocytes stabilized this normally unstable orientation (Nicklas and Koch, 1969) to the point that the spindle assembly checkpoint (SAC) was satisfied and the cells entered anaphase (Li and Nicklas, 1995). Despite the fact that PEFs are likely to influence the production of tension at kinetochores, the contribution of PEFs to kt-MT attachment stability has never been directly tested.

PEFs were initially proposed to be generated by two non-exclusive sources: chromosome-associated motor proteins and the polymerization of microtubules (Rieder et al., 1986; Rieder and Salmon, 1994). The chromokinesin KID (kinesin-10) was later identified as the principal mediator of PEF generation in vertebrate cells (Antonio et al., 2000; Brouhard and Hunt, 2005; Funabiki and Murray, 2000). No distributive disjunction (NOD) is the *D. melanogaster* kinesin-10 family member that, like KID, localizes to chromosomes and is required for

generating PEFs (Afshar et al., 1995a; Afshar et al., 1995b; Theurkauf and Hawley, 1992). However, NOD is classified as a nonmotile kinesin because it fails to exhibit activity in conventional microtubule gliding assays (Matthies et al., 2001), while KID is a bona fide plus end-directed motor (Bieling et al., 2010a; Brouhard and Hunt, 2005; Yajima et al., 2003). NOD has been shown to preferentially bind microtubule plus ends in vitro (Cui et al., 2005) and it has been postulated, based on analyses of its catalytic domain, that NOD generates force by associating with the plus ends of polymerizing microtubules – a behavior termed "end tracking" (Cochran et al., 2009). Thus, while PEF production by kinesin-10 chromokinesins is evolutionarily conserved, the molecular mechanism by which kinesin-10 motors transmit force is thought to differ.

Whether derived from motility or end-tracking, individual PEF-producing interactions are most likely weak so that the DNA is not damaged (Brouhard and Hunt, 2005). Consistent with this presumed constraint, the PEF has been measured as 0.5 pN per microtubule on mammalian chromosomes (Brouhard and Hunt, 2005) and ~1 pN in *Drosophila* embryos (Marshall et al., 2001). In principle, either motility or end-tracking could generate PEFs of this magnitude, because both motile kinesins and polymerizing microtubules generate forces in the low pN range (Dogterom and Yurke, 1997; Visscher et al., 1999). Although it is thought that NOD is nonmotile and that it produces PEFs solely by end-tracking on polymerizing microtubules, the molecular mechanism of PEF production by NOD is unclear.

3.2 Results

3.2.1 NOD overexpression stabilizes syntelic attachments in a dose-dependent manner

To experimentally manipulate PEFs in living cells, the *D. melanogaster* chromokinesin NOD (Afshar et al., 1995a; Zhang et al., 1990) was fused to mCherry and placed under the control of a copper-inducible promoter. NOD-mCherry localized exclusively to mitotic chromosomes over a broad range of expression levels that varied on a cell-by-cell basis. Using a custom-made polyclonal peptide antibody, induced NOD, but not endogenous NOD, was detectable on mitotic chromatin by immunofluorescence (IF) and was detectable by western blot (WB) of cell extracts as a ~105 kDa protein band. An inability to detect endogenous NOD by WB or IF has also been reported for another NOD antibody (Afshar et al., 1995a; Afshar et al., 1995b). Our antibody efficiently detected NOD-mCherry by IF in the highest-expressing cells, but in cells expressing lower levels of NOD the antibody's sensitivity rapidly diminished. These data suggest that endogenous NOD levels are low in mitotic cells. Despite its low abundance, NOD generates an away-from-the-pole force in mitotic *Drosophila* cells as NOD RNAi caused an inward movement of kinetochores and chromosome arms in monopolar spindles, which was also observed following Kid inhibition in vertebrate cells (Levesque and Compton, 2001; Stumpff et al., 2012; Wandke et al., 2012). Thus, our results are consistent with previous reports that NOD regulates mitotic chromosome

behavior (Goshima and Vale, 2003; Goshima et al., 2007; Rasooly et al., 1991; Zhang and Hawley, 1990).

Aberrant spindle morphologies were evident in GFP-α-tubulin expressing cells co-expressing NOD-mCherry. As observed in embryonic cells (Afshar et al., 1995b), monopolar spindles assembled in S2 cells expressing the highest levels of NOD. Cells expressing low or intermediate levels of NOD did not form monopoles but often assembled unusual spindles with robust kinetochore fibers connecting chromosomes to the same spindle pole (Figure 3.1A). At high-intermediate concentrations of NOD, spindles were often comprised of two fan-shaped half spindles, each with its own associated subset of chromosomes (Figure 3.1B). In general, the intermediate range of NOD expression levels yielded spindles lacking normal metaphase plates (Figures 3.1C and 3.1D). Despite the absence of metaphase alignment, NOD expressing cells were able to satisfy the SAC and enter anaphase (Figures 3.1A and 3.1D).

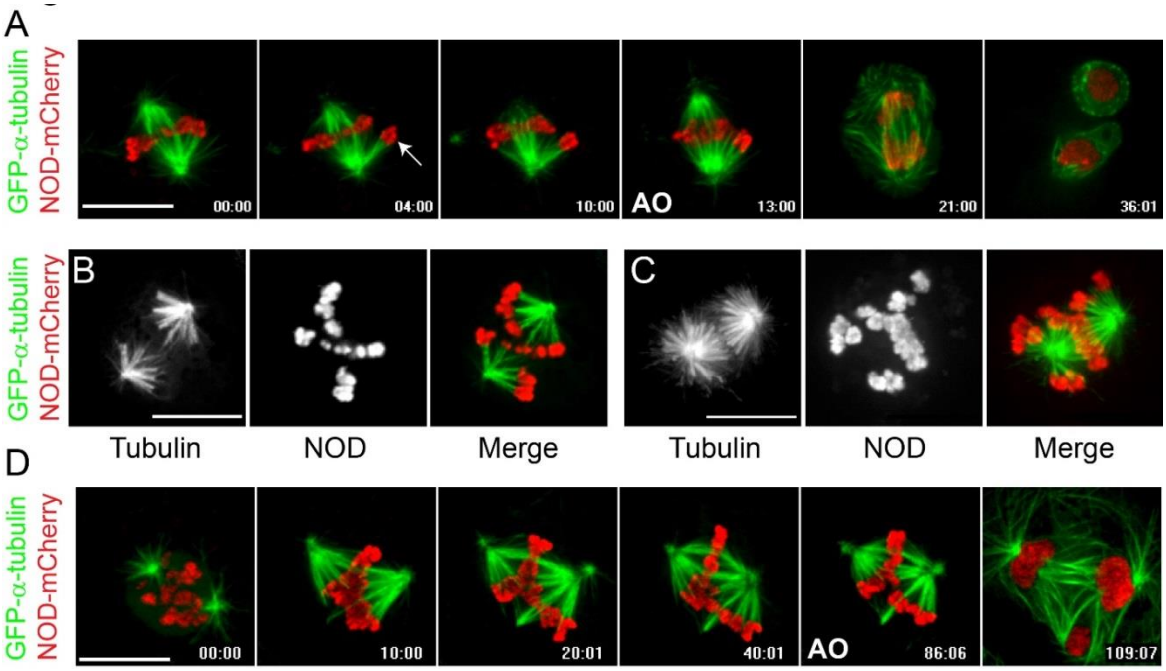

Figure 3.1: NOD-mCherry-expressing cells do not form a well-defined metaphase plate. *(A–D)* Two-color confocal imaging of GFP–α-tubulin (green)- and NOD-mCherry (red)-expressing S2 cells. *(A)* Selected frames from a time lapse of a cell with a pair of sister chromatids that are attached to the same pole (arrow). The aberrant attachment state persists and anaphase onset (AO) ensues without error correction. *(B and C)* Chromosomes move away from the poles but fail to align along a well-defined metaphase plate, particularly in cells expressing high levels of NOD-mCherry. *(D)* Selected micrographs from a time lapse of a NOD-mCherry-expressing cell as it progresses through mitosis. A mixture of attachment states are established within the first 10 min of nuclear envelope breakdown and persist until the cell enters anaphase with uncorrected syntelic attachments, resulting in chromosome missegregation and multiple nuclei. Bars, 10 µm.

The spindle morphologies in NOD expressing cells indicated a prevalence of syntelic attachments, a non-bioriented attachment state where both sister kinetochores are attached to the same spindle pole. To confirm that syntelic attachments were being formed, NOD-mCherry was co-expressed with Ndc80-GFP to label kinetochores. Persistent syntelic attachments, as defined by clearly juxtaposed sister kinetochores facing the same spindle pole, were observed following induction of NOD (Figure 3.2A). This phenotype was not due to a dominant negative effect of NOD expression as syntelic attachments still formed when NOD-mCherry was induced after targeting endogenous NOD by RNAi. Thus, NOD overexpression yielded spindles with elevated levels of syntelic attachments.

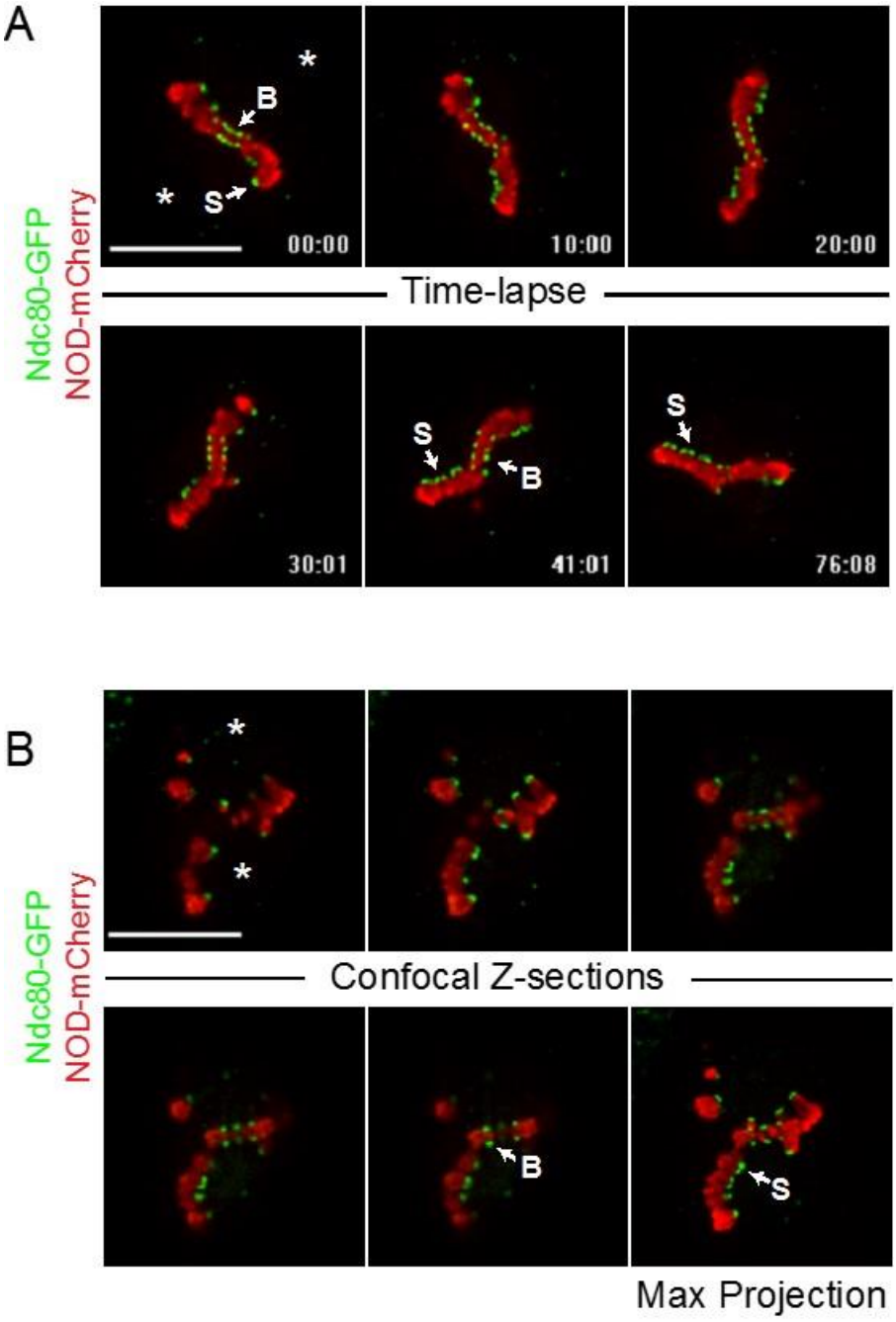

Figure 3.2: NOD-mCherry expression stabilizes syntelic attachments. *(A)* Selected frames from a confocal time lapse of a cell with both bioriented (B) and syntelic (S) attachments (approximate pole positions are marked with asterisks). Note that the syntelic attachments persist for the duration of the time lapse. *(B)* Selected confocal Z-sections showing a combination of syntelic and bioriented kinetochore pairs in the same cell. The mCherry fluorescence intensity for each cell was quantified from the maximum intensity projection of the Z-sections (rightmost panel).

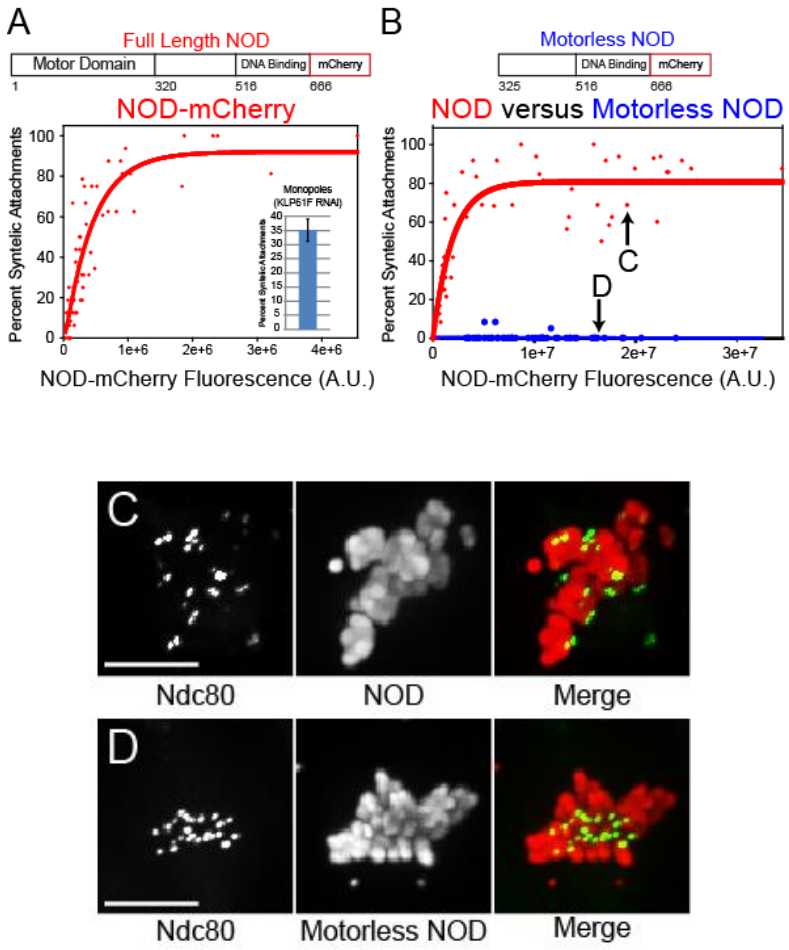

Figure 3.3: NOD-mediated stabilization of syntelic attachments is dose- and motor-dependent. *(A)* Plotting the percentage of syntelic attachments versus NOD-mCherry fluorescence reveals that NOD-mCherry stabilizes syntelic attachments in a dose-dependent fashion (*n* = 60 cells). Inset shows the mean percentage of syntelic attachments found in monopolar spindles assembled in the absence of Klp61F. *(B)* Syntelic stabilization by NOD-mCherry requires the motor domain of NOD (NOD, *n* = 57 cells; motorless NOD, *n* = 70 cells). *(C and D)* Maximum intensity projections of representative NOD-mCherry- and motorless NOD-mCherry-expressing cells with comparable expression levels (highlighted in *B*). Error bar represents the SEM. Bars, 10 µm.

The phenotypic variability exhibited by NOD overexpressing cells led to the development of a quantitative image-based assay ("PEF assay") that was applied to further characterize the effects of NOD overexpression. In brief, two-color spinning disk confocal Z-sections were acquired for individual cells co-expressing NOD-mCherry and Ndc80-GFP. NOD levels for a given cell were measured by quantifying the total integrated fluorescence intensity from the mCherry fluorophore, and each chromosome in that cell was individually scored as "bioriented", "syntelic" or "other" by examining Ndc80-GFP-labeled kinetochore pairs (Figure 3.2B). Plotting the percentage of syntelic attachments in a given cell against the NOD-mCherry fluorescence intensity for that cell, and repeating that analysis on a cell-by-cell basis over a range of expression levels, revealed that NOD stabilized syntelic attachments in a dose-dependent manner (Figure 3.3A).

3.2.2 NOD-mediated stabilization of syntelic attachments is specific and motor dependent

The prevalence of syntelic attachments in NOD expressing cells could not be attributed to monopolar spindle assembly because cells expressing the highest levels of NOD – those that assembled monopoles – were excluded from analysis. Furthermore, monopoles assembled following depletion of Klp61F (kinesin-5) contained an average of ~35% syntelic attachments – less than the average percentage of syntelic attachments seen in the high NOD expressing cells included in the analyses (Figure 3.3A). To address the possibility that NOD overexpression stabilized syntelic attachments by disrupting chromosome

structure or by mis-localizing other chromosomal components, a NOD mutant lacking the N-terminal motor domain was expressed in S2 cells. Motorless NOD localized to mitotic chromosomes as efficiently as full length NOD but did not increase the percentage of syntelic attachments (Figures 3.3B-3.3D), demonstrating that the motor domain of NOD is required to stabilize syntelic attachments.

KLP3A (kinesin-4), the other major chromokinesin in *Drosophila*, regulates spindle pole separation in prometaphase and anaphase (Kwon et al., 2004), and its vertebrate homolog regulates chromosome oscillations and midzone assembly by suppressing microtubule plus end dynamics (Bieling et al., 2010b; Bringmann et al., 2004; Hu et al., 2011; Stumpff et al., 2012; Wandke et al., 2012). Like its vertebrate counterpart, KLP3A may act as an “anti-PEF” by inhibiting the polymerization of microtubules that come into contact with chromatin. We next examined whether NOD overexpression indirectly elevated PEFs by mis-localizing the anti-PEF motor KLP3A. As previously reported (Kwon et al., 2004), KLP3A localized to interphase nuclei as well as on and around mitotic chromosomes and along midzone and midbody microtubules. KLP3A localization and chromosomal association were unaffected by elevated NOD expression (Figures 3.4A and 3.4B).

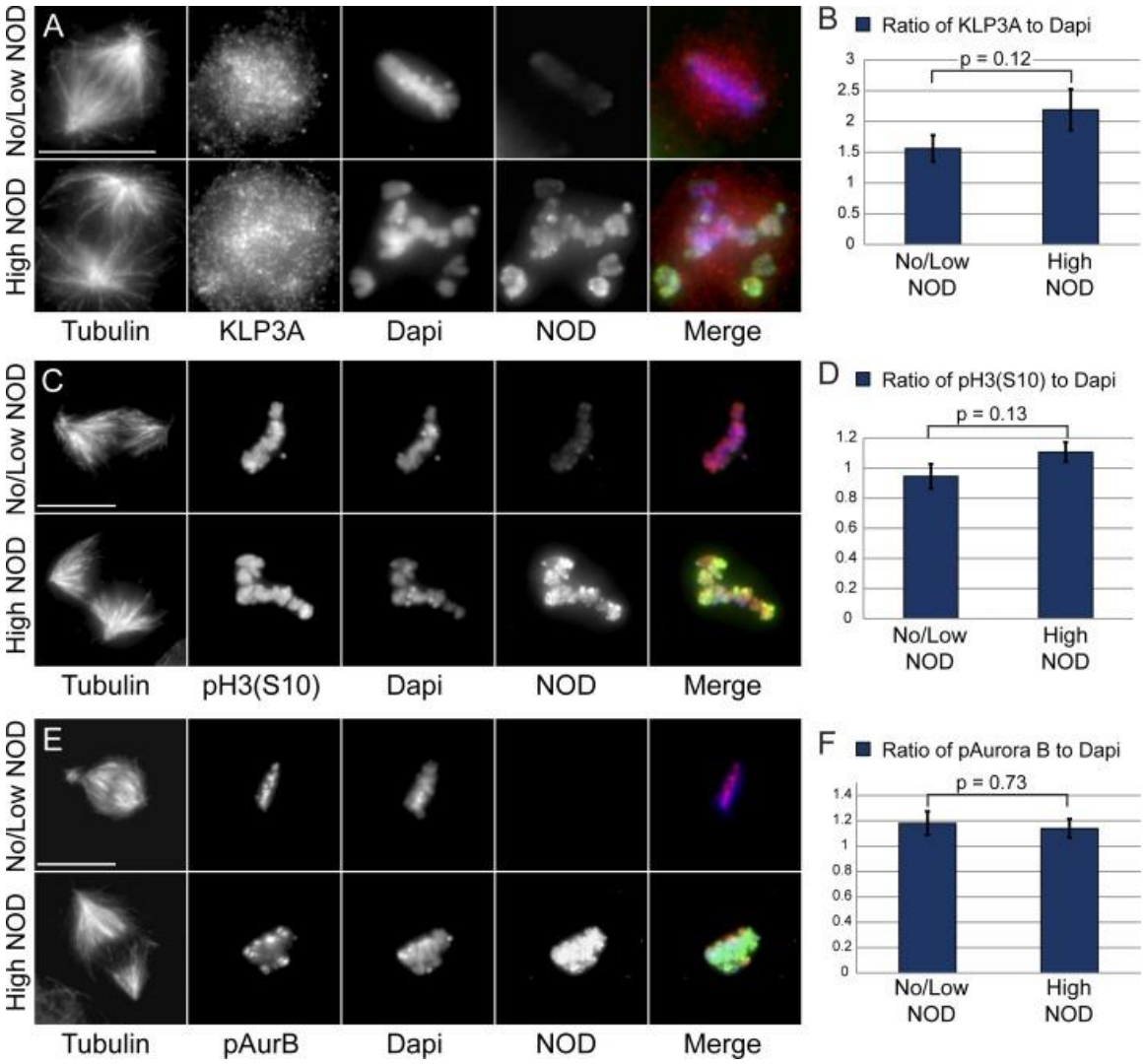

Figure 3.4: KLP3A localization and Aurora B localization and activity are not compromised in NOD-expressing cells. *(A, C, and E)* Representative maximum projections of tubulin, DAPI (blue), KLP3A (red; A), phospho-histone H3-serine 10 (red; C) or phospho-Aurora B (red; E), and NOD (green) for high and low/no NOD-expressing cells. (B, D, and F) Quantification of KLP3A (*n* = 102 cells; B), phospho-histone H3 (Serine 10; *n* = 31 cells; D), or phospho-Aurora B (*n* = 73 cells; F) signals relative to DAPI intensities for high and low/no NOD-expressing cells. There was not a statistically significant difference in levels of KLP3A, phosphor-Aurora B, or phospho-H3 (Ser10) between high and no/low NOD-expressing cells. Two-tailed p-values are shown. Error bars represent the SEM. Bars, 10 µm.

Inhibition of Aurora B kinase, which destabilizes erroneous kt-MT attachments (reviewed in (Maresca and Salmon, 2010)), results in numerous syntelic attachments near spindle poles (Ditchfield et al., 2003; Hauf et al., 2003; Lampson et al., 2004). Despite the fact that chromosomes in NOD overexpressing cells were often pushed away from the poles and the NOD overexpression phenotype was distinct from the effects of Aurora B depletion in S2 cells (Adams et al., 2001; Giet and Glover, 2001), the striking abundance of stable syntelic attachments warranted a careful investigation of Aurora B localization and activity in NOD expressing cells. We found that NOD overexpression cells did not affect the localization or activity of Aurora B as neither the phosphorylation of histone H3 at S10 (Figures 3.4C and 3.4D) nor the levels of active chromatin-associated and phosphorylated Aurora B (Figures 3.4E and 3.4F) was altered by NOD expression. The lack of syntelic attachments in motorless NOD overexpressing cells (Figure 3.3B) along with the fact that KLP3A localization and Aurora B localization/activity are unaffected by NOD overexpression strongly support the conclusion that NOD-dependent stabilization of syntelic attachments is a direct consequence of overexpressing full length NOD and requires force generation by the motor.

3.2.3 Elevated PEFs produce cold-stable syntelic kt-MT attachments with reduced Mad1 levels

Syntelic attachments are typically repaired before cells enter anaphase. However, syntelic attachments assembled in NOD expressing cells persisted until anaphase. We found that the GFP-α-tubulin fluorescence intensity of

kinetochore fibers was comparable for syntelic and amphitelic (connected to opposing spindle poles) attachments (Figures 3.5A and 3.5B). FRAP analysis of GFP-α-tubulin was done near the spindle equator in control and NOD-expressing cells to determine whether excess NOD stabilizes microtubules in general. Similar to previous observations (Goshima et al., 2008), a $t_{1/2}$ = 31 +/- 2s (n = 8 cells) was measured in control cells. NOD overexpression did not significantly alter GFP-α-tubulin turnover as a $t_{1/2}$ = 38 +/- 3s (n = 8 cells) was measured in cells expressing high levels of NOD-mCherry. Thus, turnover of non-kinetochore microtubules is largely unaffected by NOD overexpression, indicating that the prevalence of syntelics was caused, not by stabilization of microtubules in general but, rather, by stabilization of kinetochore microtubules in particular. This finding is in agreement with the observation that overexpression of the motor domain alone, which binds exclusively to microtubules, does not stabilize syntelic attachments (unpublished observation and (Afshar et al., 1995b)).

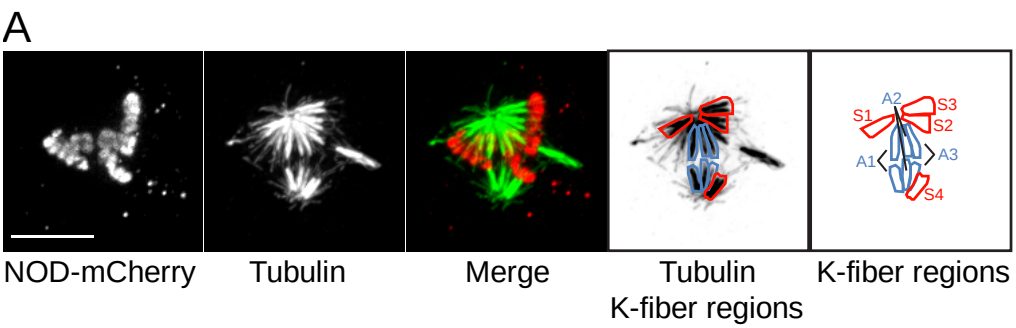

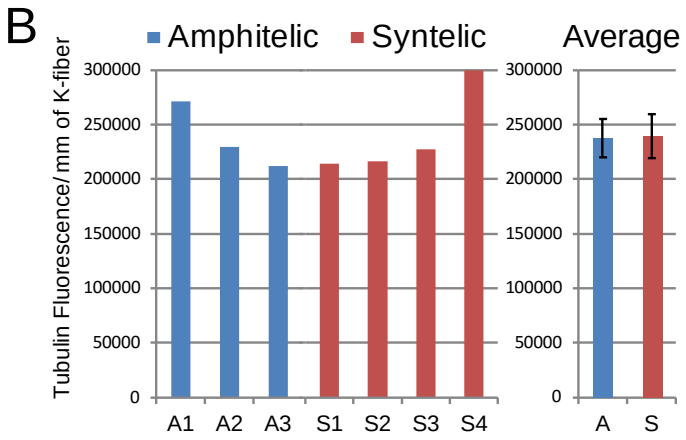

Figure 3.5: Amphitelic and NOD-mCherry-induced syntelic attachments have comparable k-fiber fluorescence intensity. *(A)* Maximum projection of two-color confocal Z-sections from a NOD-mCherry-expressing cell with syntelic attachments (S1-S4) and bioriented chromosomes with amphitelic attachments (A1-A3). *(B)* Quantification of k-fiber fluorescence intensity of the amphitelic (A1-A3) and syntelic attachments (S1-S4) highlighted in (A). The tubulin fluorescence presented in the bar graph is the integrated fluorescence intensity per micrometer of k-fiber.

We further probed the stability of NOD-induced syntelic attachments using a cold-stability assay, which selectively preserves microtubules that are stably bound to kinetochores. Induced NOD-mCherry, GFP-α-tubulin expressing cells were treated with the proteasome inhibitor MG132 to arrest mitotic cells and were kept at room temperature or placed at 4°C for 1 hour before fixing and staining the microtubules by IF (Figure 3.6A). Spindle fluorescence intensity and NOD-mCherry signals were quantified for control and cold-treated cells. Spindle fluorescence was 1.5X brighter in cells expressing high levels of NOD compared to cells with low or undetectable NOD-mCherry for both control and cold-treated cells. Only kinetochore fibers remained after 1 hour at 4°C, as reflected by a 3.7-fold reduction in the fluorescence intensity of spindle microtubules in both high and no/low NOD expressing cells (Figures 3.6B and 3.6C). The stability of syntelic attachments was further evidenced by the fact that both bioriented and syntelic attachments persisted within the same cold-treated spindles (Figure 3.6B).

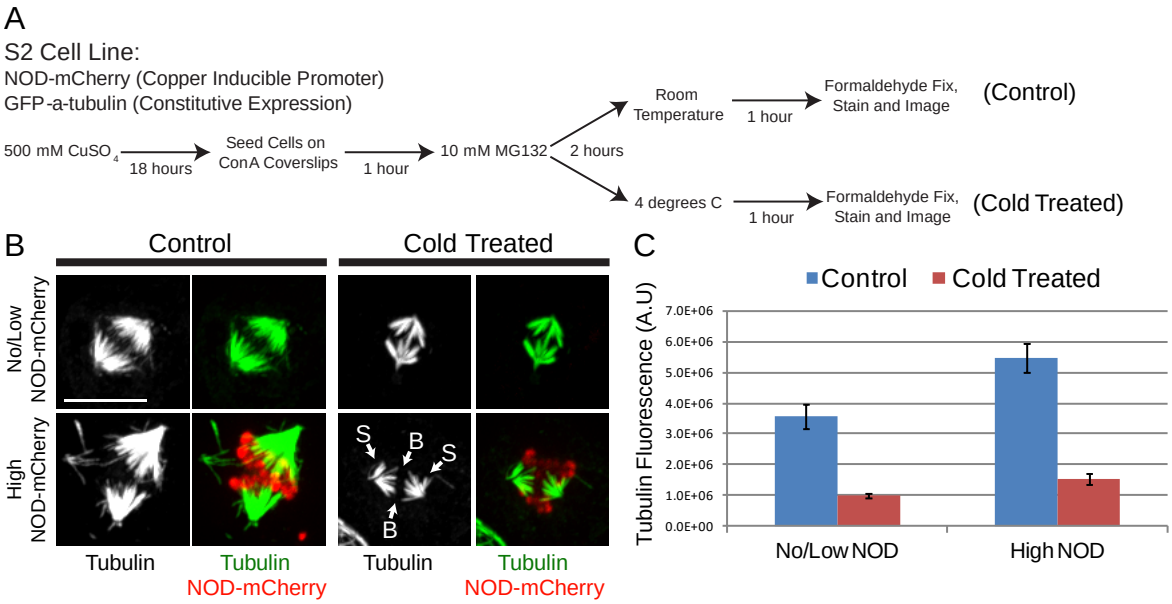

Figure 3.6: NOD-mCherry-induced syntelic attachments are cold stable. *(A)* Flow chart outlining the cold stability assay used to probe syntelic k-fiber stability. *(B)* Micrographs of no/low NOD-mCherry- and high NOD-mCherry-expressing control and cold-treated cells. Note that both syntelic (S) and bioriented (B) chromosomes retain their k-fibers equally after cold treatment. *(C)* Quantification of tubulin fluorescence intensity for no/low NOD-mCherry- and high NOD-mCherry-expressing cells for control and cold-treated cells. Error bars represent the SEM. Bars, 10 µm.

Levels of the checkpoint protein Mad1 are low at stably attached kinetochores and high at unattached kinetochores (Chen et al., 1998; Shah et al., 2004). To investigate whether Mad1 levels were reduced at the syntelic attachments produced by NOD expression, we generated and imaged a stable cell line co-expressing inducible NOD-mCherry and Mad1-YFP under the control of its endogenous promoter. Induced cells were arrested in mitosis with MG132 and the same cell was imaged by spinning disk confocal microscopy both before and after depolymerizing microtubules with colchicine (Figure 3.7A). Syntelic and bioriented kinetochores had low levels of Mad1-YFP in MG132-treated cells before colchicine treatment (Figure 3.7B). Depolymerizing microtubules with a 15-minute colchicine treatment resulted in a ~22-fold average increase in kinetochore-associated Mad1 in NOD expressing cells. The observed reduction of Mad1 at kinetochores is consistent with the observation of anaphase onset in cells with NOD-stabilized syntelic attachments. A more detailed examination of the kinetics of mitotic progression and checkpoint protein depletion from syntelic attachments will be the focus of future work. Taken together, our findings support the conclusion that the stability of syntelic attachments is comparable to the stability of bioriented attachments in NOD-expressing cells.

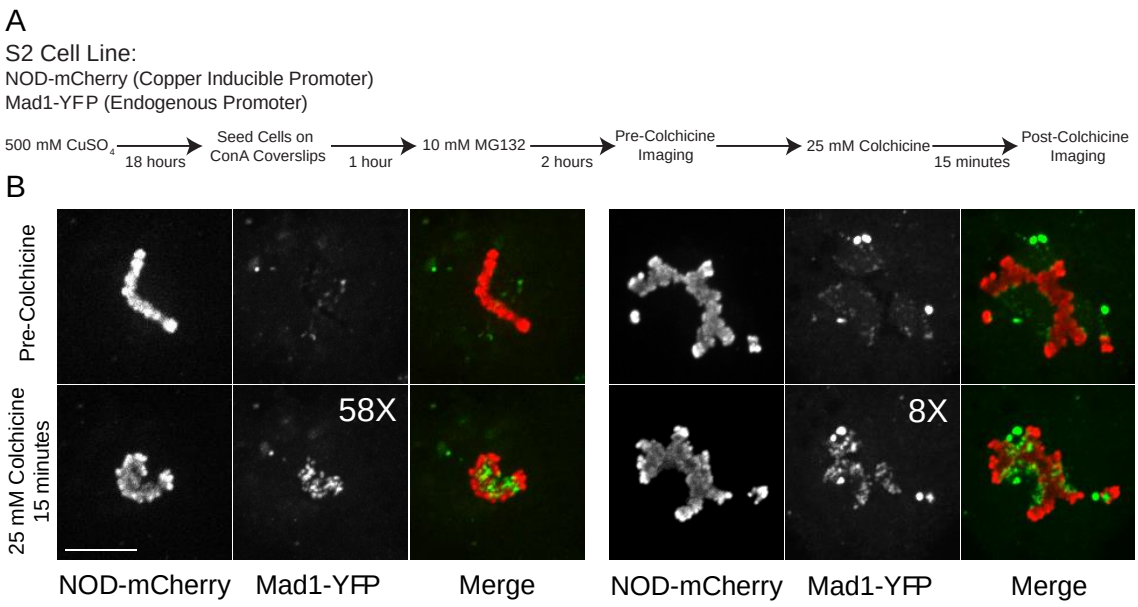

Figure 3.7: NOD-mCherry-induced syntelic attachments exhibit reduced levels of Mad1. *(A)* Flow chart outlining the protocol used to examine Mad1 reduction at syntelic attachments. *(B)* Spinning disk confocal imaging of NOD-mCherry- and Mad1-YFP-expressing cells before and after a 15-min colchicine treatment to depolymerize the spindle microtubules. The fold increase (58× and 8×) in Mad1 levels after the colchicine treatment is shown for each cell. Bars, 10 µm.

3.2.4 Two types of chromatin stretch events occur in NOD overexpressing cells via distinct microtubule-chromatin interactions

Elevated away-from-the-pole force production was evidenced by frequent chromatin stretching events in which NOD-mCherry-coated chromatin extended away from chromosome arms. Stretch events were only observed in NOD expressing cells and required microtubules (unpublished observation). Therefore, we employed near simultaneous two-color spinning disk confocal imaging of cells expressing NOD-mCherry and GFP-α-tubulin to more closely examine the relationship between chromatin stretches and dynamic microtubules (Figure 3.8A). Two distinct categories of microtubule-chromosome interactions were observed – glancing and polymerizing. In glancing interactions, chromatin laterally interacted with microtubules that extended beyond the chromosome. Polymerizing interactions, in contrast, occurred when growing microtubules collided with the chromatin in an end-on orientation. In one clear example of a glancing interaction, chromatin stretched toward the plus end of a microtubule after making lateral contact with the microtubule; the stretch persisted for ~15 seconds until the chromatin recoiled when the microtubule depolymerized (Figures 3.8B and 3.8D). The same chromosome also underwent two definitive polymerizing interactions in which stretch events coincided with polymerizing microtubules. During one of the polymerizing interactions, the growing microtubule visibly buckled as the chromatin reached maximum stretch and began to recoil (Figures 3.8C and 3.8D).

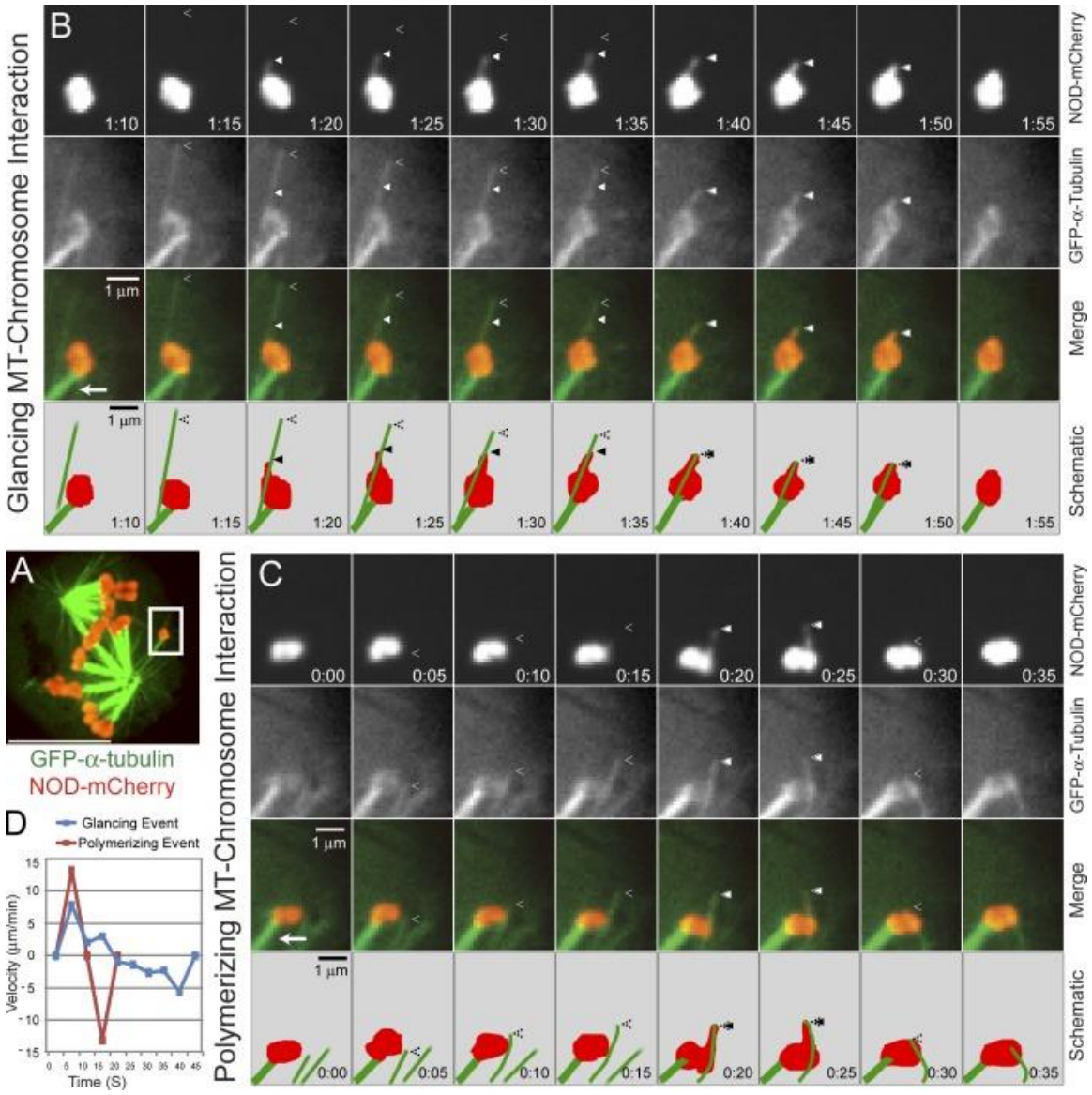

Figure 3.8: NOD-dependent chromatin stretching events are associated with two different types of microtubule-chromatin interactions. *(A)* A whole cell two-color confocal image of a GFP-α-tubulin (green)- and NOD-mCherry (red)-expressing S2 cell with the chromosome shown in B and C highlighted (white box). *(B and C)* Selected frames from confocal time-lapse imaging of chromatin stretching events. The chromosome is attached to the pole through kinetochore microtubules (bottom left corner, arrow). *(B)* An example of a chromatin stretching event extending along a microtubule that makes a glancing interaction with the chromosome. The chromatin is stretched toward the plus end before it is retracted coincident with the depolymerizing microtubule. *(C)* A chromatin stretching event that is associated with a polymerizing microtubule-chromosome interaction. Note that the chromatin stretches along with the

polymerizing microtubule before pausing and then rapidly retracting, causing the microtubule to buckle. The separation between the plus end of the microtubule and the stretched chromatin at t = 15 s is a consequence of sequential imaging. *(D)* A plot of velocity versus time for the two stretch events shown in B and C. The positive values represent extension velocities and the negative values reflect recoil velocities. Closed arrowheads denote the leading edges of stretched chromatin and open arrowheads mark the microtubule plus ends. Bars: (A) 10 µm; (B and C) 1 µm.

We reasoned that careful analysis of chromatin stretching events would provide insight into the molecular mechanism of force production by NOD. Stretched chromatin extended an average distance of 0.94 µm (0.6-1.4 µm range) from the chromosome before recoiling (Figure 3.9A). While stretch distances were largely uniform, two distinct types of stretch dynamics were observed – rapid and persistent. Stretch events were classified as "rapid" if complete extension and retraction onset occurred within 10 seconds. Events with an extension phase lasting 10 seconds or longer were deemed "persistent" (Figure 3.9A). Polymerizing microtubule-chromosome interactions coincided with rapid stretch events whereas glancing microtubule-chromosome interactions were associated with persistent events (Figures 3.8B and 3.8C). The stretched NOD-mCherry signals were reporting on chromatin dynamics, as the stretches contained phospho-histone-H3 (Figure 3.9B) and always recoiled (Figures 3.10E and 3.10F). The average extension velocity for a rapid event was 10.4 +/- 2.2 µm/min, which was more than twice the average velocity of 4.2 +/- 2.9 µm/min for persistent events (Figure 3.9C). However, rapid and persistent events were not differentiated solely by their extension velocities. Rapid events were simple: maximum extension of the chromatin was achieved within 10s at an average rate of ~10.4 +/- 2.2 µm/min (Figure 3.9D) before the chromatin completely recoiled within the next 5-10 seconds. Persistent stretch events were more complicated. The extension phase of a persistent stretch typically lasted 10-20 seconds and the extension velocity varied over time, starting at 8.1 +/- 1.1 µm/min early and decreasing over time to ~2.3 +/- 1.2 µm/min (Figure 3.9D). Because the

timescale of stretching was similar to our initial imaging frequency (5 seconds), stretch events were examined with higher temporal resolution by acquiring images at 1.5 - 2 second intervals. The additional data thereby obtained for individual stretch events afforded a more detailed view of their dynamic properties (Figures 3.10A and 3.10B). It is apparent from kymographs of chromatin stretching that rapid events are uniform in their extension and recoil phases with comparable velocities, while persistent events are complex and vary in both their extension and recoil velocities. Thus, NOD-mediated chromatin stretching events are characterized either by (i) rapid ~10 µm/min bursts that are followed by rapid recoiling, or (ii) more complicated gradual extensions and recoils that change velocity over time.

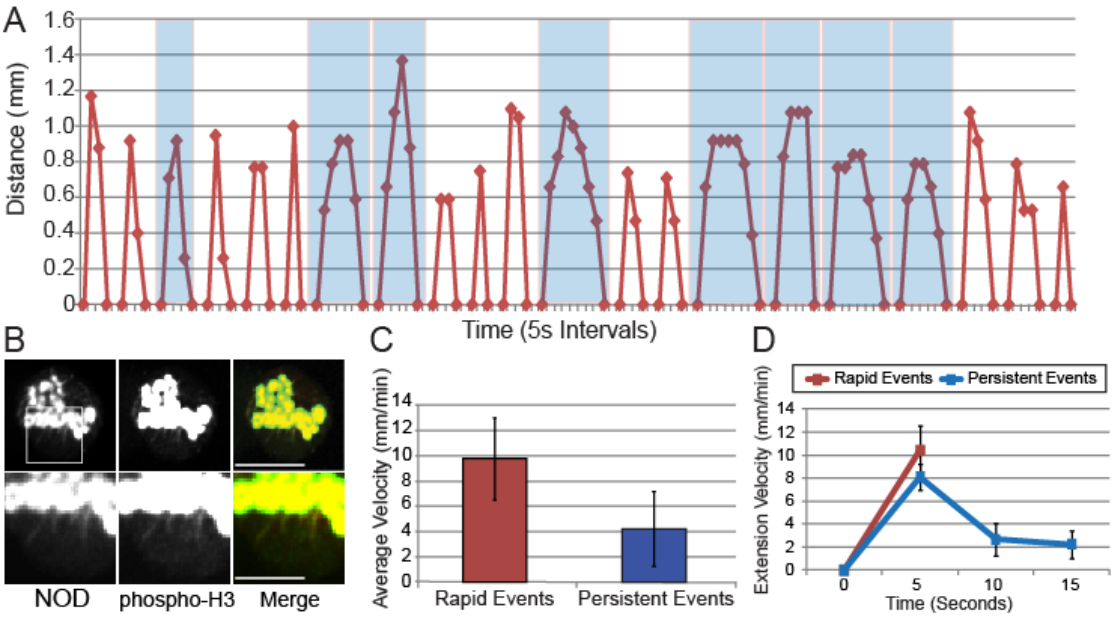

Figure 3.9: Two types of chromatin stretch events occur in NOD-mCherry-expressing cells. (A) Plot of distance versus time (5-s intervals) for 21 separate chromatin stretching events. Persistent stretch events are highlighted in blue. (B) NOD-mCherry stretches contain phospho-H3 (Serine 10)-positive chromatin. NOD is red and phospho-H3 is green in the merged image. (C) The mean extension velocities of rapid and persistent stretch events. (D) Chromatin in rapid events extends at ~10 µm/min, whereas extension in persistent events starts at ~8 µm/min and slows over time to ~2 µm/min. Bars: B, top 5 µm; B, bottom 2.5 µm.

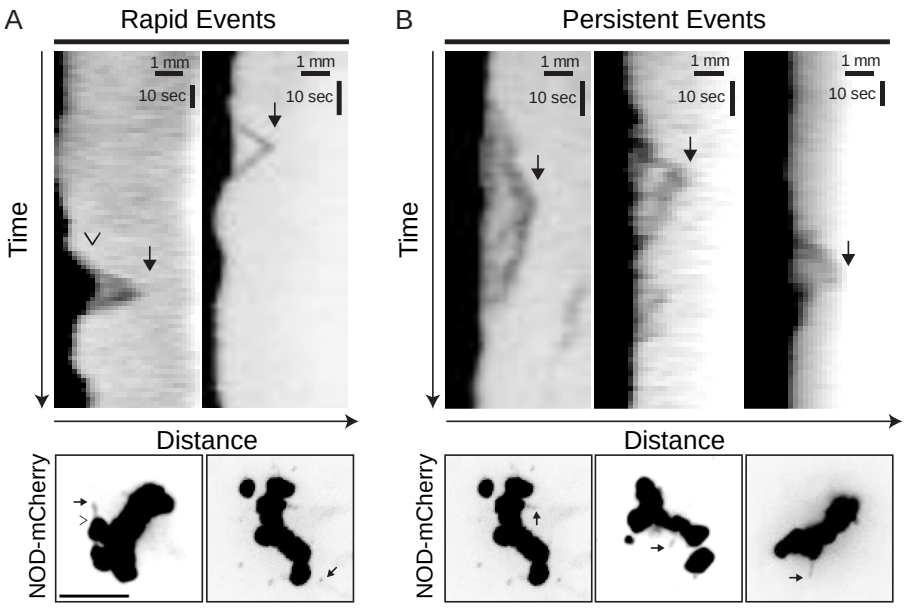

Figure 3.10: Rapid and persistent stretch events exhibit different patterns of extension and recoil velocity. *(A and B)* Kymographs of rapid and persistent stretch events imaged by spinning disk confocal microscopy with high temporal resolution (1.5-2 s intervals). Whole cell images are shown below each kymograph highlighting the stretch event that is represented in the kymograph. In the first image, the open arrowhead marks the periphery of the chromosome and the solid arrow marks the edge of the stretch event. Stretches are highlighted in subsequent images with solid arrows. *(A)* Rapid events exhibit rapid and uniform extension and recoil velocities. *(B)* Persistent stretch events exhibit variable extension and recoil velocities over time. Bars: Bottom, 5 µm; Top, 1 µm (horizontal) and 10 s (vertical).

3.2.5 NOD associates with the plus ends of polymerizing microtubules

The average extension velocity of rapid stretch events closely approximated the reported microtubule growth rate of 10.8 μm/min in mitotic S2 cells. Furthermore, physical interactions must exist between the growing plus end of a microtubule and NOD-mCherry-coated chromatin for microtubule buckling to occur (Figure 3.8C). Thus, the characteristics of NOD-dependent rapid stretch events are in agreement with the hypothesis that NOD generates PEFs by end-tracking on polymerizing microtubules. To further test if rapid stretch events associated with growing microtubule plus ends, a stable cell line co-expressing EB1-GFP, which labels the plus ends of polymerizing microtubules, and inducible NOD-mCherry was created (Figure 3.11). Rapid chromatin stretch events co-localized with EB1-GFP comets (Figures 3.11B and 3.11C) and disappearance of the EB1 comets coincided with maximal chromatin stretch, indicating that the microtubule with which the chromatin was interacting had ceased polymerizing. Small pieces of NOD-coated chromatin were sometimes torn from chromosome arms and transported through the cytoplasm. NOD-positive fragments were significantly smaller than the smallest chromosome (number 4) in *Drosophila*. A subset of motile NOD-mCherry fragments co-localized with EB1-GFP comets (Figure 3.11D). A closer look at motile NOD-mCherry fragments in cells co-expressing GFP-α-tubulin also revealed that they tracked the plus ends of microtubules (Figures 3.11E-3.11G). Thus, our data support the hypothesis that NOD is capable of generating PEFs through association with polymerizing microtubule plus ends.

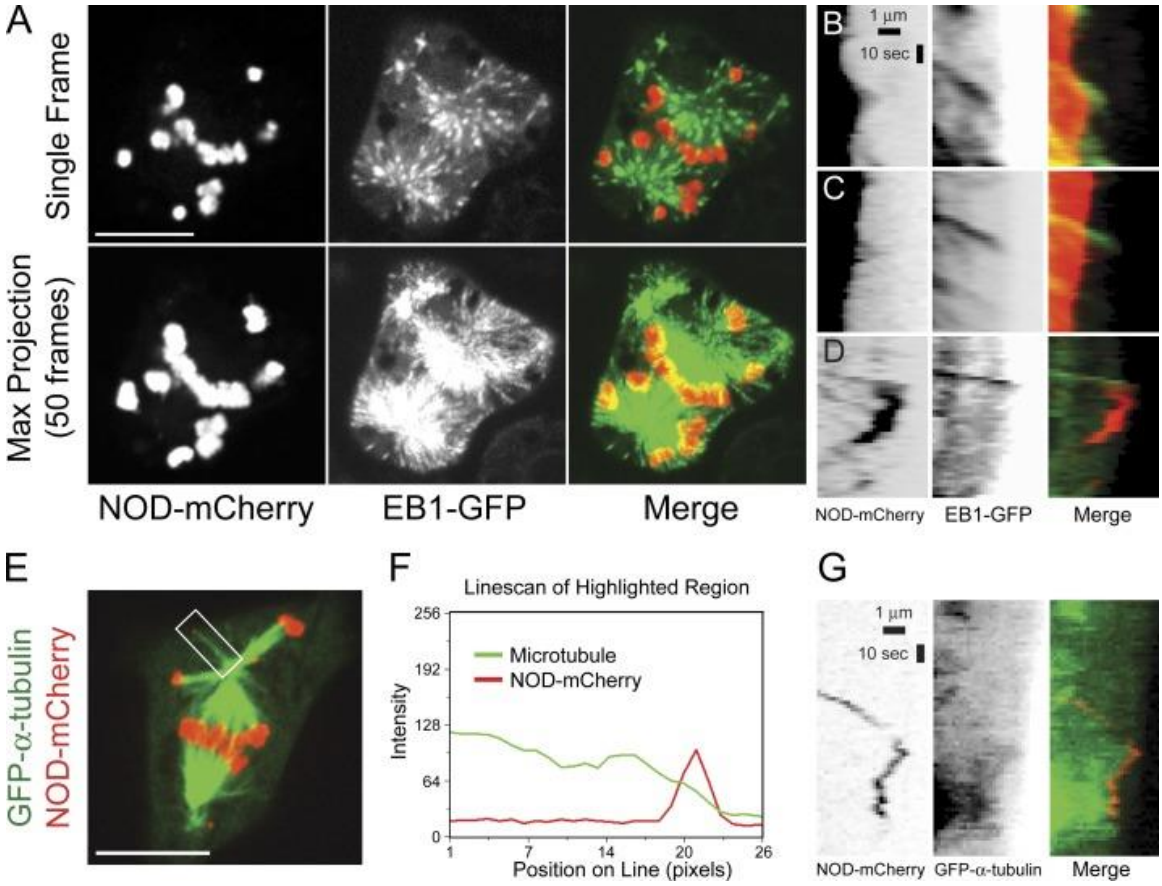

Figure 3.11: High spatial and temporal resolution imaging reveals that NOD-mCherry associates with the ends of polymerizing microtubules. *(A)* Selected frame (top) and maximum projection of 50 frames (bottom) from a confocal time lapse of an EB1-GFP (green)- and NOD-mCherry (red)-expressing S2 cell. *(B-D)* Kymographs of NOD-mCherry and EB1-GFP. *(B and C)* The extension phases of two rapid stretch events that colocalize with EB1-GFP comets are shown. *(D)* A NOD-mCherry spot that is propelled through the cytoplasm colocalizes with an EB1-GFP comet. *(E–G)* NOD-mCherry tracks on dynamic microtubules. *(E)* Selected frame from a confocal time lapse of a GFP-α-tubulin (green)- and NOD-mCherry (red)-expressing mitotic S2 cell showing a NOD-mCherry fragment localized at the microtubule plus end. The fragment is considerably smaller than the syntelically attached chromosome 4 located below it. (F) Line scan of the highlighted region shown in E. *(G)* Kymographs of NOD-mCherry and GFP-α-tubulin during a tracking event. NOD-mCherry (red) tracks the growing, shortening, and paused plus end of the microtubule (green). Bars: (A and E) 10 µm; (B-D and G) 1 µm (horizontal) and 10 s (vertical).

3.2.6 NOD chimeras with either plus end-directed motility or tip tracking activity produce PEFs

The observation of two types of chromatin stretch events associated with different chromatin-microtubule interactions suggested that PEFs could be produced by two distinct force-producing activities. To further investigate this possibility, two NOD chimeras were created to specifically isolate the contributions of plus end-directed motility and microtubule tip-tracking to kt-MT stabilization in the PEF assay (Figure 3.12A). In one chimera, the motor domain of NOD was replaced with EB1. The EB1-NOD-mCherry chimera exhibited plus end tip-tracking in interphase and became highly enriched on chromosomes during mitosis (Figures 3.12B and 3.12C). EB1-NOD-dependent stretch events were observed with lower frequency than in NOD-expressing cells although, like NOD-dependent chromatin stretching, EB1-NOD stretches extended 1-2 µm in length (Figure 3.12D). The dynamics of EB1-NOD-dependent stretches were similar to those of rapid NOD-dependent stretch events, as maximum extension in the EB1-NOD cells was completed within less than 10 seconds (average = 7.6 seconds). The average extension velocity of EB1-NOD stretches was 7.6 +/- 2.1 µm/min, which was slower than the rapid stretches observed in NOD overexpressing cells. Furthermore, pause events were more frequent during EB1-NOD stretches compared to rapid NOD-dependent stretching. Nonetheless, EB1-NOD-mCherry expression stabilized syntelic attachments in a dose-dependent manner albeit with significantly lower efficiency than wild type NOD-mCherry (Figures 3.12C, 3.12E and 3.12J).

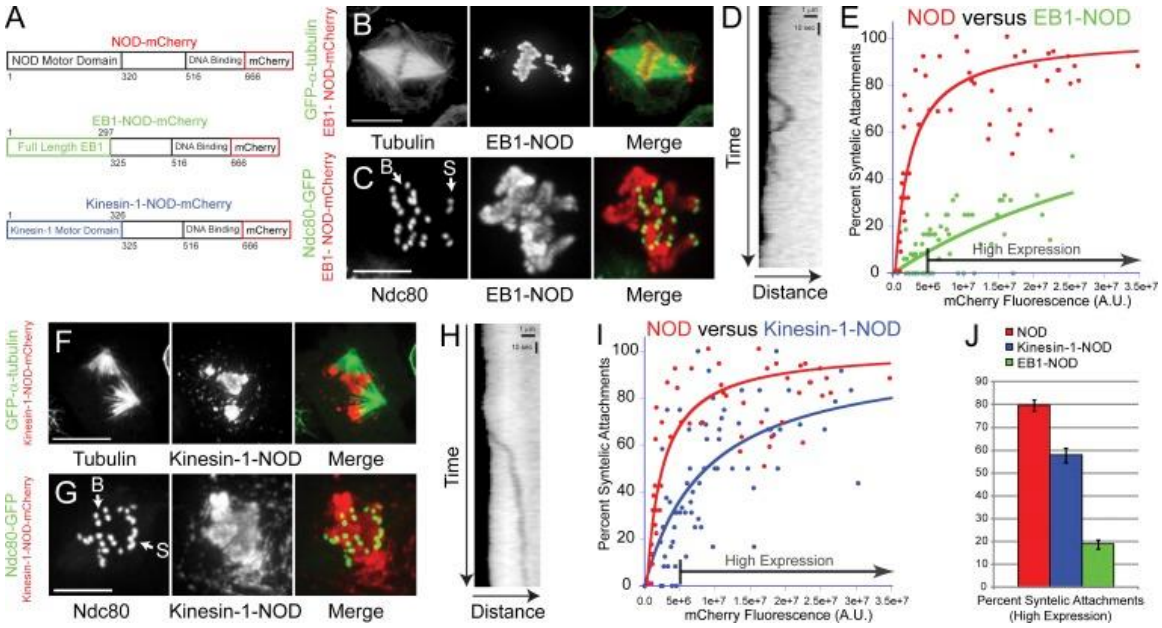

Figure 3.12: Syntelic attachments are stabilized by NOD chimeras that possess either plus end-directed motility or tip-tracking activity. *(A)* Schematic diagrams of full length NOD-mCherry and EB1- and kinesin-1-NOD-mCherry. *(B)* Maximum intensity projection of a GFP-α-tubulin (green)- and EB1-NOD-mCherry (red)-expressing S2 cell showing enrichment of EB1-NOD on chromosomes and the presence of misaligned chromosomes. *(C)* Maximum intensity projection of a cell expressing Ndc80-GFP (green) and EB1-NOD-mCherry (red) with syntelic (S) and bioriented (B) attachments. *(D)* Kymograph of a rapid EB1-NOD-mediated chromatin stretch event. *(E)* Plot of percentage of syntelic attachments versus mCherry fluorescence for EB1-NOD cells. EB1-NOD-mCherry overexpression stabilizes syntelic attachments at a significantly lower frequency than wild-type NOD-mCherry (NOD, *n* = 57 cells; EB1-NOD, *n* = 71 cells). *(F)* Maximum intensity projection of a GFP-α-tubulin (green)- and kinesin-1-NOD-mCherry (red)-expressing cell showing aberrant spindle morphology. *(G)* Maximum intensity projection of an Ndc80-GFP (green)- and kinesin-1-NOD-mCherry (red)-expressing S2 cell with a mixture of syntelic (S) and bioriented (B) attachments. *(H)* Kymograph of a persistent kinesin-1-NOD-mediated chromatin stretch event. *(I)* Plot of percentage of syntelic attachments versus mCherry fluorescence for kinesin-1-NOD cells. Kinesin-1-NOD-mCherry overexpression induces a dose-dependent increase in the percentage of syntelic attachments that rises more slowly and plateaus at a lower percentage of syntelics than the corresponding increase seen for wild-type NOD-mCherry (NOD, *n* = 57 cells; kinesin-1-NOD, *n* = 72 cells). *(J)* The percentage of syntelic attachments in high-expressing cells (defined as >5.0e6 A.U.) for NOD-, kinesin-1-NOD-, and EB1-NOD-mCherry-expressing cells. Two-tailed p-values are <0.0005. Error bars are the SEM. Curves were fit with a hyperbolic function. R

values are 0.66 (EB1-NOD), 0.7 (kinesin-1-NOD), and 0.86 (NOD). Bars: (B and F) 10 µm; (C and G) 5 µm; (D and H) 1 µm (horizontal) and 10 s (vertical).

In the second NOD chimera, the motor domain of NOD was replaced with the motor domain of human kinesin-1, a highly processive plus end-directed motor (Block et al., 1990; Hackney, 1995; Howard et al., 1989). Kinesin-1-NOD-mCherry stabilized syntelic attachments in a dose-dependent manner with greater potency than EB1-NOD but with lower efficiency than wild type NOD-mCherry (Figures 3.12G, 13.12I and 13.12J). Expression of kinesin-1-NOD-mCherry resulted in chromatin being extensively stretched from chromosome arms (Figures 3.12F-3.12H). Interestingly, neither of the chimeras, each of which possesses a unique but singular force-producing activity, was capable of stabilizing syntelics as efficiently as wild type NOD (Figures 3.12E, 3.12I and 3.12J).

Chromosomes are positioned at the periphery of monopolar spindles by PEFs (Levesque and Compton, 2001; Stumpff et al., 2012; Wandke et al., 2012). To further test if the chimeras produced PEFs we tested how expression of the NOD chimeras affected chromosome positioning in monopoles. NOD depletion resulted in the inward movement of kinetochores and chromosome arms within monopoles (Figure 3.13). Notably, the effects of NOD depletion could be rescued by overexpressing either EB1-NOD-mCherry or kinesin-1-NOD-mCherry (Figures 3.13A-3.13C). Taken together, results from the PEF and monopolar spindle assays demonstrate that a chromosome-associated protein with either plus end-directed motility or tip-tracking activity can generate PEFs.

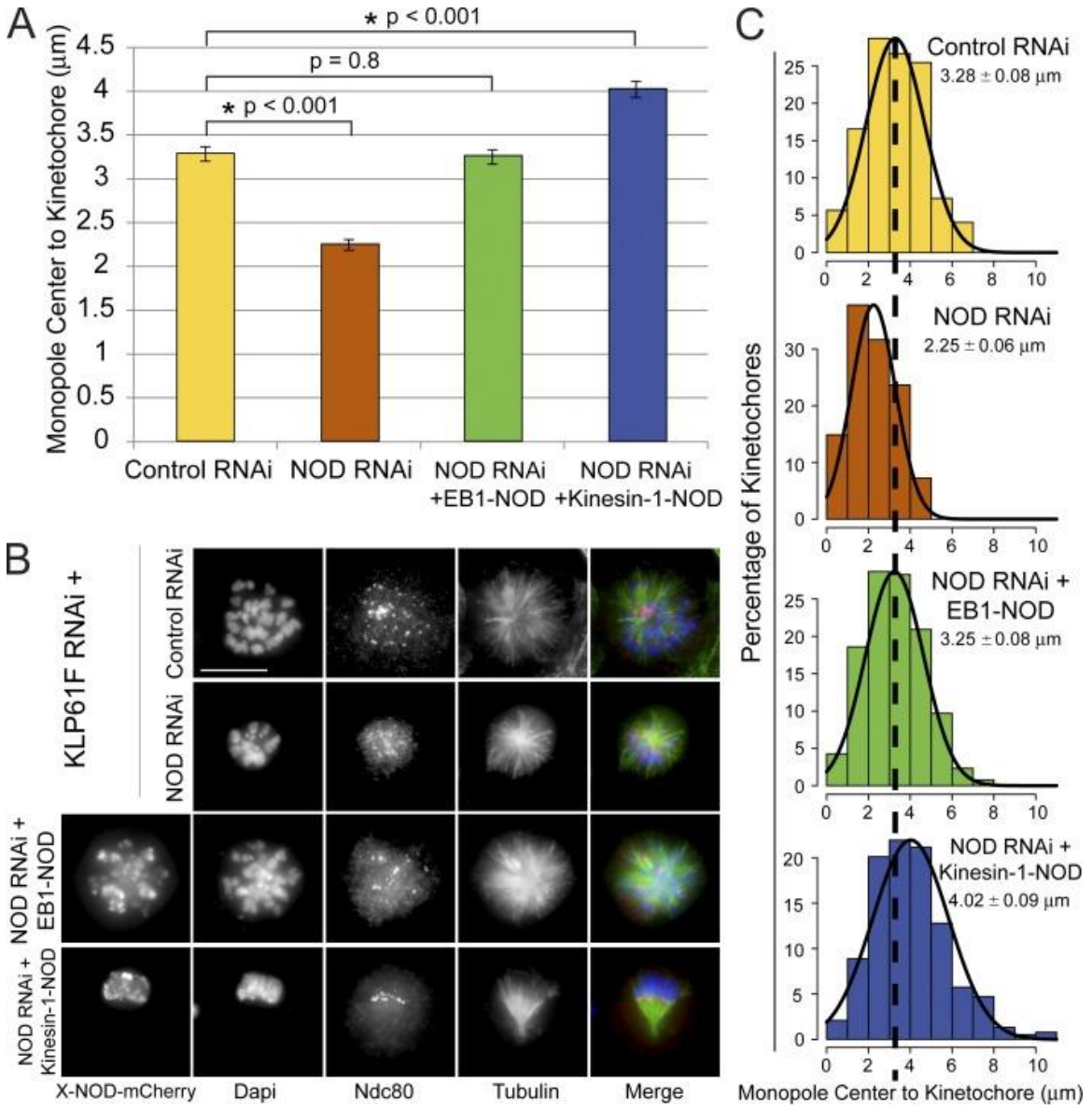

Figure 3.13: NOD chimeras with either plus end-directed motility or tip-tracking activity produce PEFs. *(A)* Distance between the monopole center and Ndc80-stained kinetochores. The distance between kinetochores and monopole centers decreased by 30% in the absence of NOD and was rescued in NOD-depleted cells by inducing either EB1-NOD-mCherry or kinesin-1-NOD-mCherry (control, *n* = 283 kinetochore pairs; NOD RNAi, *n* = 302; NOD RNAi + EB1-NOD-mCherry, *n* = 293; NOD RNAi + kinesin-1-NOD-mCherry, *n* = 383). Error bars are SEM. *(B)* Representative maximum projection images for each condition. Monopoles were generated in each condition by depleting Klp61F. The chimeric NOD-mCherry protein is shown only in black and white. In the merged images DNA is blue, Ndc80 is red, and microtubules are green. *(C)* Histograms of the distribution of pole-kinetochore measurements for the four experimental conditions each fit with a Gaussian function (black lines). The dashed line

extending through the histograms marks the mean pole-kinetochore distance in control RNAi-treated cells. Two-tailed p-values are shown. Bar, 10 µm.

3.3 Discussion

3.3.1 A live-cell assay for studying tension-dependent kt-MT stabilization

Over 40 years ago, Nicklas and Koch (Nicklas and Koch, 1969) stabilized erroneous kt-MT attachments in grasshopper spermatocytes by artificially creating tension with microneedles. We propose that NOD overexpression is the molecular equivalent of Nicklas' microneedles and that elevated PEFs produced by NOD overexpression stabilize syntelic attachments by introducing tension at kinetochores. The pioneering spermatocyte studies provided the first direct evidence that tension regulates interactions between chromosomes and the spindle. However, the use of microneedles is technically challenging, requires significant time-investment per cell/experiment, and is restricted to a small number of manipulatable cell types that are not genetically tractable. The PEF assay developed here overcomes these previous limitations because (i) force application simply requires the addition of $CuSO_4$ to the growth media, (ii) proteins of interest in *Drosophila* S2 cells can be readily manipulated by RNAi, overexpression and molecular engineering and (iii) the assay is scalable because many cells can be examined in one experiment. Consequently, we envision that the PEF assay will provide a powerful tool for studying tension-dependent regulation of kt-MT attachment stability in living cells.

3.3.2 PEFs are well-positioned to regulate chromosome oscillations and error correction

Since its discovery, the PEF has been implicated in chromosome positioning via regulation of both chromosome oscillation and congression.

During chromosome oscillations, movement is driven by the poleward moving or leading kinetochore. The poleward moving kinetochore remains attached to its depolymerizing kinetochore fiber (k-fiber) and pulls the lagging sister kinetochore, which must elongate its k-fiber by microtubule polymerization (Khodjakov and Rieder, 1996). A change in direction has been hypothesized to be triggered by the introduction of tension at the leading kinetochore as it approaches the pole and experiences increasing levels of opposing PEFs (Figure 3.14A and (Ke et al., 2009; Rieder et al., 1986; Rieder and Salmon, 1994; Skibbens et al., 1993)). Our observations support this model and are in agreement with recent cell-based examinations of the contribution of PEFs to chromosome behavior (Stumpff et al., 2012; Wandke et al., 2012) as well as the finding that the application of tension to MT-associated kinetochore particles inhibited catastrophes and promoted rescues (Akiyoshi et al., 2010). Thus, emerging evidence supports chromosome oscillation models where the introduction of tension by PEFs at the leading kinetochore promotes a directional switch by rescuing depolymerizing kt-MTs.

The fact that ~80% of the attachments in high NOD expressing cells are syntelic suggests that most chromosomes establish improper attachments before becoming bioriented. This mirrors a recent characterization of chromosome biorientation in meiosis I mouse oocytes, where ~90% of chromosomes experienced at least one round of Aurora kinase-dependent error correction before biorientation (Kitajima et al., 2011). Thus, transient formation of incorrect attachments is commonplace during cell division. Interestingly, improperly

attached chromosomes often move to the spindle poles where they remain until error correction occurs (Lampson et al., 2004). Misoriented chromosomes must experience increasingly higher levels of PEFs as they move poleward (Figure 3.14A). Hence, the fact that elevated PEFs counteract error correction presents a conundrum: the spindle pole, where error correction often takes place, is also where PEFs are highest. Over time, baseline error correction mechanisms may win out over the stabilizing effects of the PEFs. Alternatively, other kt-MT attachment destabilizing activities may exist to counter the stabilizing effects of PEFs.

Our findings also bear upon the interplay between force-dependent stabilization of kt-MT attachments and Aurora B-mediated error correction. Application of force to reconstituted kinetochore particles stabilized kt-MT attachments in the absence of Aurora B (Akiyoshi et al., 2010). We have shown that the application of force to kinetochores in living cells stabilize kt-MT attachments even in the presence of active Aurora B. Thus, kinetochore tension is capable of overpowering the ability of Aurora B to mediate error correction without compromising its activity.

3.3.3 How does NOD generate force?

Our data support the hypothesis that NOD end-tracks on polymerizing microtubules. But what is the molecular basis of NOD end-tracking? The fact that NOD fragments associated with paused and depolymerizing microtubule plus-ends, when EB1 is absent (Figure 3.11G), suggests that NOD could track

non-polymerizing microtubule ends in an EB1-independent manner although tracking on polymerizing ends by NOD may require EB1. NOD end-tracking has been envisioned as an EB1-independent phenomenon although it has never been directly demonstrated (Cochran et al., 2009). Thus, it will be important to determine whether NOD behaves like budding yeast dynein, which is targeted to microtubule plus ends independent of EB1 (Carvalho et al., 2004; Markus et al., 2011), or like MCAK (kinesin-13), which contains an S/TxIP motif and exhibits EB1-dependent tip tracking (Domnitz et al., 2012).

Since NOD has never been shown to possess plus end-directed motility in vitro, it is currently classified as a non-motile kinesin. However, the observation of persistent chromatin stretching events that moved along the sides of microtubules towards the plus ends provides compelling evidence that NOD could exhibit plus end-directed motility in cells. We feel this work strongly supports the NOD end-tracking hypothesis but does not rule out plus end-directed motility as another potential source of force production by NOD. It will be worthwhile to further test the hypothesis that NOD possesses two force-producing activities.

3.3.4 PEF generation through multiple mechanisms

Microtubule polymerization and molecular motors have long been proposed as possible sources of the PEF (Rieder et al., 1986; Rieder and Salmon, 1994) and the focus has rightfully been placed on molecular motors since the discovery of chromokinesins. Here we report that PEFs can be

generated, not only by plus end-directed chromokinesins, but also by chromosome-associated factors that associate with polymerizing plus ends (Figure 3.14B). Thus, it may be time to look beyond the motility of kinesin-10 motors and consider chromosome-based tip-tracking factors as potential mediators of PEF production.

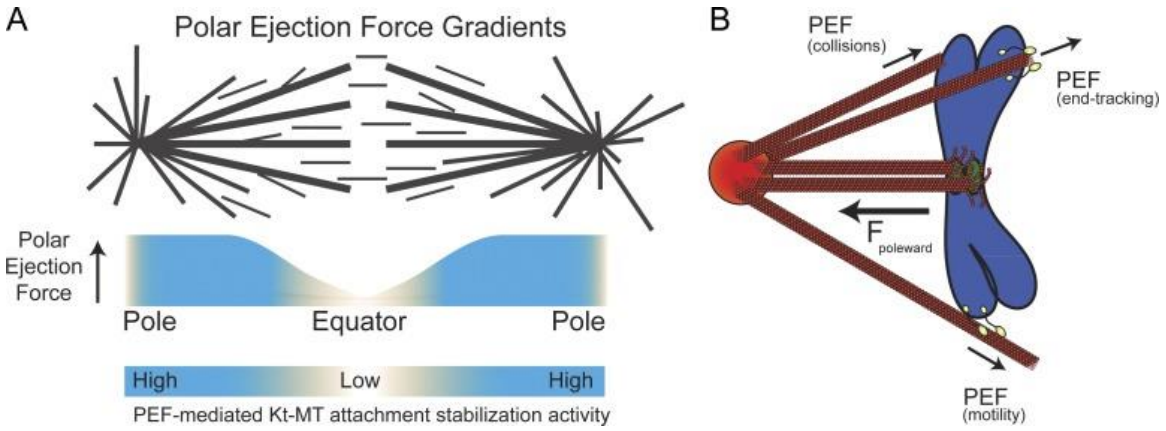

Figure 3.14: Models for PEF-based modulation of error correction around spindle poles and sources of PEF production. *(A)* A model of PEF gradients across the metaphase spindle predicts that as a chromosome approaches a spindle pole it will experience progressively higher levels of PEF-mediated kt-MT stabilization because of elevated tension at kinetochores. *(B)* Model for generation of PEFs that oppose kinetochore-mediated pulling forces to create tension at kinetochores. We propose that chromosome-associated proteins with either plus end-directed motility or end tracking activity can generate PEFs.

3.4 Materials and methods

3.4.1 Cell culture

Drosophila S2 cells were cultured at 24°C in Schneider's media (Life Technologies) supplemented with 10% heat inactivated fetal bovine serum (Life Technologies) and 0.5X antibiotic-antimycotic cocktail (Life Technologies).

3.4.2. Generation of S2 cell lines

The *Drosophila melanogaster* NOD gene (CG1763) was amplified from cDNA clone SD02282 with a 5' KpnI site and 3' SpeI site. The resulting product was inserted into the multiple cloning site of a pMT/V5 His-B vector (Invitrogen) containing the mCherry gene. The NOD-EGFP construct was generated by inserting the NOD gene between the 5' KpnI and 3' SpeI sites in the pMT/V5 His-B vector containing the EGFP gene, lacking a stop codon, inserted between the second XbaI and SacII sites. Motorless NOD was produced by PCR amplification of the portion of the NOD gene corresponding to aa 325-666. The Kin1-NOD and EB1-NOD cells were both produced by ligating the Kinesin 1 and EB1 regions into the motorless NOD vector. For the Kin1-NOD cells, the motor domain (corresponding to aa 1-326) of Human kinesin-1 (gift of Jennifer Ross, UMASS, Amherst) was amplified with 5' XbaI and 3' KpnI cut sites flanking the gene by PCR. To produce the EB1-NOD cell line, a full length *Drosophila* EB1 isoform variant A (CG 3265) was amplified from a cDNA clone with 5' XbaI and 3' KpnI sites and inserted upstream of motorless NOD-mCherry. See Table I for the primers used in cloning. All cell lines were generated by transfecting DNA

constructs into S2 cells using the Effectene Transfection Reagent system (Qiagen), according to product directions. The transfected cells were grown in Schneider's media (Invitrogen) containing 10% Fetal Bovine Serum (Invitrogen). After 4 days, they were transferred to a 25 cm^2 flask. Cells were then grown in media containing Blasticidin at a concentration of 0.025 mg/ml until cell death ceased. At that point cells were maintained in media containing no Blasticidin. Cell lines were induced by adding 500 µM $CuSO_4$ for 6-18 hours. .

3.4.3 Production of double-stranded RNAs (dsRNAs)

DNA templates for NOD (CG1763) and KLP61F (CG9191) were produced to contain approximately 500 bp of complementary sequence flanked with the T7 promoter sequence. dsRNAs were synthesized overnight at 37°C from the DNA templates using the T7 RiboMax™ Express Large Scale RNA Production System (Promega). For RNAi experiments, media was aspirated off semi-adhered cells at 25% confluence and replaced with 1 ml of serum-free Schneider's medium containing ~20 µg of dsRNA. After 1 hour, 1 ml of fresh Schneider's + FBS was added to the wells and incubated for 2-4 days at 24°C.

3.4.4 Live-cell imaging

Cells were seeded onto Concanavalin A (Sigma) treated acid-washed coverslips (Corning) for 1 hour. The coverslips were assembled into rose chambers containing Schneider's media and imaged at room temperature. Cells were imaged on two different spinning disk confocal systems: 1) a Nikon TE300 microscope stand equipped with a CSU10 spinning disk confocal head

(Yokogawa) attached to a cooled CCD Orca ER camera (Hamamatsu) using a Nikon 100X 1.4 NA Plan Apochromat (Apo) differential interference contrast (DIC) objective, and 2) a Nikon TiE inverted microscope with a CSU-X1 spinning disk confocal head (Yokogawa) and an iXON EMCCD camera (Andor Technology) using a Nikon 100X 1.4 NA Plan Apo violet corrected (VC) series DIC objective. MetaMorph software (Molecular Devices) was used to control the imaging systems. Images for all figures were processed in Photoshop (Adobe).

3.4.5 PEF assay

Ndc80-GFP, NOD-mCherry S2 cells were treated with 500 µM $CuSO_4$ for 6-18 hours to induce expression of NOD-mCherry. Two color Z-series consisting of ~30 planes at 0.2 µm intervals were then acquired for both the mCherry and Ndc80-GFP channels. A region of interest was drawn around the mCherry-positive chromosomes in a maximum intensity projection of the mCherry Z-series. After recording the integrated fluorescence intensity (IFI) of the chromosomal area, the region of interest was moved to a non-chromosomal area and the background IFI was measured and then subtracted from the chromosomal mCherry signal to yield the corrected mCherry values, which are presented in the PEF assay graphs. The Z-series from the Ndc80-GFP channel was then carefully examined by eye and the percentage of syntelic attachments, defined as those with a pair of juxtaposed kinetochores facing the same pole, was recorded. Cells with evident monopolar chromosomal arrangements were not imaged.

3.4.6 Antibody production

A polyclonal peptide antibody (antibody 5444) was generated in a rabbit and affinity purified by GenScript (Piscataway, NJ). The peptide sequence to which the antibody was raised was EAPYRQFLGRREPSC, corresponding to amino acids 15-28 of the NOD protein. Recombinant GST-KLP3A tail domain (a gift from Jonathan Scholey, University of California at Davis) was expressed in BL21 cells with 1 mM IPTG and purified using Glutathione Sepharose 4B (GE Healthcare) following the manufacturer's protocol. Cells were lysed in a buffer containing 50 mM Tris, 10 mM KCl, 1% Triton X-100, 10% Glycerol, 1 mM $MgCl_2$, 1 mM EGTA, 1 mM DTT, 0.2 mM PMSF, and protease inhibitors (Roche), and the protein was eluted in 10 mM reduced L-glutathione. Anti-KLP3A was affinity purified against GST-KLP3A by immobilizing the purified protein on a nitrocellulose membrane (BioRad). The antibody was eluted using 0.2 M Glycine, pH 2.3, and immediately neutralized with 1 M Tris, pH 8.0.

3.4.7 IF

S2 cells were allowed to adhere to ConA-coated coverslips before being quickly rinsed in BRB80 and then fixed in 10% paraformaldehyde. Cells were then permeabilized for 10 minutes in 1xPBS+ 1% Triton, washed three times for 5 minutes each in 1xPBS + 0.1% Triton, and blocked in Boiled Donkey Serum for 30-60 minutes. Primary antibodies were diluted into Boiled Donkey Serum. Anti-KLP3A (a gift of Jonathan Scholey, UC Davis) was used at a concentration of 1:100, anti-phospho-H3 Serine 10 (Abcam) at 1:20,000, anti-phospho-Aurora A/B/C (Cell Signaling Technology) at 1:500, and anti-NOD (Genscript) at 1:1000.

All secondary antibodies (Jackson ImmunoResearch) were diluted 1:200 in Boiled Donkey Serum. Cells were treated with DAPI (1:100) and sealed in mounting media containing 20 mM Tris (pH8.0), 0.5% N-propyl gallate and 90% glycerol. The ratio of the fluorescence intensities of KLP3A, phospho-H3 or phospho-Aurora B (as appropriate) to DAPI were done similar to previous work (Maresca and Salmon, 2009) – larger and smaller regions were drawn manually in MetaMorph around the chromosomes and the regions were transferred to the images to be quantified (KLP3A, phospho-H3, or phospho-Aurora B). The total intensity measurements were then normalized to the Dapi total intensity. The following equations were used: Background signal = (integrated fluorescence intensity of big area - Integrated fluorescence intensity of small area)/(big area - small area). Total intensity = integrated fluorescence intensity of small area x (background signal x small area).

3.4.8 Western blotting

A total of 10 µg of protein was loaded into a 10% SDS-PAGE gel, run out and transferred to PVDF membrane (BioRad) in transfer buffer containing 10% methanol. All antibodies were diluted in TBS with 0.1% Tween and 5% milk. The membrane was first incubated with either anti-GFP serum (gift of Magdalena Bezanilla, UMASS Amherst) at 1:50 or anti-NOD antibody (antibody 5444) at 1:500 and then probed with DM1α (anti-α-Tubulin antibody) (Sigma-Aldrich) at 1:1000. Rabbit and mouse HRP secondary antibodies (Jackson ImmunoResearch) were used in conjunction with their respective primaries and imaged with a GBox system controlled by GeneSnap software (Syngene).

CHAPTER 4

INSIGHTS FROM AN ERRONEOUS KINETOCHORE-MICROTUBULE ATTACHMENT STATE

Whenever a cell divides it is faced with the incredibly complex challenge of evenly distributing its entire complement of replicated chromosome into two daughter cells. Amazingly, healthy cells accurately divvy up their genomes 99 out of every 100 times that they divide (Thompson and Compton, 2008). So how do cells pull off such a herculean task with such high fidelity? The solution is provided, in large part, by two critical and convergent cellular networks (Nezi and Musacchio, 2009): the error correction pathway, which destabilizes improper interactions between chromosomes and spindle microtubules, and the spindle assembly checkpoint (SAC) pathway, which delays anaphase onset until every chromosome interacts properly with spindle microtubules.

"Proper interaction", in this context, refers to chromosome biorientation - the geometric configuration that best ensures sister chromatids will end up in different daughter cells. During the initial phases of cell division, a complex called the kinetochore, consisting of multiple copies of more than 100 different proteins, assembles on the centromeres of sister chromatids, which remain held together through DNA catenation and protein-based cohesion. The kinetochore consists of domains with distinct molecular compositions. The inner kinetochore contains DNA-binding components and, consequently, interfaces with the centromeric chromatin whereas the microtubule-attachment factors reside in the outer kinetochore (Cheeseman and Desai, 2008; Santaguida and Musacchio, 2009). The core kt-MT attachment complex consists of 8-9 proteins (depending

on the organism) and is referred to as the KMN (KNL1/Blinkin, Mis12 complex, Ndc80 complex) network (Cheeseman et al., 2006; DeLuca et al., 2006; Kiyomitsu et al., 2007). Thus, the kinetochore connects the chromosomes to spindle microtubules. The kinetochore also serves as the physical locale from which the SAC signal originates. Checkpoint proteins including Mad1 and BubR1 accumulate at improperly attached kinetochores (Hoffman et al., 2001) and delay anaphase onset by catalyzing the assembly of a soluble inhibitor of the anaphase promoting complex/cyclosome (APC/C) (Chao et al., 2012; Hardwick et al., 2000; Sudakin et al., 2001). Not surprisingly, the error correction and SAC pathways converge at kinetochores to promote segregation of bioriented chromosomes.

Chromosomes become bioriented when their sister kinetochores attach to dynamic microtubules emanating from opposite spindle poles. Chromosome biorientation generates tension across sister kinetochores because kinetochore-microtubules (kt-MTs) pull the physically linked chromatids in opposite directions. In turn, tension increases the affinity of kinetochore-associated microtubule-binding factors for microtubules (Akiyoshi et al., 2010; King and Nicklas, 2000; Li and Nicklas, 1995; Nicklas and Koch, 1969). Thus, bioriented attachments are selectively stabilized. While bioriented attachments may be the most stable kt-MT interaction, erroneous, non-bioriented kt-MT attachments form very frequently. In fact, a recent analysis of meiosis I kinetochores in mouse oocytes revealed that nearly 90% of kinetochores established improper kt-MT interactions at least once before becoming bioriented (Kitajima et al., 2011). However,

erroneous kt-MT attachments are transient because they are destabilized by a centromere enriched kinase called aurora B kinase (ABK) (Cimini et al., 2006; Lampson et al., 2004), which reduces the affinity of improperly attached kinetochores for microtubules via phosphorylation of KMN components including the microtubule-binding factor Ndc80 (Cheeseman et al., 2006; DeLuca et al., 2006).

Bioriented kinetochores under tension are not subjected to error correction nor do they contribute to production of an inhibitory SAC signal (Li and Nicklas, 1995; Nicklas and Ward, 1994). Does production of tension merely correlate with the cessation of error correction and SAC signaling or does it actively contribute to their suppression? We and others have demonstrated that experimentally applying tension to misoriented kinetochores in living cells overrides ABK-mediated error correction and production of the SAC signal (see Chapter 3 above and (Li and Nicklas, 1995; Nicklas and Koch, 1969)). The data reveal that tension plays an active role in opposing the error correction and SAC pathways although the means by which it does so are not entirely clear. For example, it has been hotly debated as to whether kinetochore tension is capable of providing a direct input to production of a SAC signal or if the soluble inhibitory signal is only generated by unattached kinetochores (Maresca and Salmon, 2010). While it is our opinion that existing data are insufficient to definitively rule out a direct contribution of tension to SAC signaling, the fact that tension stabilizes kt-MT interactions places tension upstream of attachment in the SAC pathway;

therefore, we believe tension must be considered an important regulator of SAC signaling.

We recently developed a live-cell polar ejection force (PEF) assay in *Drosophila melanogaster* S2 cells to more closely examine the effects of force and the tension it produces at kinetochores (see Chapter 3). The PEF assay takes advantage of an intrinsic force-producing cellular component, specifically the chromokinesin NOD (*Drosophila* kinesin-10) (Afshar et al., 1995a; Theurkauf and Hawley, 1992; Zhang et al., 1990), to experimentally elevate the force, known as the polar ejection force (Rieder et al., 1986; Rieder and Salmon, 1994), that pushes chromosome arms away from spindle poles. In the PEF assay, inducible NOD overexpression results in a dose-dependent increase in the percentage of a specific type of erroneous kt-MT interaction called a syntelic attachment, in which both sister kinetochores are attached to the same spindle pole. Syntelic attachments are normally short-lived due to the activity of ABK. We postulate that syntelic attachments, despite being misoriented, are stabilized in the PEF assay through a tension-dependent mechanism in which the poleward pulling force generated by kt-MTs (Khodjakov and Rieder, 1996; Skibbens et al., 1993) is opposed by the away-from-the-pole pushing force produced by NOD (Theurkauf and Hawley, 1992). In turn, elevated tension at the syntelic kinetochores overwhelms ABK-mediated error correction and the SAC is satisfied in the presence of erroneous yet artificially stabilized kt-MT attachments. The ability to experimentally produce high numbers of stable syntelic attachments in

the PEF assay offers a valuable opportunity to study the nature of these transient kt-MT interactions and how they contribute to production of a SAC signal.

In order to evaluate the checkpoint response to the syntelic attachments produced in NOD-overexpressing cells, a cell line was generated expressing both NOD-mCherry and an EYFP-tagged version of the checkpoint protein Mad1. A sharp reduction of Mad1 levels at the kinetochore, due in part to dynein-mediated “stripping” and poleward transport along kt-MTs, accompanies SAC satisfaction and precedes anaphase onset (Howell et al., 2000; Howell et al., 2001; Howell et al., 2004). In accordance with the observation that NOD-expressing cells enter anaphase in the presence of syntelic attachments, we found that Mad1-EYFP levels were reduced at both bioriented and syntelic attachments in cells arrested in metaphase with the proteasome inhibitor MG132 (see Chapter 3).

While NOD-expressing S2 cells clearly satisfied the SAC in the presence of stable syntelic attachments, they did so more slowly than wild type cells. Furthermore, the duration of mitosis increased with the number of syntelic attachments (unpublished observation). To better understand why mitotic progression was slower in the presence of stable syntelic attachments, we examined kinetochore Mad1-EYFP dynamics as cells progressed through cell division in the absence of MG132. Interestingly, Mad1 depletion often occurred more rapidly at bioriented kinetochores than at syntelic attachments (Figure 4.1A). In support of our previous observation that stable syntelic attachments established robust kinetochore fibers (see Chapter 3), Mad1-EYFP particles

could be seen streaming poleward along kt-MTs (Figure 4.1). Thus, dynein actively depletes Mad1 from NOD-stabilized syntelic attachments.

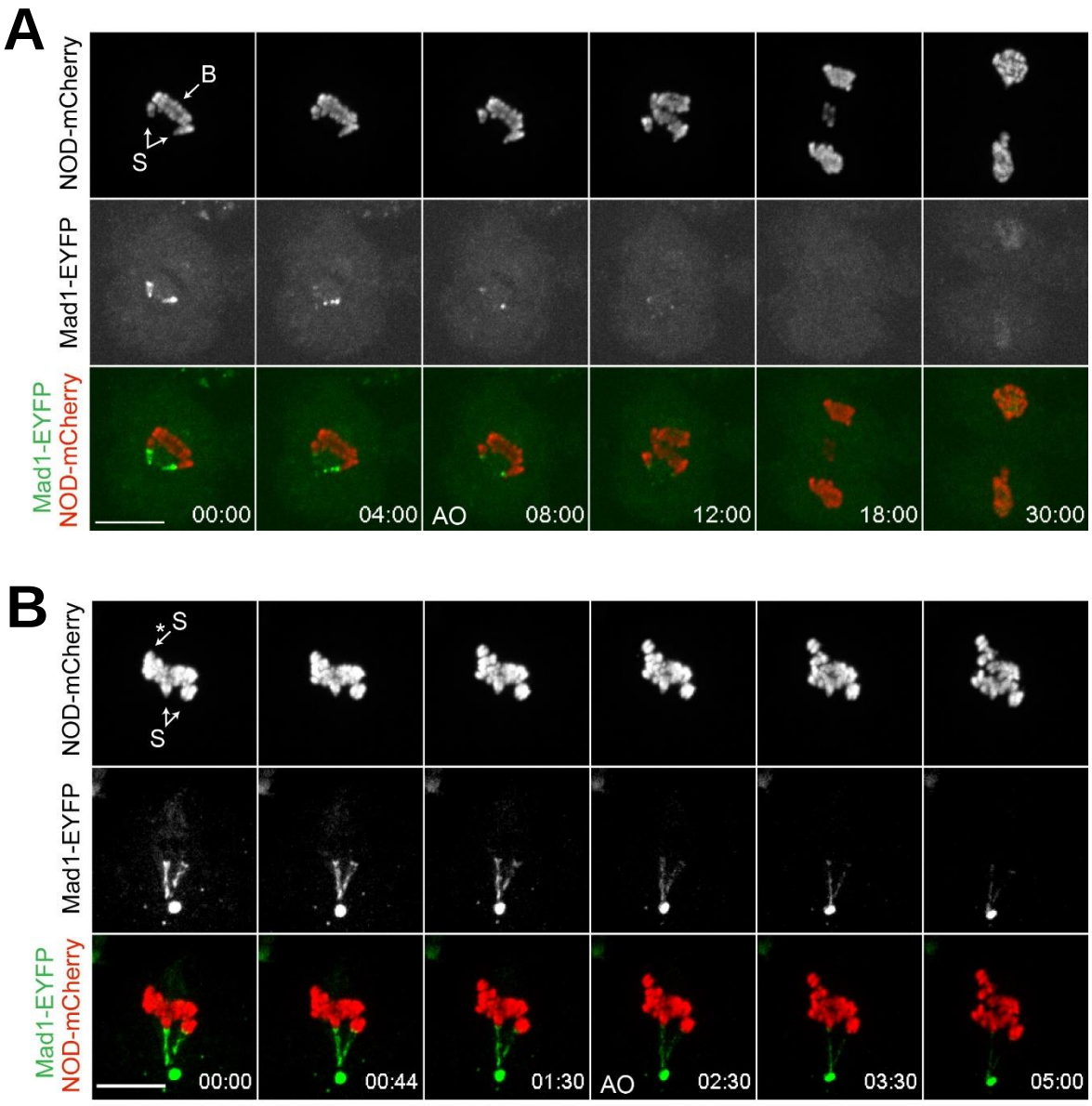

Figure 4.1: Mad1 depletion from syntelic attachments is often gradual and incomplete before anaphase onset. *(A)* Still images of time-lapse microscopy showing a cell with a mixture of syntelic and bioriented kinetochores. Mad1-EYFP persists at the syntelic kinetochores after it has been depleted from bioriented kinetochores. *(B)* Still images of time-lapse microscopy showing a different cell with syntelic and bioriented attachments. One syntelic (arrow with asterisk) lacks detectable Mad1 but Mad1 persists at two other syntelics (arrows). In both A and B, the cells enter anaphase (AO) despite having detectable (though reduced) levels of Mad1 at two syntelic attachments. In each case, Mad1 can also be seen streaming away from the syntelic attachments along kinetochore fibers. In merged images NOD-mCherry is red and Mad1-EYFP is green. Scale bars are 10 μm. *Materials and Methods*: *Drosophila* S2 cells expressing kinesin 1-NOD-mCherry and Mad1-EYFP (Chapter 3) were

cultured in Schneider's media (Life Technologies) supplemented with 10% heat inactivated fetal bovine serum (Life Technologies) and 0.5X antibiotic-antimycotic cocktail (Life Technologies). The cells were seeded onto concanavalin A (Sigma) treated acid-washed coverslips (Corning) for 1 hour after an overnight treatment with 500 μM $CuSO_4$ to induce NOD expression. The coverslips were next assembled into rose chambers containing Schneider's media and imaged at room temperature on a Nikon TiE inverted microscope with a CSU-X1 spinning disk confocal head (Yokogawa) and an iXON EMCCD camera (Andor Technology) using a Nikon 100X 1.4 NA Plan Apo violet corrected (VC) series DIC objective. Confocal images of the EYFP and mCherry channels were acquired every 2 minutes (Figure 4.1A) or every 15 seconds (Figure 4.1B).

Why, then, do the syntelic attachments often lose Mad1 more slowly than bioriented attachments? Ultimately, depletion of kinetochore-associated Mad1 depends on its off-rate, which is regulated by dynein-mediated stripping, being greater than its on-rate. While Mad1 is clearly being stripped from the stable syntelic kinetochores, the relatively slow pace of its reduction suggests that it is also being replenished and, moreover, that the Mad1 on-rate is higher at these sites than at bioriented attachments. This difference warrants further investigation especially because (i) NOD-mediated syntelic attachments were found to be as stable as bioriented attachments (Chapter 3) and (ii) Mad1 levels are generally believed to reflect the degree of kt-MT attachment stability.

Anaphase onset normally occurs ~10 minutes after the Mad1 binding partner Mad2 is completely lost from the kinetochores of the last chromosome to align on the metaphase plate (Howell et al., 2000). However, we observed that Mad1 was detectable at some syntelically attached kinetochores at anaphase onset, albeit at significantly lower levels than at the start of imaging (Figures 4.1A and 4.1B). While this discrepancy could reflect a difference in the dynamics of Mad1 versus Mad2 depletion from kinetochores, we presume that low levels of Mad2 are also present at the stable syntelic attachments where Mad1 persists. Thus, we favor the idea that Mad1/Mad2 at stable syntelic attachments contributes to production of a wait-anaphase signal, but that once kinetochore-associated levels of Mad1/Mad2 drop below a critical, but still observable, threshold the signal is no longer strong enough to block anaphase onset. A logical extension of this hypothesis is that the SAC is mediated by a titratable

inhibitory signal derived from the sum total of the signal inputs from each kinetochore. This would result in the production of wait-anaphase signals of variable potencies, reflected in varying degrees of mitotic delay, rather than an "all-or-none" signal. Such a mechanism would explain why the duration of mitosis increases with the number of stable syntelic attachments. Not only does the model predict that a cell with a greater number of stable syntelics will spend a longer time in mitosis than a cell with fewer; it also predicts that the more syntelically attached kinetochores with detectable Mad1 are found in a given cell, the greater the Mad1 reduction that must occur at each such kinetochore before anaphase onset can occur. This prediction is currently being tested.

It is also notable that not all stable syntelic attachments behave in the same manner. For example, often Mad1-EYFP was absent from some syntelic attachments yet detectable at other syntelics in the same cell (Figure 4.1B). We do not currently understand what causes this stochasticity; however, the fact that Mad1 is depleted from syntelic attachments to the same extent as from bioriented chromosomes following a two-hour MG132 treatment suggests that the non-uniform behavior seen in untreated cells may be related to the age of the syntelic attachment. We propose that Mad1 is depleted gradually from stable syntelics because the dynein-driven off-rate of Mad1 is only slightly greater than its on-rate. The observation of anaphase onset with detectable levels of kinetochore-associated Mad1 and active Mad1 streaming has additional implications for checkpoint regulation. First, it suggests that the kinetochore fiber-associated Mad1-containing particles do not produce a sufficiently potent

wait-anaphase signal to maintain a mitotic delay. Since Mad1 was not replenished at kinetochores following anaphase onset (Figures 4.1A and 4.1B) key regulators of the Mad1 on-rate must change at the metaphase to anaphase transition.

We next quantitatively examined the levels of a second checkpoint protein called BubR1 at stable syntelic attachments. In close agreement with previous findings (Howell et al., 2000), unattached kinetochores in cells treated with colchicine to eliminate kinetochore-microtubule attachments exhibited a 3.2-fold increase in kinetochore-associated BubR1 relative to bioriented kinetochores in DMSO-treated control cells (Figures 4.2A and 4.2C). In contrast, syntelically attached kinetochore pairs had 1.7-fold higher levels of BubR1 relative to their bioriented counterparts (Figure 4.2B), which represents ~50% of the amount of BubR1 at unattached kinetochores. BubR1 levels at the bioriented and syntelic attachments (Figure 4.2B) were measured after a two-hour MG132 treatment to arrest cells in metaphase – the same treatment that resulted in comparable depletion of kinetochore-associated Mad1 from both types of attachments (Chapter 3). Thus, a sub-population of BubR1 in S2 cells behaves differently than Mad1, which, given enough time, is lost from stable syntelic attachments. BubR1, like Mad1, may be stripped from kinetochores through dynein-mediated streaming along kinetochore fibers (Howell et al., 2001; Whyte et al., 2008), although this behavior has not been evident in *Drosophila* cells (Buffin et al., 2005). Our data suggest that only a sub-population of BubR1 can be removed from stable syntelic attachments, possibly through dynein-mediated stripping,

and that the remaining ~50% is regulated through different molecular mechanisms. In summary, kinetochore levels of BubR1 at stable syntelic attachments are lower than at unattached kinetochores but higher than at bioriented attachments, while the kinetics of Mad1 depletion from syntelic attachments are often slower than the kinetics at bioriented attachments (Figure 4.3).

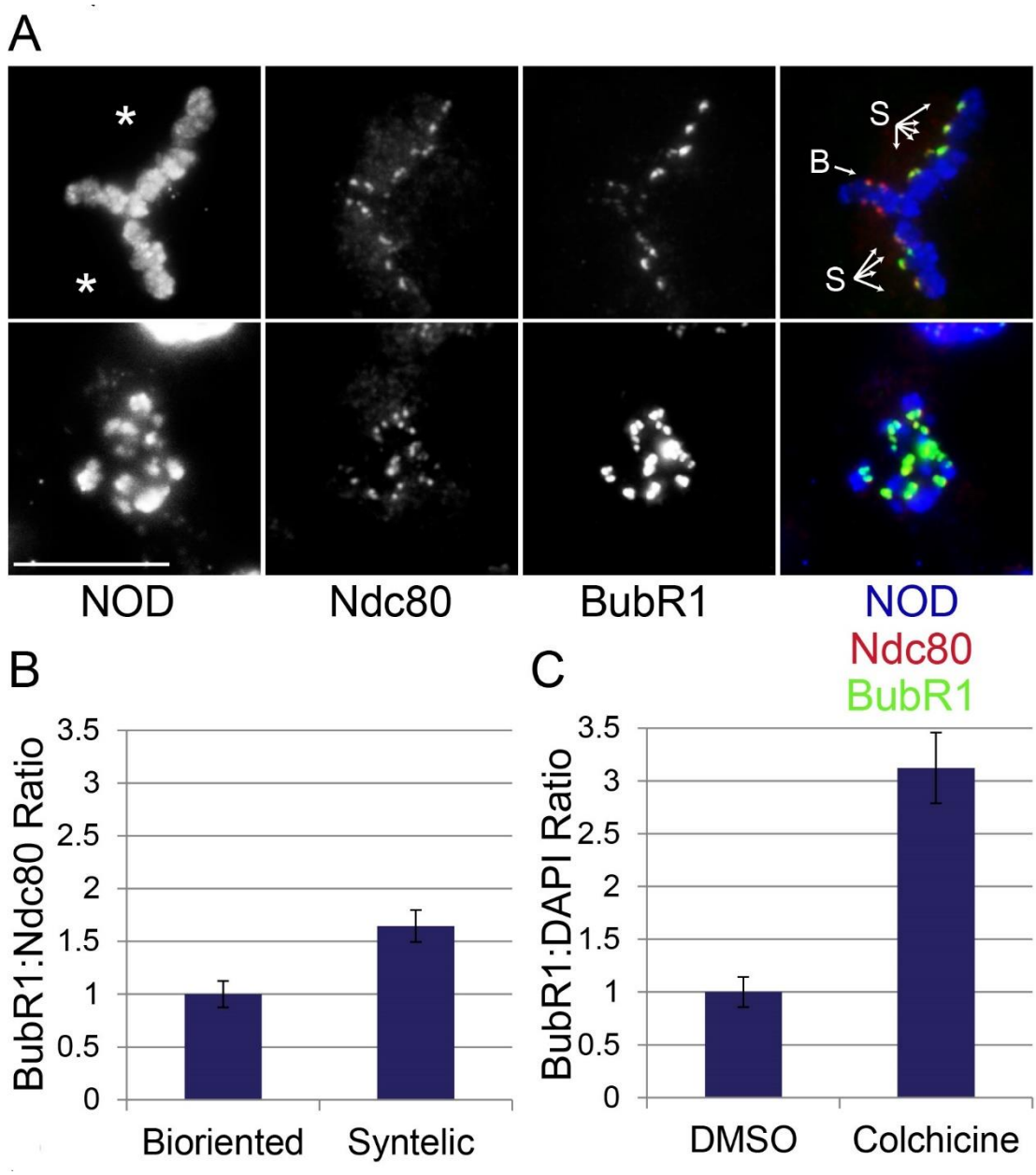

Figure 4.2: BubR1 levels at syntelic attachments are intermediate between levels at unattached and bioriented kinetochores. *(A),(B).* BubR1 levels at syntelic attachments (S) are measured by quantitative immunofluorescence to be ~1.7 fold higher at syntelics relative to bioriented (B) attachments. In merged images NOD is blue, Ndc80 is red and BubR1 is green. Scale bars are 10 µm. Error bars represent the SEM. *(C)* Unattached kinetochores in colchicine-treated cells exhibit a 3.2 fold increase of BubR1 levels relative to bioriented attachments in DMSO-treated controls. Error bars represent the SEM. *(figure and legend continued next page)*

D

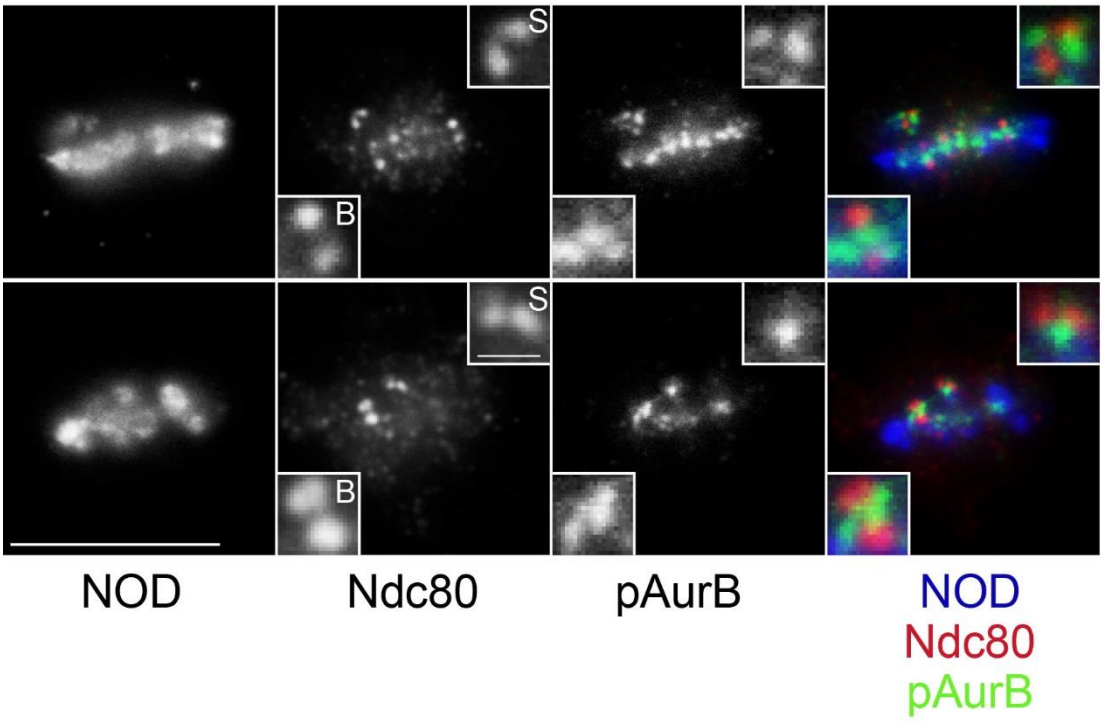

Figure 4.2 *(continued)*: BubR1 levels at syntelic attachments are intermediate between levels at unattached and bioriented kinetochores. *(D)* ABK is properly localized and active (phosphorylated) at syntelic attachments, but the erroneous attachments are not corrected. The insets show 4× zooms of representative attachments (bioriented [B] in the lower left and syntelics [S] in the upper right). In merged images NOD is blue, Ndc80 is red and phospho-Aurora B (pAurB) is green. Scale bars are 10 μm and 1 μm in insets. *Materials and Methods*: S2 cells expressing BubR1-GFP and NOD-mCherry (A, B, C) or only NOD-EGFP (D), after overnight induction with 25 μM $CuSO_4$ and a two hour treatment with 10 μM MG132 (Sigma) (A, B and C) followed by a 1 hour treatment with either 0.1% DMSO or 25 μM colchicine (A and C only) were adhered to concanavalin A-coated coverslips before being rinsed in BRB80 and fixed in 10% paraformaldehyde. Cells were then permeabilized for 10 minutes in 1xPBS + 1% Triton X-100, washed 3X for 5 minutes in 1xPBS + 0.1% Triton, and blocked in Boiled Donkey Serum for 30-60 minutes. The cells were stained overnight at 4°C with either chicken anti-Ndc80 (Maresca lab) diluted 1:100 or rabbit anti-phospho-Aurora A/B/C (Cell Signaling Technology) at 1:1000 in Boiled Donkey Serum. Coverslips were washed 3X for 5 minutes in 1xPBS + 0.1% Triton and then incubated at room temperature for 45 minutes with appropriate secondary antibodies (Jackson ImmunoResearch) at 1:200 and DAPI (1:100) diluted in Boiled Donkey Serum. Coverslips were washed 3X for 5 minutes in 1xPBS + 0.1% Triton before mounting them in media containing 20 mM Tris (pH 8.0), 0.5% N-propyl gallate and 90% glycerol. The ratio of the total fluorescence intensities of BubR1-GFP to Ndc80 (B) or Dapi (C) were quantified as previously described (Chapter 3).

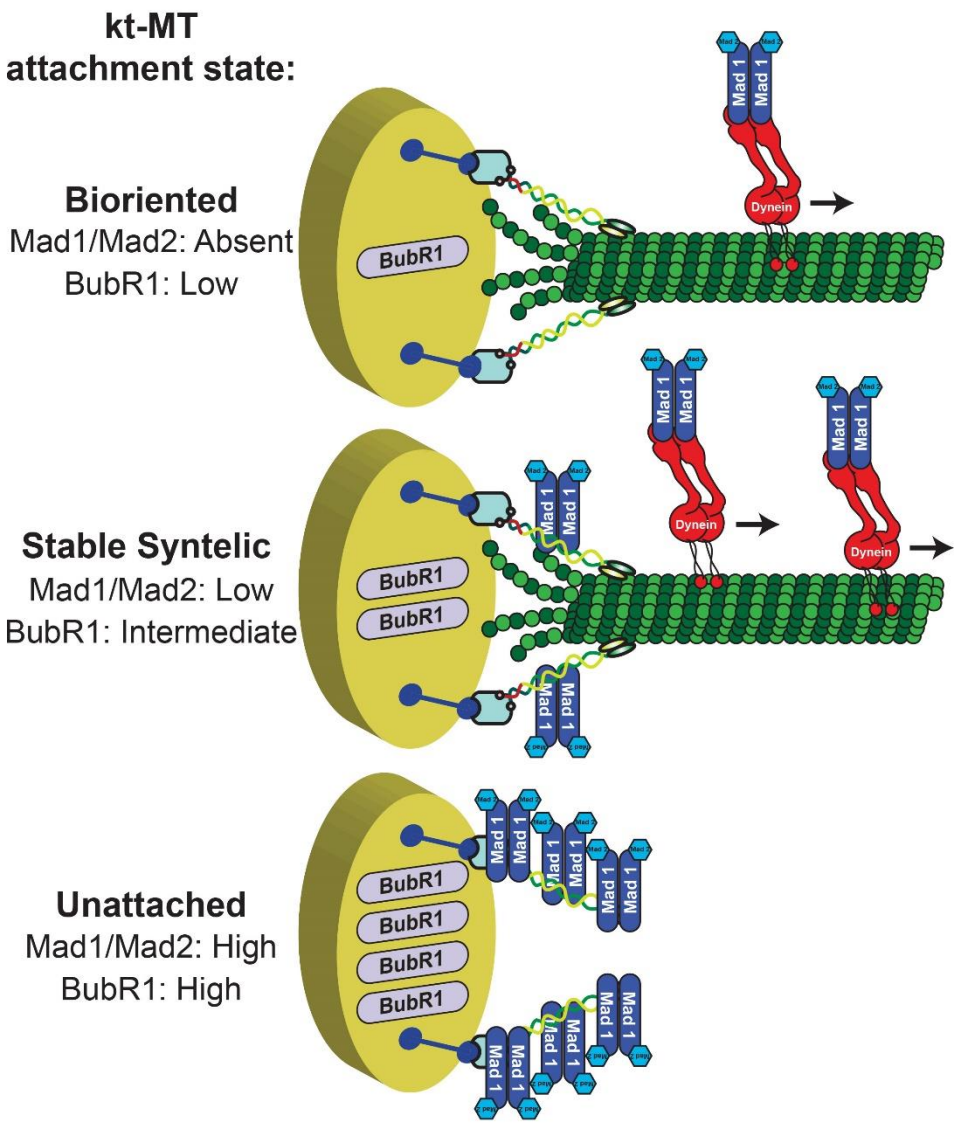

Figure 4.3: Graphical summary of Mad1 and BubR1 levels at bioriented, NOD-stabilized syntelic and unattached kinetochores. Unattached kinetochores have the highest levels of Mad1 and BubR1. Mad1 levels are very low at bioriented attachments while BubR1 is detectable but reduced ~3.2 fold relative to unattached kinetochores. Mad1 is stripped from syntelic attachments by dynein although it is depleted with slower kinetics than from bioriented attachments. Syntelic attachments have intermediate levels of BubR1, which are ~50% the amount seen at fully unattached kinetochores but ~1.7 fold higher than the levels at bioriented attachments.

We next examined the behavior of ABK in NOD-expressing cells because the localization of BubR1 and the Mad proteins to kinetochores is regulated by ABK (Ditchfield et al., 2003; Hauf et al., 2003). Active phosphorylated ABK localized properly to the inner centromere in both bioriented and stable syntelic attachments (Figure 4.2D). Thus, neither the persistence of syntelic attachments nor the changes in kinetochore checkpoint protein levels at these attachments can be attributed to significant changes in ABK localization or activity following NOD overexpression.

Our NOD overexpression studies also had obvious implications for another important unresolved question in the field: How does tension stabilize kt-MT attachments? There are presently two major models for tension-dependent stabilization of kt-MT attachments. The models will be referred to here as (i) spatial positioning and (ii) catch bond. Spatial positioning posits that kt-MT attachment affinity is increased by repositioning attachment factors further away from ABK through a tension-dependent structural change within the kinetochore called intrakinetochore stretch (Maresca and Salmon, 2009; Maresca and Salmon, 2010; Uchida et al., 2009). For simplicity's sake, spatial positioning will be presented here although related models have been proposed that do not evoke spatial positioning of attachment factors relative to ABK (Campbell and Desai, 2013). Ultimately, these alternative models, like spatial positioning, involve tension-dependent silencing of ABK-mediated error correction. The catch bond model, on the other hand, postulates that tension increases the affinity of attachment factors for microtubules via purely mechanical means and

independent of ABK (Akiyoshi et al., 2010). The spatial positioning and catch bond models are not mutually exclusive, and it is believed that both contribute to tension-mediated stabilization of kt-MT attachments in cells, but it remains to be seen whether that is indeed the case and, if so, what the relative contribution of each mechanism is to kt-MT attachment stability.

In catch bonds, the interaction between two components becomes stronger when force is applied to them. Purified budding yeast kinetochore particles, lacking ABK, exhibit catch bond properties as the lifetime of their interactions with dynamic microtubules was found to increase with the application of increasing force using an optical trap (Akiyoshi et al., 2010). Furthermore, increased tension caused the single microtubule to which a particle was attached to undergo fewer catastrophes and more frequent rescues. While the data strongly suggest that budding yeast kt-MT attachments act as catch-bonds and that tension regulates kt-MT dynamics, the molecular mechanisms underlying these observations are currently unknown. We now propose a mechano-molecular hypothesis to explain the kinetochore catch bond. We acknowledge that the model outlined here is speculative, and we do not consider it to be comprehensive or to preclude other potential catch bond mechanisms. Rather, we view the model as an important discussion point within the broader conversation surrounding the question of how tension stabilizes kt-MT attachments.

The model focuses on the interface between kinetochore microtubules and a core attachment factor called Ndc80 (also known as highly expressed in

cancer 1 (HEC1)) that localizes to the outer kinetochore. Microtubule structure and dynamics are key components of the model. Catastrophe, or the transition from assembly to disassembly, is accompanied by a dramatic change in the structure of protofilaments at the plus end of the microtubule from straight to curved. Conversely, rescue events and subsequent polymerization most likely require a majority of protofilaments at the plus end to be in a straight conformation. Thus, protofilament plus ends adopt distinct structural states depending on the polymerization state of the microtubule: straight when the microtubule is polymerizing and curved when it is depolymerizing. Microtubule dynamics also produce force. Polymerization can generate a pushing force of ~3-4 piconewtons (pN) against a barrier (Dogterom and Yurke, 1997) while measurements of the force produced by depolymerizing microtubules have suggested that each curving protofilament can generate up to 5 pN (Grishchuk et al., 2005).

Kinetochore microtubules in budding yeast must transition between polymerization and depolymerization since each kinetochore associates with a single microtubule (Winey et al., 1995), assembly and disassembly only takes place at the plus ends (Maddox et al., 2000), and pre-anaphase centromere movements occur at rates similar to those of growing and shrinking plus ends of astral microtubules (Pearson et al., 2001). The fact that metaphase chromosomes oscillate in many vertebrate cell types indicates that kt-MTs also transition between polymerization and depolymerization at kinetochores bound to multiple microtubules. Interestingly, a majority of metazoan kt-MTs analyzed by

electron tomography exist in a curved/depolymerizing configuration regardless of their oscillatory state (McIntosh et al., 2008; VandenBeldt et al., 2006). Nonetheless, kt-MTs were also found to contain some straightened protofilaments with one study reporting that ~1/3 of kt-MT plus ends were in a straightened/polymerizing state (VandenBeldt et al., 2006). Our model presumes that, regardless of whether a kinetochore interacts with a single or multiple microtubules, (i) kt-MTs transition between assembly and disassembly and (ii) the conformation of the kt-MT plus ends and the extent of protofilament curvature changes accordingly, with depolymerizing ends being more curved and polymerizing ends being more straight.

The core kt-MT attachment factor Ndc80 interacts with microtubules through an N-terminal calponin homology domain via its so-called “toe” (Alushin et al., 2010). Ndc80 can bind both α and β tubulin monomers (Alushin et al., 2010; Wilson-Kubalek et al., 2008) – a property that distinguishes it from most microtubule-associated proteins, which typically interact with α/β heterodimers. More specifically, the Ndc80 toe binds to a hinge point between each tubulin monomer that is proposed to pivot with protofilament curvature in a manner that reduces the affinity of Ndc80 for a curved lattice (Alushin et al., 2010). Accordingly, the Ndc80 complex exhibits greater affinity for straight microtubules than for curved microtubule substrates (Alushin et al., 2010; Schmidt et al., 2012). Thus, the Ndc80 toe is postulated to act as a microtubule conformation sensor that causes the Ndc80 complex to associate preferentially with straight protofilaments (Figure 4.4A – inset 1).

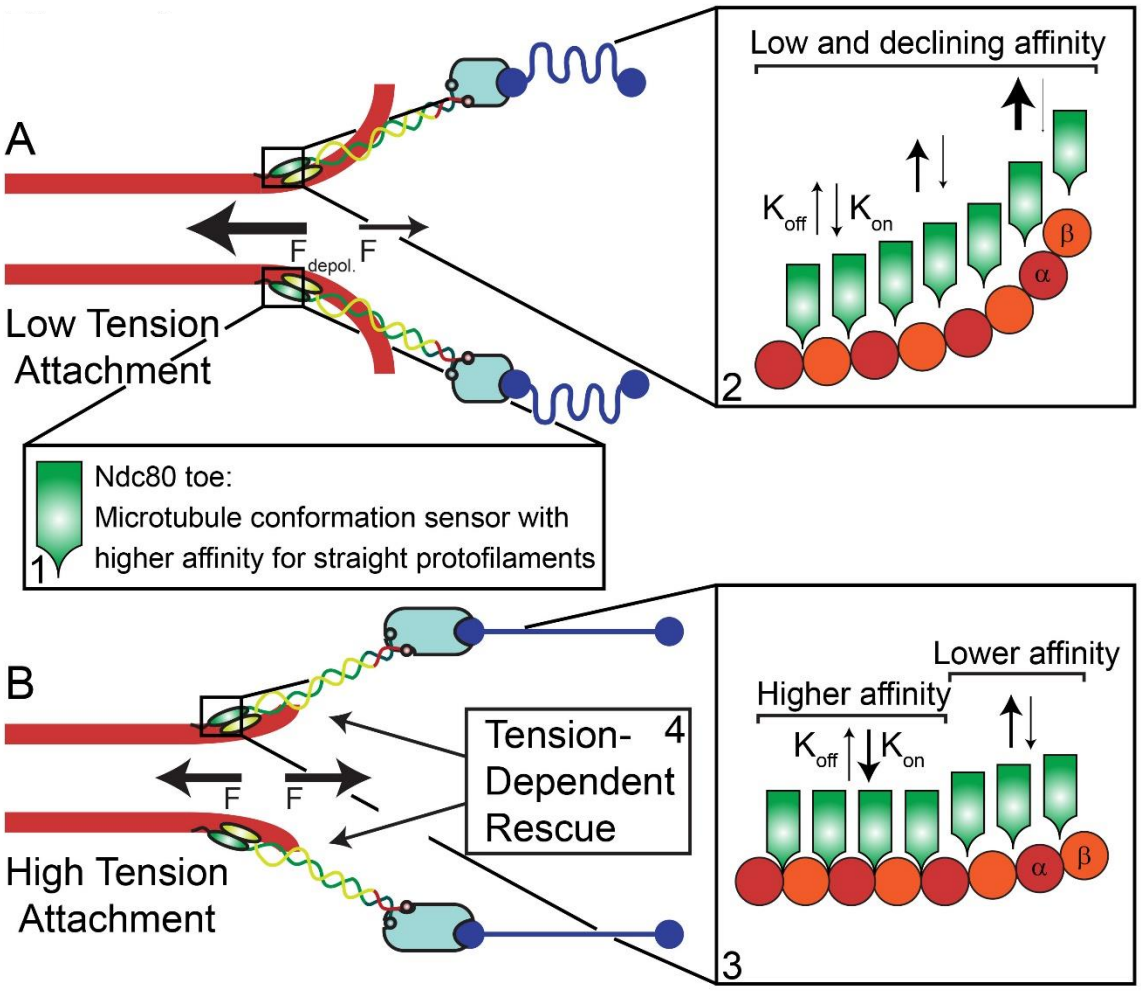

Figure 4.4: Mechano-molecular model of a kinetochore catch bond. *(A)* When Ndc80 makes initial end-on contact with a dynamic microtubule that has transitioned into a depolymerizing state, the kinetochore is pulled poleward by the force of microtubule depolymerization. Ndc80 maintains load-bearing interactions with the shrinking microtubule through biased diffusion that results from preferential binding of the Ndc80 toe (insert 1) to the straight regions of protofilaments at some distance from the curling plus ends. While these initial interactions are load bearing we propose that the curved conformation of the depolymerizing plus ends prevents high affinity Ndc80 toe interactions (insert 2). *(B)* When opposing forces produce kinetochore tension, internal kinetochore elements (light and dark blue) extend through stretching and/or reorientation and microtubule protofilaments straighten at the plus end. The model posits that tension-dependent straightening of protofilaments increases the affinity of Ndc80 for the microtubule by presenting higher affinity binding sites for the Ndc80 toe (insert 3) and promotes rescue once protofilament straightening reaches a critical threshold (insert 4).

We propose that when the kinetochore makes initial end-on contact with a microtubule that has transitioned into a depolymerizing state, the Ndc80 complexes will bind weakly to the microtubule lattice with the highest affinity interactions being found along the straight portions of protofilaments at some distance from the highly curved plus ends (Figure 4.4A – inset 2). This early kt-MT interaction will result in the kinetochore moving poleward as the force generated by microtubule depolymerization dominates and Ndc80 complexes remain loosely associated with the shortening microtubule through biased diffusion (Alushin et al., 2010; Powers et al., 2009). The model next envisions that increasing levels of opposing force - for example, from chromosome biorientation - will reduce the curvature of kt-MT plus ends (Figure 4.4B). In this case, the interaction between Ndc80 and the microtubule would behave like a catch bond as tension-dependent straightening of protofilaments increases the affinity of Ndc80 for kt-MTs by creating more accessible binding sites for the Ndc80 toe (Figure 4.4B – inset 3). We also propose that the microtubule would eventually transition into a polymerizing state once tension-mediated straightening of the protofilaments reaches a critical threshold (Figure 4.4B – inset 4).

The full picture in dividing cells is certainly more complicated than our model. While the model focuses on Ndc80 to highlight a potential tension-dependent mechanism for increasing the kinetochore's affinity for microtubules, the catch bond mechanism almost certainly depends on other critical properties of the kinetochore that the model does not discuss. These include, but are not

limited to: (i) the number of Ndc80 molecules, (ii) the 3-dimensional arrangement of Ndc80 attachment sites on the lattice and (iii) the number, arrangement and functions of other kinetochore associated proteins such as the Dam1 complex in budding yeast or the Ska complex in vertebrate cells. It should be noted that the model does not require that tension-dependent rescues be mediated by the Ndc80 complex; per se, but only that they depend on straightening of the protofilaments, which could be accomplished by other kinetochore components. Indeed, like the purified kinetochore particles, application of tension to purified Dam1 complex-microtubule attachments also increased the rescue rate and reduced the catastrophe frequency (Franck et al., 2007). Regardless of what molecules impart tension-dependent straightening of the protofilament; our model proposes that the result will be the same - higher affinity interactions between the Ndc80 toe and the microtubule.

Kinetochore-microtubule attachment stability, especially during the initial establishment of end-on attachments, most likely depends on the combined inputs from phospho-regulation through spatial positioning and mechano-regulation via the catch bond pathway (Figure 4.5). We propose that distinct contributions from the two pathways would yield a gradient of kt-MT attachment affinities - the highest affinity coming when Ndc80 is associated with straight protofilaments and dephosphorylated (Figure 4.5A) and the lowest affinity interaction coming from phosphorylated Ndc80 with a prevalence of curved protofilaments in its vicinity (Figure 4.5D). Since it is unclear whether one mechanism or the other dominates in modulating the affinity of Ndc80 for

microtubules the exact order of affinities in our proposed attachment stability gradient is not clear; however, intermediate attachment affinities would be expected if Ndc80 was phosphorylated but protofilaments were straight (Figure 4.5B) or if Ndc80 was dephosphorylated and protofilaments were curved (Figure 4.5C). An additional layer of complexity exists for kinetochores that bind numerous microtubules as individual kt-MT interactions with varying affinities may exist within the same kinetochore.

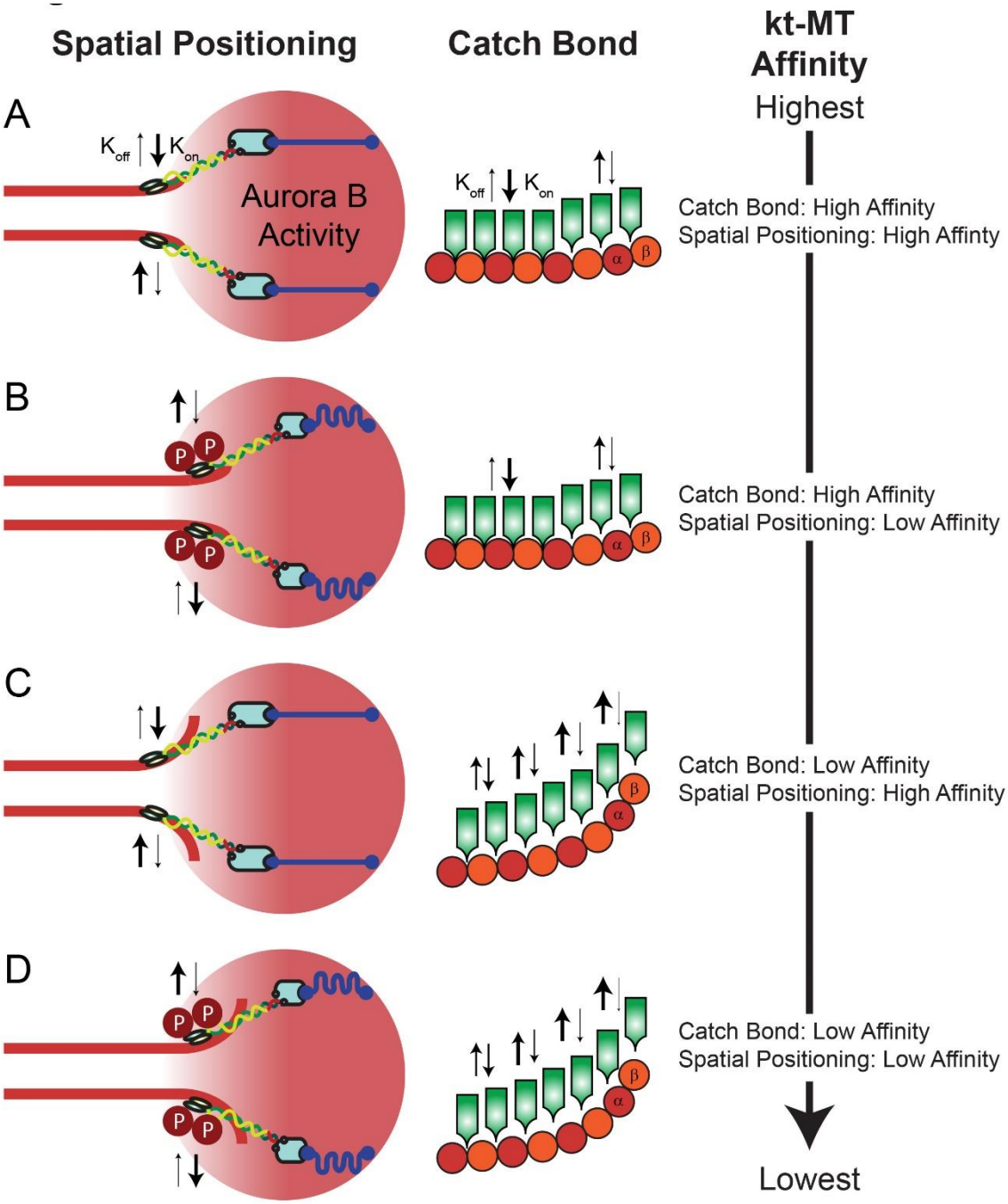

Figure 4.5: The combined contribution of spatial positioning and catch bond mechanisms could create a kt-MT attachment affinity gradient. *(A)* In spatial positioning, tension repositions the Ndc80 complex further away from ABK by stretching (or reorienting) internal kinetochore elements (light and dark blue) resulting in reduced phosphorylation and increasing the affinity of the complex for microtubules. In the proposed catch bond mechanism, tension

straightens protofilaments thereby increasing the affinity of the Ndc80 toe for microtubules. Dephosphorylated Ndc80 associated with straight protofilaments produces the highest affinity kt-MT interaction. Lower affinity interactions would result if Ndc80 was phosphorylated but associated with straight protofilaments *(B)* or if Ndc80 was dephosphorylated and associated with curved protofilaments *(C)* although it is unclear which of these combinations would exhibit higher affinity. *(D)* The lowest affinity kt-MT interaction would result from phosphorylated Ndc80 associated with curved protofilaments.

Elevating PEFs via NOD overexpression has provided key insights into how tension produced at kinetochores upon chromosome biorientation regulates kt-MT attachment stability in unperturbed cells. Further experimentation employing the PEF assay (Chapter 3) should promote a more refined understanding of the mechanisms involved in attachment stabilization and of the relative contributions of factors such as spatial positioning and catch bond interactions at the outer kinetochore.

CHAPTER 5

FUTURE DIRECTIONS

Future work in the areas of inquiry described in the preceding chapters, in addition to further efforts to measure outer kinetochore phosphorylation in the shortened CENP-C cell lines, could include experiments designed to more fully rescue the attachment instability phenotype seen in those cell lines. One seemingly feasible approach is to combine the two different treatments that have produced partial rescues, *i.e.*, Aurora B inhibition and length restoration, and to determine whether in combination they produce stable kinetochore-microtubule attachments comparable to the wild type condition.

If a more complete rescue is not achievable, it would be important to reconsider the possibility that a functional domain has been lost in the course of making the truncation mutants. In the literature, one report identified a CENP-C region unique to, but apparently well conserved among, members of the Drosophilid family (Heeger et al., 2005); the authors named this the “Drosophilid homology” region, and mapped it to the general vicinity of amino acid residue 550. They reported that a CENP-C construct lacking this region did not rescue certain phenotypic abnormalities seen in CENP-C mutant embryos. The CENP-C Drosophilid homology region does not seem to have appeared in any subsequent literature, so no particular function has been ascribed to it, but conceivably the lack of this region (or of some other region within the middle portion of CENP-C) could have an effect on kinetochore-microtubule attachment stability.

The successful manipulations of CENP-C stretch reported here also suggest an avenue for examining the usefulness of the “dog leash” model in which INCENP flexibly tethers Aurora B at a variable distance from the outer kinetochore. In theory, a combination of INCENP stretch and CENP-C stretch could well give rise jointly to a system that would generate a range of outer kinetochore phosphorylation states. A recent analysis proposes that if the central region of INCENP were to behave like the structurally similar myosin 10, then INCENP could, in principle, stretch out to a fully extended length of 80 nm. In any event, experiments involving manipulation of INCENP length had already begun while the work described in Chapter Two was still in its earliest stages, and further progress seems quite possible in view of the experience gained from the CENP-C work reported here.

Another line of investigation already in progress will examine the *in vitro* force-extension behavior of the middle region of CENP-C in an optical trap. This work has the potential to be informative in two different ways: The force required to extend this protein segment by 20-25 nm in the trap is further evidence for the amount of force experienced *in vivo* by each CENP-C molecule, supplementing work that has already been completed in living cells. In that work, which has not yet been published, an extendible domain of the focal adhesion protein Talin was inserted into CENP-C and employed as a calibrated force sensor according to the method described in (del Rio et al., 2009). Conversely, with the force experienced by each CENP-C molecule having previously been determined experimentally using the Talin-based force sensor, continuous application of that

amount of force (1-2 pN) to a CENP-C segment in the trap would be expected to stretch the molecule by 20-25 nm.

Finally, it could be worthwhile to examine a curious result that emerges from the kinetochore length calculations discussed in Chapter Two. In the original intrakinetochore stretch work (Maresca and Salmon, 2009), the metaphase distance from Cid to a fluorescent label near the Ndc80 C terminus was found to be ~100 nm. If that is so, then it would seem that the overall distance from Cid to the microtubule binding interface, including now the previously uncounted portion of Ndc80, should be in the neighborhood of 125-135 nm in S2 cells. By the measurements obtained in Chapter Two, however, the metaphase distance from the CENP-C C terminus to the microtubule binding interface is something closer to 100 nm – the sum of stretched CENP-C (~25 nm), the Mis12 complex (~23 nm) and the Ndc80 complex (~50 nm). The difference between the two sets of measurements can be taken to imply that there is a 30 nm gap separating Cid from the CENP-C C terminus. Intriguingly, Schittenhelm *et al*. found Cid to be “well separated” from the CENP-C C terminus in experimentally squashed *Drosophila* embryos (Schittenhelm et al., 2007). There appear to have been no reports to date identifying an additional protein or other intervening structure situated between CENP-A/Cid and the DNA-binding region of CENP-C, but the question may deserve a closer look.

BIBLIOGRAPHY

Adams, R.R., H. Maiato, W.C. Earnshaw, and M. Carmena. 2001. Essential roles of Drosophila inner centromere protein (INCENP) and aurora B in histone H3 phosphorylation, metaphase chromosome alignment, kinetochore disjunction, and chromosome segregation. *J Cell Biol*. 153:865-880.

Afshar, K., N.R. Barton, R.S. Hawley, and L.S. Goldstein. 1995a. DNA binding and meiotic chromosomal localization of the Drosophila nod kinesin-like protein. *Cell*. 81:129-138.

Afshar, K., J. Scholey, and R.S. Hawley. 1995b. Identification of the chromosome localization domain of the Drosophila nod kinesin-like protein. *J Cell Biol*. 131:833-843.

Akiyoshi, B., K.K. Sarangapani, A.F. Powers, C.R. Nelson, S.L. Reichow, H. Arellano-Santoyo, T. Gonen, J.A. Ranish, C.L. Asbury, and S. Biggins. 2010. Tension directly stabilizes reconstituted kinetochore-microtubule attachments. *Nature*. 468:576-579.

Alushin, G.M., V. Musinipally, D. Matson, J. Tooley, P.T. Stukenberg, and E. Nogales. 2012. Multimodal microtubule binding by the Ndc80 kinetochore complex. *Nat Struct Mol Biol*. 19:1161-1617.

Alushin, G.M., V.H. Ramey, S. Pasqualato, D.A. Ball, N. Grigorieff, A. Musacchio, and E. Nogales. 2010. The Ndc80 kinetochore complex forms oligomeric arrays along microtubules. *Nature*. 467:805-810.

Anderson, B.R., and H.L. Granzier. 2012. Titin-based tension in the cardiac sarcomere: molecular origin and physiological adaptations. *Prog Biophys Mol Biol*. 110:204-217.

Andrews, P.D., Y. Ovechkina, N. Morrice, M. Wagenbach, K. Duncan, L. Wordeman, and J.R. Swedlow. 2004. Aurora B regulates MCAK at the mitotic centromere. *Dev Cell*. 6:253-268.

Antonio, C., I. Ferby, H. Wilhelm, M. Jones, E. Karsenti, A.R. Nebreda, and I. Vernos. 2000. Xkid, a chromokinesin required for chromosome alignment on the metaphase plate. *Cell*. 102:425-435.

Arai, R., H. Ueda, A. Kitayama, N. Kamiya, and T. Nagamune. 2001. Design of the linkers which effectively separate domains of a bifunctional fusion protein. *Protein Eng*. 14:529-532.

Bieling, P., I. Kronja, and T. Surrey. 2010a. Microtubule motility on reconstituted meiotic chromatin. *Current biology : CB*. 20:763-769.

Bieling, P., I.A. Telley, and T. Surrey. 2010b. A minimal midzone protein module controls formation and length of antiparallel microtubule overlaps. *Cell*. 142:420-432.

Block, S.M., L.S. Goldstein, and B.J. Schnapp. 1990. Bead movement by single kinesin molecules studied with optical tweezers. *Nature*. 348:348-352.

Blower, M.D., and G.H. Karpen. 2001. The role of Drosophila CID in kinetochore formation, cell-cycle progression and heterochromatin interactions. *Nat Cell Biol*. 3:730-739.

Bringmann, H., G. Skiniotis, A. Spilker, S. Kandels-Lewis, I. Vernos, and T. Surrey. 2004. A kinesin-like motor inhibits microtubule dynamic instability. *Science*. 303:1519-1522.

Brouhard, G.J., and A.J. Hunt. 2005. Microtubule movements on the arms of mitotic chromosomes: polar ejection forces quantified in vitro. *Proc Natl Acad Sci U S A*. 102:13903-13908.

Buchan, D.W., F. Minneci, T.C. Nugent, K. Bryson, and D.T. Jones. 2013. Scalable web services for the PSIPRED Protein Analysis Workbench. *Nucleic Acids Res*. 41:W349-357.

Buffin, E., C. Lefebvre, J. Huang, M.E. Gagou, and R.E. Karess. 2005. Recruitment of Mad2 to the kinetochore requires the Rod/Zw10 complex. *Current biology : CB*. 15:856-861.

Caldas, G.V., and J.G. DeLuca. 2014. KNL1: bringing order to the kinetochore. *Chromosoma*. 123:169-181.

Campbell, C.S., and A. Desai. 2013. Tension sensing by Aurora B kinase is independent of survivin-based centromere localization. *Nature*. 497:118-121.

Carmena, M., M. Wheelock, H. Funabiki, and W.C. Earnshaw. 2012. The chromosomal passenger complex (CPC): from easy rider to the godfather of mitosis. *Nat Rev Mol Cell Biol*. 13:789-803.

Carvalho, P., M.L. Gupta, Jr., M.A. Hoyt, and D. Pellman. 2004. Cell cycle control of kinesin-mediated transport of Bik1 (CLIP-170) regulates microtubule stability and dynein activation. *Dev Cell*. 6:815-829.

Cassimeris, L., C.L. Rieder, and E.D. Salmon. 1994. Microtubule assembly and kinetochore directional instability in vertebrate monopolar spindles: implications for the mechanism of chromosome congression. *J Cell Sci*. 107 (Pt 1):285-297.

Chan, G.K., S.T. Liu, and T.J. Yen. 2005. Kinetochore structure and function. *Trends Cell Biol*. 15:589-598.

Chao, W.C., K. Kulkarni, Z. Zhang, E.H. Kong, and D. Barford. 2012. Structure of the mitotic checkpoint complex. *Nature*. 484:208-213.

Cheerambathur, D.K., and A. Desai. 2014. Linked in: formation and regulation of microtubule attachments during chromosome segregation. *Curr Opin Cell Biol*. 26:113-122.

Cheeseman, I.M. 2014. The kinetochore. *Cold Spring Harb Perspect Biol*. 6:a015826.

Cheeseman, I.M., J.S. Chappie, E.M. Wilson-Kubalek, and A. Desai. 2006. The conserved KMN network constitutes the core microtubule-binding site of the kinetochore. *Cell*. 127:983-997.

Cheeseman, I.M., and A. Desai. 2008. Molecular architecture of the kinetochore-microtubule interface. *Nat Rev Mol Cell Biol*. 9:33-46.

Chen, C.C., M.L. Dechassa, E. Bettini, M.B. Ledoux, C. Belisario, P. Heun, K. Luger, and B.G. Mellone. 2014. CAL1 is the Drosophila CENP-A assembly factor. *J Cell Biol*. 204:313-329.

Chen, R.H., A. Shevchenko, M. Mann, and A.W. Murray. 1998. Spindle checkpoint protein Xmad1 recruits Xmad2 to unattached kinetochores. *J Cell Biol*. 143:283-295.

Ciferri, C., S. Pasqualato, E. Screpanti, G. Varetti, S. Santaguida, G. Dos Reis, A. Maiolica, J. Polka, J.G. De Luca, P. De Wulf, M. Salek, J. Rappsilber, C.A. Moores, E.D. Salmon, and A. Musacchio. 2008. Implications for kinetochore-microtubule attachment from the structure of an engineered Ndc80 complex. *Cell*. 133:427-439.

Cimini, D., X. Wan, C.B. Hirel, and E.D. Salmon. 2006. Aurora kinase promotes turnover of kinetochore microtubules to reduce chromosome segregation errors. *Current biology : CB*. 16:1711-1718.

Cochran, J.C., C.V. Sindelar, N.K. Mulko, K.A. Collins, S.E. Kong, R.S. Hawley, and F.J. Kull. 2009. ATPase cycle of the nonmotile kinesin NOD allows microtubule end tracking and drives chromosome movement. *Cell*. 136:110-122.

Cui, W., L.R. Sproul, S.M. Gustafson, H.J. Matthies, S.P. Gilbert, and R.S. Hawley. 2005. Drosophila Nod protein binds preferentially to the plus ends of microtubules and promotes microtubule polymerization in vitro. *Mol Biol Cell*. 16:5400-5409.

del Rio, A., R. Perez-Jimenez, R. Liu, P. Roca-Cusachs, J.M. Fernandez, and M.P. Sheetz. 2009. Stretching single talin rod molecules activates vinculin binding. *Science*. 323:638-641.

DeLuca, J.G., W.E. Gall, C. Ciferri, D. Cimini, A. Musacchio, and E.D. Salmon. 2006. Kinetochore microtubule dynamics and attachment stability are regulated by Hec1. *Cell*. 127:969-982.

DeLuca, J.G., and A. Musacchio. 2012. Structural organization of the kinetochore-microtubule interface. *Curr Opin Cell Biol*. 24:48-56.

DeLuca, K.F., S.M. Lens, and J.G. DeLuca. 2011. Temporal changes in Hec1 phosphorylation control kinetochore-microtubule attachment stability during mitosis. *J Cell Sci*. 124:622-634.

Ditchfield, C., V.L. Johnson, A. Tighe, R. Ellston, C. Haworth, T. Johnson, A. Mortlock, N. Keen, and S.S. Taylor. 2003. Aurora B couples chromosome alignment with anaphase by targeting BubR1, Mad2, and Cenp-E to kinetochores. *J Cell Biol*. 161:267-280.

Dogterom, M., and B. Yurke. 1997. Measurement of the force-velocity relation for growing microtubules. *Science*. 278:856-860.

Domnitz, S.B., M. Wagenbach, J. Decarreau, and L. Wordeman. 2012. MCAK activity at microtubule tips regulates spindle microtubule length to promote robust kinetochore attachment. *J Cell Biol*. 197:231-237.

Dumont, J., K. Oegema, and A. Desai. 2010. A kinetochore-independent mechanism drives anaphase chromosome separation during acentrosomal meiosis. *Nat Cell Biol*. 12:894-901.

Duro, E., and A.L. Marston. 2015. From equator to pole: splitting chromosomes in mitosis and meiosis. *Genes Dev*. 29:109-122.

Espeut, J., D.K. Cheerambathur, L. Krenning, K. Oegema, and A. Desai. 2012. Microtubule binding by KNL-1 contributes to spindle checkpoint silencing at the kinetochore. *Journal of Cell Biology*. 196:469-482.

Fahrenkrog, B., and U. Aebi. 2003. The nuclear pore complex: nucleocytoplasmic transport and beyond. *Nat Rev Mol Cell Biol*. 4:757-766.

Foley, E.A., and T.M. Kapoor. 2013. Microtubule attachment and spindle assembly checkpoint signalling at the kinetochore. *Nat Rev Mol Cell Biol*. 14:25-37.

Franck, A.D., A.F. Powers, D.R. Gestaut, T. Gonen, T.N. Davis, and C.L. Asbury. 2007. Tension applied through the Dam1 complex promotes microtubule elongation providing a direct mechanism for length control in mitosis. *Nat Cell Biol*. 9:832-837.

Funabiki, H., and A.W. Murray. 2000. The Xenopus chromokinesin Xkid is essential for metaphase chromosome alignment and must be degraded to allow anaphase chromosome movement. *Cell*. 102:411-424.

Ghongane, P., M. Kapanidou, A. Asghar, S. Elowe, and V.M. Bolanos-Garcia. 2014. The dynamic protein Knl1 - a kinetochore rendezvous. *J Cell Sci*. 127:3415-3423.

Giet, R., and D.M. Glover. 2001. Drosophila aurora B kinase is required for histone H3 phosphorylation and condensin recruitment during chromosome condensation and to organize the central spindle during cytokinesis. *J Cell Biol*. 152:669-682.

Godek, K.M., L. Kabeche, and D.A. Compton. 2015. Regulation of kinetochore-microtubule attachments through homeostatic control during mitosis. *Nat Rev Mol Cell Biol*. 16:57-64.

Gorbsky, G.J., and W.A. Ricketts. 1993. Differential expression of a phosphoepitope at the kinetochores of moving chromosomes. *J Cell Biol*. 122:1311-1321.

Gordon, D.J., B. Resio, and D. Pellman. 2012. Causes and consequences of aneuploidy in cancer. *Nat Rev Genet*. 13:189-203.

Goshima, G., M. Mayer, N. Zhang, N. Stuurman, and R.D. Vale. 2008. Augmin: a protein complex required for centrosome-independent microtubule generation within the spindle. *J Cell Biol*. 181:421-429.

Goshima, G., and R.D. Vale. 2003. The roles of microtubule-based motor proteins in mitosis: comprehensive RNAi analysis in the Drosophila S2 cell line. *J Cell Biol*. 162:1003-1016.

Goshima, G., R. Wollman, S.S. Goodwin, N. Zhang, J.M. Scholey, R.D. Vale, and N. Stuurman. 2007. Genes required for mitotic spindle assembly in Drosophila S2 cells. *Science*. 316:417-421.

Grishchuk, E.L., M.I. Molodtsov, F.I. Ataullakhanov, and J.R. McIntosh. 2005. Force production by disassembling microtubules. *Nature*. 438:384-388.

Guse, A., C.W. Carroll, B. Moree, C.J. Fuller, and A.F. Straight. 2011. In vitro centromere and kinetochore assembly on defined chromatin templates. *Nature*. 477:354-358.

Hackney, D.D. 1995. Highly processive microtubule-stimulated ATP hydrolysis by dimeric kinesin head domains. *Nature*. 377:448-450.

Hardwick, K.G., R.C. Johnston, D.L. Smith, and A.W. Murray. 2000. MAD3 encodes a novel component of the spindle checkpoint which interacts with Bub3p, Cdc20p, and Mad2p. *J Cell Biol*. 148:871-882.

Hauf, S., R.W. Cole, S. LaTerra, C. Zimmer, G. Schnapp, R. Walter, A. Heckel, J. van Meel, C.L. Rieder, and J.M. Peters. 2003. The small molecule Hesperadin reveals a role for Aurora B in correcting kinetochore-microtubule attachment and in maintaining the spindle assembly checkpoint. *J Cell Biol*. 161:281-294.

Heeger, S., O. Leismann, R. Schittenhelm, O. Schraidt, S. Heidmann, and C.F. Lehner. 2005. Genetic interactions of separase regulatory subunits reveal the diverged Drosophila Cenp-C homolog. *Genes Dev*. 19:2041-2053.

Hegyi, H., E. Schad, and P. Tompa. 2007. Structural disorder promotes assembly of protein complexes. *BMC Struct Biol*. 7:65.

Hoffman, D.B., C.G. Pearson, T.J. Yen, B.J. Howell, and E.D. Salmon. 2001. Microtubule-dependent changes in assembly of microtubule motor proteins and mitotic spindle checkpoint proteins at PtK1 kinetochores. *Mol Biol Cell*. 12:1995-2009.

Hori, T., M. Amano, A. Suzuki, C.B. Backer, J.P. Welburn, Y.M. Dong, B.F. McEwen, W.H. Shang, E. Suzuki, K. Okawa, I.M. Cheeseman, and T. Fukagawa. 2008. CCAN Makes Multiple Contacts with Centromeric DNA to Provide Distinct Pathways to the Outer Kinetochore. *Cell*. 135:1039-1052.

Hornung, P., M. Maier, G.M. Alushin, G.C. Lander, E. Nogales, and S. Westermann. 2011. Molecular architecture and connectivity of the budding yeast Mtw1 kinetochore complex. *J Mol Biol*. 405:548-559.

Howard, J., A.J. Hudspeth, and R.D. Vale. 1989. Movement of microtubules by single kinesin molecules. *Nature*. 342:154-158.

Howell, B.J., D.B. Hoffman, G. Fang, A.W. Murray, and E.D. Salmon. 2000. Visualization of Mad2 dynamics at kinetochores, along spindle fibers, and at spindle poles in living cells. *J Cell Biol*. 150:1233-1250.

Howell, B.J., B.F. McEwen, J.C. Canman, D.B. Hoffman, E.M. Farrar, C.L. Rieder, and E.D. Salmon. 2001. Cytoplasmic dynein/dynactin drives kinetochore protein transport to the spindle poles and has a role in mitotic spindle checkpoint inactivation. *J Cell Biol*. 155:1159-1172.

Howell, B.J., B. Moree, E.M. Farrar, S. Stewart, G. Fang, and E.D. Salmon. 2004. Spindle checkpoint protein dynamics at kinetochores in living cells. *Current biology : CB*. 14:953-964.

Hu, C.K., M. Coughlin, C.M. Field, and T.J. Mitchison. 2011. KIF4 regulates midzone length during cytokinesis. *Current biology : CB*. 21:815-824.

Indjeian, V.B., and A.W. Murray. 2007. Budding yeast mitotic chromosomes have an intrinsic bias to biorient on the spindle. *Current biology : CB*. 17:1837-1846.

Jones, D.T., and D. Cozzetto. 2015. DISOPRED3: precise disordered region predictions with annotated protein-binding activity. *Bioinformatics*. 31:857-863.

Kato, H., J. Jiang, B.R. Zhou, M. Rozendaal, H. Feng, R. Ghirlando, T.S. Xiao, A.F. Straight, and Y. Bai. 2013. A conserved mechanism for centromeric nucleosome recognition by centromere protein CENP-C. *Science*. 340:1110-1113.

Ke, K., J. Cheng, and A.J. Hunt. 2009. The distribution of polar ejection forces determines the amplitude of chromosome directional instability. *Current biology : CB*. 19:807-815.

Khodjakov, A., and C.L. Rieder. 1996. Kinetochores moving away from their associated pole do not exert a significant pushing force on the chromosome. *J Cell Biol*. 135:315-327.

King, J.M., and R.B. Nicklas. 2000. Tension on chromosomes increases the number of kinetochore microtubules but only within limits. *J Cell Sci*. 113 Pt 21:3815-3823.

Kitajima, T.S., M. Ohsugi, and J. Ellenberg. 2011. Complete kinetochore tracking reveals error-prone homologous chromosome biorientation in mammalian oocytes. *Cell*. 146:568-581.

Kiyomitsu, T., C. Obuse, and M. Yanagida. 2007. Human Blinkin/AF15q14 is required for chromosome alignment and the mitotic checkpoint through direct interaction with Bub1 and BubR1. *Dev Cell*. 13:663-676.

Klare, K., J.R. Weir, F. Basilico, T. Zimniak, L. Massimiliano, N. Ludwigs, F. Herzog, and A. Musacchio. 2015. CENP-C is a blueprint for constitutive centromere-associated network assembly within human kinetochores. *J Cell Biol*. 210:11-22.

Kwon, M., S. Morales-Mulia, I. Brust-Mascher, G.C. Rogers, D.J. Sharp, and J.M. Scholey. 2004. The chromokinesin, KLP3A, dives mitotic spindle pole separation during prometaphase and anaphase and facilitates chromatid motility. *Mol Biol Cell*. 15:219-233.

Lampert, F., and S. Westermann. 2011. A blueprint for kinetochores - new insights into the molecular mechanics of cell division. *Nat Rev Mol Cell Biol*. 12:407-412.

Lampson, M.A., and I.M. Cheeseman. 2011. Sensing centromere tension: Aurora B and the regulation of kinetochore function. *Trends Cell Biol*. 21:133-140.

Lampson, M.A., K. Renduchitala, A. Khodjakov, and T.M. Kapoor. 2004. Correcting improper chromosome-spindle attachments during cell division. *Nat Cell Biol*. 6:232-237.

Levesque, A.A., and D.A. Compton. 2001. The chromokinesin Kid is necessary for chromosome arm orientation and oscillation, but not congression, on mitotic spindles. *J Cell Biol*. 154:1135-1146.

Li, X., and R.B. Nicklas. 1995. Mitotic forces control a cell-cycle checkpoint. *Nature*. 373:630-632.

Lim, R.Y., N.P. Huang, J. Koser, J. Deng, K.H. Lau, K. Schwarz-Herion, B. Fahrenkrog, and U. Aebi. 2006. Flexible phenylalanine-glycine nucleoporins as entropic barriers to nucleocytoplasmic transport. *Proc Natl Acad Sci U S A*. 103:9512-9517.

Lipinszki, Z., S. Lefevre, M.S. Savoian, M.R. Singleton, D.M. Glover, and M.R. Przewloka. 2015. Centromeric binding and activity of Protein Phosphatase 4. *Nat Commun*. 6:5894.

Liu, D., G. Vader, M.J.M. Vromans, M.A. Lampson, and S.M.A. Lens. 2009. Sensing Chromosome Bi-Orientation by Spatial Separation of Aurora B Kinase from Kinetochore Substrates. *Science*. 323:1350-1353.

London, N., and S. Biggins. 2014. Signalling dynamics in the spindle checkpoint response. *Nat Rev Mol Cell Biol*. 15:736-747.

Lu, P., and M.G. Feng. 2008. Bifunctional enhancement of a beta-glucanase-xylanase fusion enzyme by optimization of peptide linkers. *Appl Microbiol Biotechnol*. 79:579-587.

Maddox, P.S., K.S. Bloom, and E.D. Salmon. 2000. The polarity and dynamics of microtubule assembly in the budding yeast Saccharomyces cerevisiae. *Nat Cell Biol*. 2:36-41.

Magidson, V., C.B. O'Connell, J. Loncarek, R. Paul, A. Mogilner, and A. Khodjakov. 2011. The spatial arrangement of chromosomes during prometaphase facilitates spindle assembly. *Cell*. 146:555-567.

Maiato, H., J. DeLuca, E.D. Salmon, and W.C. Earnshaw. 2004. The dynamic kinetochore-microtubule interface. *J Cell Sci*. 117:5461-5477.

Maiato, H., P.J. Hergert, S. Moutinho-Pereira, Y. Dong, K.J. Vandenbeldt, C.L. Rieder, and B.F. McEwen. 2006. The ultrastructure of the kinetochore and kinetochore fiber in Drosophila somatic cells. *Chromosoma*. 115:469-480.

Malvezzi, F., G. Litos, A. Schleiffer, A. Heuck, K. Mechtler, T. Clausen, and S. Westermann. 2013. A structural basis for kinetochore recruitment of the Ndc80 complex via two distinct centromere receptors. *Embo J*. 32:409-423.

Maresca, T.J., and E.D. Salmon. 2009. Intrakinetochore stretch is associated with changes in kinetochore phosphorylation and spindle assembly checkpoint activity. *Journal of Cell Biology*. 184:373-381.

Maresca, T.J., and E.D. Salmon. 2010. Welcome to a new kind of tension: translating kinetochore mechanics into a wait-anaphase signal. *J Cell Sci*. 123:825-835.

Markus, S.M., K.M. Plevock, B.J. St Germain, J.J. Punch, C.W. Meaden, and W.L. Lee. 2011. Quantitative analysis of Pac1/LIS1-mediated dynein targeting: Implications for regulation of dynein activity in budding yeast. *Cytoskeleton (Hoboken)*. 68:157-174.

Marshall, W.F., J.F. Marko, D.A. Agard, and J.W. Sedat. 2001. Chromosome elasticity and mitotic polar ejection force measured in living Drosophila embryos by four-dimensional microscopy-based motion analysis. *Current biology : CB*. 11:569-578.

Maskell, D.P., X.W. Hu, and M.R. Singleton. 2010. Molecular architecture and assembly of the yeast kinetochore MIND complex. *J Cell Biol*. 190:823-834.

Matthies, H.J., R.J. Baskin, and R.S. Hawley. 2001. Orphan kinesin NOD lacks motile properties but does possess a microtubule-stimulated ATPase activity. *Mol Biol Cell*. 12:4000-4012.

McEwen, B.F., C.E. Hsieh, A.L. Mattheyses, and C.L. Rieder. 1998. A new look at kinetochore structure in vertebrate somatic cells using high-pressure freezing and freeze substitution. *Chromosoma*. 107:366-375.

McIntosh, J.R. 1991. Structural and mechanical control of mitotic progression. *Cold Spring Harb Symp Quant Biol*. 56:613-619.

McIntosh, J.R. 2012. Motors or dynamics: what really moves chromosomes? *Nat Cell Biol*. 14:1234.

McIntosh, J.R., E.L. Grishchuk, M.K. Morphew, A.K. Efremov, K. Zhudenkov, V.A. Volkov, I.M. Cheeseman, A. Desai, D.N. Mastronarde, and F.I. Ataullakhanov. 2008. Fibrils connect microtubule tips with kinetochores: a mechanism to couple tubulin dynamics to chromosome motion. *Cell*. 135:322-333.

Meraldi, P. 2012. Keeping kinetochores on track. *Eur J Cell Biol*. 91:103-106.

Musacchio, A., and E.D. Salmon. 2007. The spindle-assembly checkpoint in space and time. *Nat Rev Mol Cell Biol*. 8:379-393.

Nezi, L., and A. Musacchio. 2009. Sister chromatid tension and the spindle assembly checkpoint. *Curr Opin Cell Biol*. 21:785-795.

Nicklas, R.B., and C.A. Koch. 1969. Chromosome micromanipulation. 3. Spindle fiber tension and the reorientation of mal-oriented chromosomes. *J Cell Biol*. 43:40-50.

Nicklas, R.B., and S.C. Ward. 1994. Elements of error correction in mitosis: microtubule capture, release, and tension. *J Cell Biol*. 126:1241-1253.

Nicklas, R.B., S.C. Ward, and G.J. Gorbsky. 1995. Kinetochore chemistry is sensitive to tension and may link mitotic forces to a cell cycle checkpoint. *J Cell Biol*. 130:929-939.

Nicklas, R.B., J.C. Waters, E.D. Salmon, and S.C. Ward. 2001. Checkpoint signals in grasshopper meiosis are sensitive to microtubule attachment, but tension is still essential. *J Cell Sci*. 114:4173-4183.

Nishino, T., F. Rago, T. Hori, K. Tomii, I.M. Cheeseman, and T. Fukagawa. 2013. CENP-T provides a structural platform for outer kinetochore assembly. *Embo J*. 32:424-436.

Orr, B., O. Afonso, T. Feijao, and C.E. Sunkel. 2010. Driving chromosome segregation: lessons from the human and Drosophila centromere-kinetochore machinery. *Biochem Soc Trans*. 38:1667-1675.

Orr, B., K.M. Godek, and D. Compton. 2015. Aneuploidy. *Current biology : CB*. 25:R538-542.

Orr, B., and C.E. Sunkel. 2011. Drosophila CENP-C is essential for centromere identity. *Chromosoma*. 120:83-96.

Pearson, C.G., P.S. Maddox, E.D. Salmon, and K. Bloom. 2001. Budding yeast chromosome structure and dynamics during mitosis. *J Cell Biol*. 152:1255-1266.

Perpelescu, M., and T. Fukagawa. 2011. The ABCs of CENPs. *Chromosoma*. 120:425-446.

Petrovic, A., S. Mosalaganti, J. Keller, M. Mattiuzzo, K. Overlack, V. Krenn, A. De Antoni, S. Wohlgemuth, V. Cecatiello, S. Pasqualato, S. Raunser, and A. Musacchio. 2014. Modular Assembly of RWD Domains on the Mis12 Complex Underlies Outer Kinetochore Organization. *Mol Cell*. 53:591-605.

Petrovic, A., S. Pasqualato, P. Dube, V. Krenn, S. Santaguida, D. Cittaro, S. Monzani, L. Massimiliano, J. Keller, A. Tarricone, A. Maiolica, H. Stark, and A. Musacchio. 2010. The MIS12 complex is a protein interaction hub for outer kinetochore assembly. *J Cell Biol*. 190:835-852.

Phansalkar, R., P. Lapierre, and B.G. Mellone. 2012. Evolutionary insights into the role of the essential centromere protein CAL1 in Drosophila. *Chromosome research : an international journal on the molecular, supramolecular and evolutionary aspects of chromosome biology*. 20:493-504.

Powers, A.F., A.D. Franck, D.R. Gestaut, J. Cooper, B. Gracyzk, R.R. Wei, L. Wordeman, T.N. Davis, and C.L. Asbury. 2009. The Ndc80 kinetochore complex forms load-bearing attachments to dynamic microtubule tips via biased diffusion. *Cell*. 136:865-875.

Powers, J., D.J. Rose, A. Saunders, S. Dunkelbarger, S. Strome, and W.M. Saxton. 2004. Loss of KLP-19 polar ejection force causes misorientation and missegregation of holocentric chromosomes. *J Cell Biol*. 166:991-1001.

Przewloka, M.R., Z. Venkei, V.M. Bolanos-Garcia, J. Debski, M. Dadlez, and D.M. Glover. 2011. CENP-C Is a Structural Platform for Kinetochore Assembly. *Curr Biol*. 21:399-405.

Przewloka, M.R., Z. Venkei, and D.M. Glover. 2009. Searching for Drosophila Dsn1 kinetochore protein. *Cell Cycle*. 8:1292-1293.

Rago, F., and I.M. Cheeseman. 2013. Review series: The functions and consequences of force at kinetochores. *J Cell Biol*. 200:557-565.

Rago, F., K.E. Gascoigne, and I.M. Cheeseman. 2015. Distinct organization and regulation of the outer kinetochore KMN network downstream of CENP-C and CENP-T. *Current biology : CB*. 25:671-677.

Rasooly, R.S., C.M. New, P. Zhang, R.S. Hawley, and B.S. Baker. 1991. The lethal(1)TW-6cs mutation of Drosophila melanogaster is a dominant antimorphic allele of nod and is associated with a single base change in the putative ATP-binding domain. *Genetics*. 129:409-422.

Ricke, R.M., K.B. Jeganathan, and J.M. van Deursen. 2011. Bub1 overexpression induces aneuploidy and tumor formation through Aurora B kinase hyperactivation. *J Cell Biol*. 193:1049-1064.

Rieder, C.L. 1981. The structure of the cold-stable kinetochore fiber in metaphase PtK1 cells. *Chromosoma*. 84:145-158.

Rieder, C.L., R.W. Cole, A. Khodjakov, and G. Sluder. 1995. The checkpoint delaying anaphase in response to chromosome monoorientation is mediated by an inhibitory signal produced by unattached kinetochores. *J Cell Biol*. 130:941-948.

Rieder, C.L., E.A. Davison, L.C. Jensen, L. Cassimeris, and E.D. Salmon. 1986. Oscillatory movements of monooriented chromosomes and their position relative to the spindle pole result from the ejection properties of the aster and half-spindle. *J Cell Biol*. 103:581-591.

Rieder, C.L., and E.D. Salmon. 1994. Motile kinetochores and polar ejection forces dictate chromosome position on the vertebrate mitotic spindle. *J Cell Biol*. 124:223-233.

Rosic, S., F. Kohler, and S. Erhardt. 2014. Repetitive centromeric satellite RNA is essential for kinetochore formation and cell division. *J Cell Biol*. 207:335-349.

Salimian, K.J., E.R. Ballister, E.M. Smoak, S. Wood, T. Panchenko, M.A. Lampson, and B.E. Black. 2011. Feedback control in sensing chromosome biorientation by the Aurora B kinase. *Current biology : CB*. 21:1158-1165.

Samejima, K., M. Platani, M. Wolny, H. Ogawa, G. Vargiu, P.J. Knight, M. Peckham, and W.C. Earnshaw. 2015. The Inner Centromere Protein (INCENP) Coil Is a Single alpha-Helix (SAH) Domain That Binds Directly to Microtubules and Is Important for Chromosome Passenger Complex (CPC) Localization and Function in Mitosis. *J Biol Chem*. 290:21460-21472.

Santaguida, S., and A. Musacchio. 2009. The life and miracles of kinetochores. *Embo J*. 28:2511-2531.

Sarangapani, K.K., and C.L. Asbury. 2014. Catch and release: how do kinetochores hook the right microtubules during mitosis? *Trends Genet*. 30:150-159.

Schittenhelm, R.B., F. Althoff, S. Heidmann, and C.F. Lehner. 2010. Detrimental incorporation of excess Cenp-A/Cid and Cenp-C into Drosophila centromeres is prevented by limiting amounts of the bridging factor Cal1. *J Cell Sci*. 123:3768-3779.

Schittenhelm, R.B., R. Chaleckis, and C.F. Lehner. 2009. Intrakinetochore localization and essential functional domains of Drosophila Spc105. *Embo J*. 28:2374-2386.

Schittenhelm, R.B., S. Heeger, F. Althoff, A. Walter, S. Heidmann, K. Mechtler, and C.F. Lehner. 2007. Spatial organization of a ubiquitous eukaryotic kinetochore protein network in Drosophila chromosomes. *Chromosoma*. 116:385-402.

Schleiffer, A., M. Maier, G. Litos, F. Lampert, P. Hornung, K. Mechtler, and S. Westermann. 2012. CENP-T proteins are conserved centromere receptors of the Ndc80 complex. *Nat Cell Biol*. 14:604-613.

Schmidt, J.C., H. Arthanari, A. Boeszoermenyi, N.M. Dashkevich, E.M. Wilson-Kubalek, N. Monnier, M. Markus, M. Oberer, R.A. Milligan, M. Bathe, G. Wagner, E.L. Grishchuk, and I.M. Cheeseman. 2012. The kinetochore-bound Ska1 complex tracks depolymerizing microtubules and binds to curved protofilaments. *Dev Cell*. 23:968-980.

Screpanti, E., A. De Antoni, G.M. Alushin, A. Petrovic, T. Melis, E. Nogales, and A. Musacchio. 2011. Direct Binding of Cenp-C to the Mis12 Complex Joins the Inner and Outer Kinetochore. *Curr Biol*. 21:391-398.

Shah, J.V., E. Botvinick, Z. Bonday, F. Furnari, M. Berns, and D.W. Cleveland. 2004. Dynamics of centromere and kinetochore proteins; implications for checkpoint signaling and silencing. *Current biology : CB*. 14:942-952.

Shrestha, R.L., and V.M. Draviam. 2013. Lateral to end-on conversion of chromosome-microtubule attachment requires kinesins CENP-E and MCAK. *Current biology : CB*. 23:1514-1526.

Sickmeier, M., J.A. Hamilton, T. LeGall, V. Vacic, M.S. Cortese, A. Tantos, B. Szabo, P. Tompa, J. Chen, V.N. Uversky, Z. Obradovic, and A.K. Dunker. 2007. DisProt: the Database of Disordered Proteins. *Nucleic Acids Res*. 35:D786-793.

Skibbens, R.V., V.P. Skeen, and E.D. Salmon. 1993. Directional instability of kinetochore motility during chromosome congression and segregation in mitotic newt lung cells: a push-pull mechanism. *J Cell Biol*. 122:859-875.

Smurnyy, Y., A.V. Toms, G.R. Hickson, M.J. Eck, and U.S. Eggert. 2010. Binucleine 2, an isoform-specific inhibitor of Drosophila Aurora B kinase, provides insights into the mechanism of cytokinesis. *ACS Chem Biol*. 5:1015-1020.

Stumpff, J., M. Wagenbach, A. Franck, C.L. Asbury, and L. Wordeman. 2012. Kif18A and chromokinesins confine centromere movements via microtubule growth suppression and spatial control of kinetochore tension. *Dev Cell*. 22:1017-1029.

Sudakin, V., G.K. Chan, and T.J. Yen. 2001. Checkpoint inhibition of the APC/C in HeLa cells is mediated by a complex of BUBR1, BUB3, CDC20, and MAD2. *J Cell Biol*. 154:925-936.

Sullivan, B.A., M.D. Blower, and G.H. Karpen. 2001. Determining centromere identity: cyclical stories and forking paths. *Nat Rev Genet*. 2:584-596.

Sundin, L.J., G.J. Guimaraes, and J.G. Deluca. 2011. The NDC80 complex proteins Nuf2 and Hec1 make distinct contributions to kinetochore-microtubule attachment in mitosis. *Mol Biol Cell*. 22:759-768.

Suzuki, A., B.L. Badger, X.H. Wan, J.G. DeLuca, and E.D. Salmon. 2014. The Architecture of CCAN Proteins Creates a Structural Integrity to Resist Spindle Forces and Achieve Proper Intrakinetochore Stretch. *Dev Cell*. 30:717-730.

Suzuki, A., T. Hori, T. Nishino, J. Usukura, A. Miyagi, K. Morikawa, and T. Fukagawa. 2011. Spindle microtubules generate tension-dependent changes in the distribution of inner kinetochore proteins. *J Cell Biol*. 193:125-140.

Tanaka, T.U. 2010. Kinetochore-microtubule interactions: steps towards bi-orientation. *Embo J*. 29:4070-4082.

Tanaka, T.U., N. Rachidi, C. Janke, G. Pereira, M. Galova, E. Schiebel, M.J.R. Stark, and K. Nasmyth. 2002. Evidence that the Ipl1-Sli15 (Aurora knase-INCENP) complex by altering promotes chromosome bi-orientation kinetochore-spindle pole connections. *Cell*. 108:317-329.

Tantos, A., L. Kalmar, and P. Tompa. 2015. The role of structural disorder in cell cycle regulation, related clinical proteomics, disease development and drug targeting. *Expert Rev Proteomics*. 12:221-233.

Theurkauf, W.E., and R.S. Hawley. 1992. Meiotic spindle assembly in Drosophila females: behavior of nonexchange chromosomes and the effects of mutations in the nod kinesin-like protein. *J Cell Biol*. 116:1167-1180.

Thompson, S.L., and D.A. Compton. 2008. Examining the link between chromosomal instability and aneuploidy in human cells. *J Cell Biol*. 180:665-672.

Tokai-Nishizumi, N., M. Ohsugi, E. Suzuki, and T. Yamamoto. 2005. The chromokinesin Kid is required for maintenance of proper metaphase spindle size. *Mol Biol Cell*. 16:5455-5463.

Tompa, P. 2002. Intrinsically unstructured proteins. *Trends Biochem Sci*. 27:527-533.

Tompa, P. 2005. The interplay between structure and function in intrinsically unstructured proteins. *FEBS Lett*. 579:3346-3354.

Tooley, J., and P.T. Stukenberg. 2011. The Ndc80 complex: integrating the kinetochore's many movements. *Chromosome Res*. 19:377-391.

Uchida, K.S., K. Takagaki, K. Kumada, Y. Hirayama, T. Noda, and T. Hirota. 2009. Kinetochore stretching inactivates the spindle assembly checkpoint. *J Cell Biol*. 184:383-390.

Umbreit, N.T., and T.N. Davis. 2012. Mitosis puts sisters in a strained relationship: force generation at the kinetochore. *Exp Cell Res*. 318:1361-1366.

van der Horst, A., and S.M. Lens. 2014. Cell division: control of the chromosomal passenger complex in time and space. *Chromosoma*. 123:25-42.

van der Lee, R., M. Buljan, B. Lang, R.J. Weatheritt, G.W. Daughdrill, A.K. Dunker, M. Fuxreiter, J. Gough, J. Gsponer, D.T. Jones, P.M. Kim, R.W. Kriwacki, C.J. Oldfield, R.V. Pappu, P. Tompa, V.N. Uversky, P.E. Wright, and M.M. Babu. 2014. Classification of intrinsically disordered regions and proteins. *Chem Rev*. 114:6589-6631.

van der Waal, M.S., R.C. Hengeveld, A. van der Horst, and S.M. Lens. 2012. Cell division control by the Chromosomal Passenger Complex. *Exp Cell Res*. 318:1407-1420.

VandenBeldt, K.J., R.M. Barnard, P.J. Hergert, X. Meng, H. Maiato, and B.F. McEwen. 2006. Kinetochores use a novel mechanism for coordinating the dynamics of individual microtubules. *Current biology : CB*. 16:1217-1223.

Varma, D., S. Chandrasekaran, L.J. Sundin, K.T. Reidy, X. Wan, D.A. Chasse, K.R. Nevis, J.G. DeLuca, E.D. Salmon, and J.G. Cook. 2012. Recruitment of the human Cdt1 replication licensing protein by the loop domain of Hec1 is required for stable kinetochore-microtubule attachment. *Nat Cell Biol*. 14:593-603.

Varma, D., X. Wan, D. Cheerambathur, R. Gassmann, A. Suzuki, J. Lawrimore, A. Desai, and E.D. Salmon. 2013. Spindle assembly checkpoint proteins are positioned close to core microtubule attachment sites at kinetochores. *J Cell Biol*. 202:735-746.

Venkei, Z., M.R. Przewloka, and D.M. Glover. 2011. Drosophila Mis12 complex acts as a single functional unit essential for anaphase chromosome movement and a robust spindle assembly checkpoint. *Genetics*. 187:131-140.

Visscher, K., M.J. Schnitzer, and S.M. Block. 1999. Single kinesin molecules studied with a molecular force clamp. *Nature*. 400:184-189.

Wan, X.H., R.P. O'Quinn, H.L. Pierce, A.P. Joglekar, W.E. Gall, J.G. DeLuca, C.W. Carroll, S.T. Liu, T.J. Yen, B.F. McEwen, T. Stukenberg, A. Desai, and E.D. Salmon. 2009. Protein Architecture of the Human Kinetochore Microtubule Attachment Site. *Cell*. 137:672-684.

Wandke, C., M. Barisic, R. Sigl, V. Rauch, F. Wolf, A.C. Amaro, C.H. Tan, A.J. Pereira, U. Kutay, H. Maiato, P. Meraldi, and S. Geley. 2012. Human chromokinesins promote chromosome congression and spindle microtubule dynamics during mitosis. *J Cell Biol*. 198:847-863.

Ward, J.J., L.J. McGuffin, K. Bryson, B.F. Buxton, and D.T. Jones. 2004. The DISOPRED server for the prediction of protein disorder. *Bioinformatics*. 20:2138-2139.

Wei, R.R., P.K. Sorger, and S.C. Harrison. 2005. Molecular organization of the Ndc80 complex, an essential kinetochore component. *Proc Natl Acad Sci U S A*. 102:5363-5367.

Welburn, J.P., M. Vleugel, D. Liu, J.R. Yates, 3rd, M.A. Lampson, T. Fukagawa, and I.M. Cheeseman. 2010. Aurora B phosphorylates spatially distinct targets to differentially regulate the kinetochore-microtubule interface. *Mol Cell*. 38:383-392.

Westermann, S., and A. Schleiffer. 2013. Family matters: structural and functional conservation of centromere-associated proteins from yeast to humans. *Trends Cell Biol*. 23:260-269.

Whyte, J., J.R. Bader, S.B. Tauhata, M. Raycroft, J. Hornick, K.K. Pfister, W.S. Lane, G.K. Chan, E.H. Hinchcliffe, P.S. Vaughan, and K.T. Vaughan. 2008. Phosphorylation regulates targeting of cytoplasmic dynein to kinetochores during mitosis. *J Cell Biol*. 183:819-834.

Wignall, S.M., and A.M. Villeneuve. 2009. Lateral microtubule bundles promote chromosome alignment during acentrosomal oocyte meiosis. *Nat Cell Biol*. 11:839-844.

Wilson-Kubalek, E.M., I.M. Cheeseman, C. Yoshioka, A. Desai, and R.A. Milligan. 2008. Orientation and structure of the Ndc80 complex on the microtubule lattice. *J Cell Biol*. 182:1055-1061.

Winey, M., C.L. Mamay, E.T. O'Toole, D.N. Mastronarde, T.H. Giddings, Jr., K.L. McDonald, and J.R. McIntosh. 1995. Three-dimensional ultrastructural analysis of the Saccharomyces cerevisiae mitotic spindle. *J Cell Biol*. 129:1601-1615.

Wright, P.E., and H.J. Dyson. 2015. Intrinsically disordered proteins in cellular signalling and regulation. *Nat Rev Mol Cell Biol*. 16:18-29.

Yajima, J., M. Edamatsu, J. Watai-Nishii, N. Tokai-Nishizumi, T. Yamamoto, and Y.Y. Toyoshima. 2003. The human chromokinesin Kid is a plus end-directed microtubule-based motor. *Embo J*. 22:1067-1074.

Yang, C.H., J. Tomkiel, H. Saitoh, D.H. Johnson, and W.C. Earnshaw. 1996. Identification of overlapping DNA-binding and centromere-targeting domains in the human kinetochore protein CENP-C. *Mol Cell Biol*. 16:3576-3586.

Yang, Z., U.S. Tulu, P. Wadsworth, and C.L. Rieder. 2007. Kinetochore dynein is required for chromosome motion and congression independent of the spindle checkpoint. *Current biology : CB*. 17:973-980.

Ye, A.A., J. Deretic, C.M. Hoel, A.W. Hinman, D. Cimini, J.P. Welburn, and T.J. Maresca. 2015. Aurora A Kinase Contributes to a Pole-Based Error Correction Pathway. *Current biology : CB*. 25:1842-1851.

Zaytsev, A.V., L.J. Sundin, K.F. DeLuca, E.L. Grishchuk, and J.G. DeLuca. 2014. Accurate phosphoregulation of kinetochore-microtubule affinity requires unconstrained molecular interactions. *J Cell Biol*. 206:45-59.

Zhang, P., and R.S. Hawley. 1990. The genetic analysis of distributive segregation in Drosophila melanogaster. II. Further genetic analysis of the nod locus. *Genetics*. 125:115-127.

Zhang, P., B.A. Knowles, L.S. Goldstein, and R.S. Hawley. 1990. A kinesin-like protein required for distributive chromosome segregation in Drosophila. *Cell*. 62:1053-1062.